Universidade Estadual de Campinas
Instituto de Computação

Leticia da Silva Bomfim

Characterization of Brazilian Pre-Salt Reservoirs Based on Image Analysis and Machine Learning

Caracterização de Reservatórios do Pré-Sal Brasileiro Baseada em Análise de Imagens e Aprendizado de Máquina

CAMPINAS
2024

Leticia da Silva Bomfim

Characterization of Brazilian Pre-Salt Reservoirs Based on Image Analysis and Machine Learning

Caracterização de Reservatórios do Pré-Sal Brasileiro Baseada em Análise de Imagens e Aprendizado de Máquina

Tese apresentada ao Instituto de Computação da Universidade Estadual de Campinas como parte dos requisitos para a obtenção do título de Doutora em Ciência da Computação.

Thesis presented to the Institute of Computing of the University of Campinas in partial fulfillment of the requirements for the degree of Doctor in Computer Science.

Supervisor/Orientador: Prof. Dr. Hélio Pedrini
Co-supervisor/Coorientador: Prof. Dr. Alexandre Campane Vidal

Este exemplar corresponde à versão final da
Tese defendida por Leticia da Silva Bomfim
e orientada pelo Prof. Dr. Hélio Pedrini.

CAMPINAS

2024

Ficha catalográfica
Universidade Estadual de Campinas (UNICAMP)
Biblioteca do Instituto de Matemática, Estatística e Computação Científica
Ana Regina Machado - CRB 8/5467

Informações Complementares

Universidade Estadual de Campinas
Instituto de Computação

Leticia da Silva Bomfim

Characterization of Brazilian Pre-Salt Reservoirs Based on Image Analysis and Machine Learning

Caracterização de Reservatórios do Pré-Sal Brasileiro Baseada em Análise de Imagens e Aprendizado de Máquina

Banca Examinadora:

- Prof. Dr. Hélio Pedrini
  IC/UNICAMP

- Profa. Dra. Camila Duelis Viana
  IGc/USP

- Prof. Dr. Ronaldo Cristiano Prati
  CMCC/UFABC

- Prof. Dr. Emilson Pereira Leite
  IG/UNICAMP

- Prof. Dr. Andre Santanche
  IC/UNICAMP

A ata da defesa, assinada pelos membros da Comissão Examinadora, consta no SIGA/Sistema de Fluxo de Dissertação/Tese e na Secretaria do Programa da Unidade.

Campinas, 31 de julho de 2024

Acknowledgments

The journey to this specific moment in my life has been guided by many people who have helped shape who I am today. Of all who have passed through and still remain, I would like to first thank my family, especially the women in my life: Fernanda, my mother, and Laís, my sister. Both have always been my safe haven, reminding me of who I am and where I can go. I also thank my father, Dorierlan, for providing me with support and affection on this journey so far. My entire family has my eternal gratitude for the trust and encouragement they have given me. I can only say that I am the result of my faith in God and the love of all of them, my grandparents, uncles, aunts, and cousins.

I am grateful to all the teachers with whom I have had the opportunity to interact, especially my advisor, Prof. Hélio Pedrini, who made the research journey light, enriching, and inspiring. Despite the many challenges that the doctorate presents us with, your guidance has enabled me to finish this stage eager to provide my future students with the same environment that I had the opportunity to experience.

The development of this research would not have been possible without the collaboration of my colleagues from the Reservoir Geological Modeling Laboratory (MGR). Special thanks to Marcus Vinicius Theodoro, for the countless research discussions, partnership, and support; to Michelle, for always being willing to help and collaborate; to my co-advisor, Prof. Alexandre Vidal, for all the opportunities and teachings; and to all the other group colleagues who shared these four years with me. I also thank the colleagues and friends from the Institute of Computing and the Computer Vision Laboratory for everything we experienced together.

I am thankful for the friends I have made over the years in Campinas, who are now part of my life beyond academia, making the distance from my family less difficult. All of you have a special place in my heart: Danielle, Sara, Sandra, Eva, Francisco, Marianna, Guilherme, Ana, and Jonathan.

I thank my fiancé, Marcos Vinicius, for all the companionship up to this point. Throughout my academic journey, his presence has been a special constant, being able to closely follow each of my steps. I am certain that everything I have achieved has been enriched by his aid, teachings, academic discussions, encouragement, and, most importantly, love.

Resumo

Os reservatórios carbonáticos têm a heterogeneidade como uma de suas principais características. Essa particularidade, quando vinculada à análise e à caracterização de poços e reservatórios, agrega desafios à interpretação e à definição de um modelo geológico concreto. Além disso, todo o processo de conceitualização de um reservatório inclui o enfrentamento de incertezas geológicas voltadas à sua estrutura física, bem como incertezas econômicas voltadas ao custo e investimento. No Brasil, a Bacia de Santos se apresenta como grande produtora do ramo de óleo e gás, o que reúne grandes esforços para a compreensão e modelagem do campo. Porém, sua formação geológica derivada de rochas carbonáticas apresenta diversos desafios envolvendo sua constituição altamente heterogênea. Assim, estratégias que permitem aprofundar e produzir generalizações desses ambientes viabilizam a otimização e maior sucesso na exploração de um reservatório. Para automatizar e aprimorar os procedimentos envolvidos nessa tarefa, diversas abordagens no campo da visão computacional têm sido aplicadas ao longo dos anos, e podem ser observadas desde a aquisição de dados até a modelagem final dos reservatórios. Metodologias desenvolvidas para essa caracterização geológica demonstram uma forte sinergia entre técnicas de processamento de imagens e aprendizado de máquina. Essa colaboração mutualística contribui para o avanço de ambas as tecnologias, fornecendo coletivamente uma variedade de soluções para os diversos desafios encontrados na modelagem geológica de reservatórios. Dessa forma, por meio desta pesquisa, buscamos contextualizar o uso de análise de imagens e aprendizado de máquina na caracterização de reservatórios, bem como apresentar de forma prática a aplicação desse recurso em três tarefas importantes da modelagem geológica: o tratamento de imagens de poço ruidosas para possibilitar a análise dos dados, a classificação de fácies sísmicas por meio das redes convolucionais e a identificação de falhas em dados sísmicos utilizando modelos Transformers. Na primeira aplicação, foi desenvolvida uma metodologia que utiliza o algoritmo de Retinex Multiescala com preservação de cor para eliminar o ruído causado por sombreamento, seguida da aplicação de um algoritmo de quantização dos canais de cor da imagem para segmentação precisa das estruturas de interesse. Em relação à classificação de fácies, foi implementada uma rede U-Net que alcançou uma média de IoU de 95,48% na classificação de cinco diferentes tipos de fácies em dados sísmicos. Por fim, na tarefa de extração de falhas, investigamos o uso de Transformers através da rede TransUnet, que superou redes convolucionais tradicionais, obtendo um coeficiente Dice superior a 88% na identificação dessas estruturas. Todos esses processos foram avaliados de forma quantitativa e qualitativa, e corresponderam positivamente aos métodos aplicados. As abordagens utilizadas reforçam o poder da computação visual como uma ferramenta aliada à caracterização de reservatórios, impulsionando a precisão, a automação e a eficiência, bem como promovendo avanços significativos na exploração e modelagem geológica.

Abstract

Carbonate reservoirs feature heterogeneity as one of their main characteristics. This peculiarity, when linked to well and reservoir analysis and characterization, adds challenges to the interpretation and definition of a concrete geological model. Additionally, the entire process of conceptualizing a reservoir involves addressing geological uncertainties related to its physical structure, as well as economic uncertainties regarding cost and investment. In Brazil, the Santos Basin stands out as a major producer in the oil and gas sector, which gathers significant efforts for field understanding and modeling. However, its geological formation derived from carbonate rocks presents various challenges due to its highly heterogeneous constitution. Therefore, strategies that enable deeper insights and generalizations of these environments facilitate optimization and greater success in reservoir exploration. To automate and enhance the procedures involved in this task, various approaches in the field of computer vision have been applied over the years, observable from data acquisition to final reservoir modeling. Methodologies developed for this geological characterization demonstrate a strong synergy between image processing techniques and machine learning. This mutually beneficial collaboration contributes to advancing both technologies, collectively providing a range of solutions to the diverse challenges encountered in geological reservoir modeling. Thus, through this research, we aim to contextualize the use image analysis and machine learning in reservoir characterization, as well as to practically demonstrate the application of this resource in three important tasks of the geological modeling workflow: noise reduction in well images to enable pore analysis, seismic facies classification through convolutional networks, and fault identification in seismic data using Transformer models. In the first application, a methodology was developed that employs the Multiscale Retinex algorithm with color preservation to eliminate noise caused by fogging, followed by the application of a color channel quantization algorithm for precise segmentation of the structures of interest. Regarding facies classification, a U-Net network was implemented, achieving an average IoU of 95.48% in the classification of five different types of facies in seismic data. Finally, in the task of fault extraction, we investigated the use of Transformers through the TransUnet network, which outperformed traditional convolutional networks, obtaining a Dice coefficient higher than 88% in the identification of these structures. All these processes were evaluated quantitatively and qualitatively, yielding positive outcomes for the applied methods. This approach reinforces visual computing as an essential and powerful tool in reservoir characterization, driving precision, automation, and efficiency, and fostering significant advancements in geological exploration and modeling.

List of Figures

List of Tables

List of Abbreviations and Acronyms

1D	One-Dimensional
2D	Two-Dimensional
3D	Three-Dimensional
4D	Four-Dimensional
AAM	Active Attention Module
ANP	Agência Nacional do Petróleo, Gás Natural e Biocombustíveis
BHI	Borehole Image Log
BMP	Bitmap
CCUS	Carbon Capture, Utilization and Storage
cDC-GAN	Conditional Deep Convolutional Generative Neural Network
CDF	Cumulative Distribution Function
CGAN	Conditional Generative Adversarial Networks
CLAHE	Contrast Limited Adaptive Histogram Equalization
CNN	Convolutional Neural Network
CO_2	Carbon Dioxide
CT	Computed Tomography
CWT	Continuous Wavelet Transforms
DICOM	Digital Imaging and Communications in Medicine
DL	Deep Learning
DSGAN	Deep Convolutional Generative Adversarial Networks
FESEM	Field Emission Scanning Electron Microscopy
FITS	Flexible Image Transport System
FMI	Fullbore Formation MicroImager
FMS	Formation MicroScanner
FN	False Negative
FP	False Positive
GAN	Generative Adversarial Network
GANSim	Generative Adversarial Network-based Geomodeling Simulation
GIF	Graphics Interchange Format
HE	Histogram Equalization
IoU	Intersection over Union
IQA	Image Quality Assessment
JPEG	Joint Photographic Experts Group
LN	Layer Normalization
LSFM	Laser Scanning Fluorescence Microscopy
MLP	Multi-Layer Perceptron

MSA	Multihead Self-Attention
MsNet	Multiscale Convolutional Neural Network
MSR	Multi-Scale Retinex
MSRCP	Multi-Scale Retinex with Color Preservation
MSRCR	Multi-Scale Retinex with Color Restoration
NLP	Natural Language Processing
OpenCV Library	Open Source Computer Vision Library
P	Precision
PCAS	Pores (Particles) and Cracks Analysis System
PLM	Polarized Light Microscopy
PSNR	Peak Signal to Noise Ratio
R	Recall
RAGAN	Relativistic Average Generative Adversarial Network
ReLU	Rectified Linear Unit
R, G, B	Red, Green, Blue
RGBQ	Red, Green, Blue Image Quantization
SAGANs	Spatially Assembled Generative Adversarial Network
SCWT	Scattering Wavelet Transform
SEG	Society of Exploration Geophysicists
SEM	Scanning Electron Microscope
SinGAN	Generative Adversarial Network based on a Single Image
SR-CNN	Super Resolution Convolutional Neural Network
SSIM	Structural Similarity Index Measure
SSR	Single-Scale Retinex
T	Threshold
TgCNN	Theory-guided Convolutional Neural Network
TIFF	Tagged Image File Format
TN	True Negative
TP	True Positive
UBI	Ultrasonic Borehole Imager
VGG	Visual Geometry Group
ViT	Vision Transformer
WGAN-GP	Wasserstein GAN with Gradient Penalty

Contents

Chapter 1

Introduction

This chapter outlines the problem to be investigated, presents the main motivations of the research topic, describes the main objectives, the expected contributions of the work, and the research questions. Additionally, it provides an overview of the text organization and a list of publications carried out during the execution of the research.

1.1 Problem Characterization

Oil is the most important raw material in the world, and its primary use today is as fuel, with 97% of transportation relying on this resource [174]. In the petrochemical industry, its use goes beyond energy generation; its derivatives enable the production of plastics, synthetic rubbers, paints, dyes, adhesives, solvents, detergents, explosives, pharmaceuticals, cosmetics, and other items [210]. However, the extraction of this resource requires a lengthy process, beginning with the exploration of the raw material's existence feasibility. During this stage, geological studies and geophysical methods determine the conditions for exploration, given the characteristics of sedimentary basins with the capacity to accumulate hydrocarbons [156].

In the Brazilian context, we have the Pre-Salt, which has great exploration potential, and reserve estimates indicate there are approximately 70 to 100 billion barrels of oil. A significant portion of its location is in the Santos Basin, which, due to its production, ranks among the five largest reserves globally [45]. However, despite these significant qualities, the exploration of these reserves faces a series of challenges, both in terms of the cost of the tools used in this process, and in the environment encountered post-drilling (enormous pressures and temperatures, salt behavior, porosity, and heterogeneity of carbonate reservoirs) [173].

Furthermore, the geological characterization of these reservoirs encompasses the understanding and the methods used to characterize their heterogeneity [131]. According to Jia et al. [96], this task is a combined technology associated with geostatistics, geophysics, petrophysics, geology and reservoir engineering, where the main objective is to describe the reservoir in sufficient detail. For this, realistic 3D/4D models are constructed based on petrophysical properties to obtain greater chances of resource capture, through an optimized process, where efforts are applied to reduce uncertainties and increase pro-

ductivity. This process presents numerous difficulties due to the different methods for the construction of a reservoir framework, including the accurate representation of the reservoir geometry, the structural modeling and a detailed stratigraphic layers definition [96].

To provide the necessary geological information to deal with all the encountered barriers, several technologies (Figure 1.1) have been used to understand the prospects of a reservoir at a wide range of scales. Through the image acquisition process, different types of data provide the visualization and comprehension necessary to explore the subsurface region effectively. Moreover, this work encompasses the investigation of: (i) kilometer-scale seismic images to resolve the volumetric distribution of reservoir layers and its geological bodies within the sedimentary basin (for instance, [13, 25, 141, 233]); (ii) meter-scale borehole wall image logs, core and sidewall core sample images to depict the vertical layering of different rock types throughout the reservoir interval (for instance, [148, 195]); and (iii) thin sections, scanning electron microscope (SEM), and X-ray computed tomography (CT) images derived from rock samples to further address their microscopic properties such as porosity, permeability, and composition) (for instance, [15, 84]).
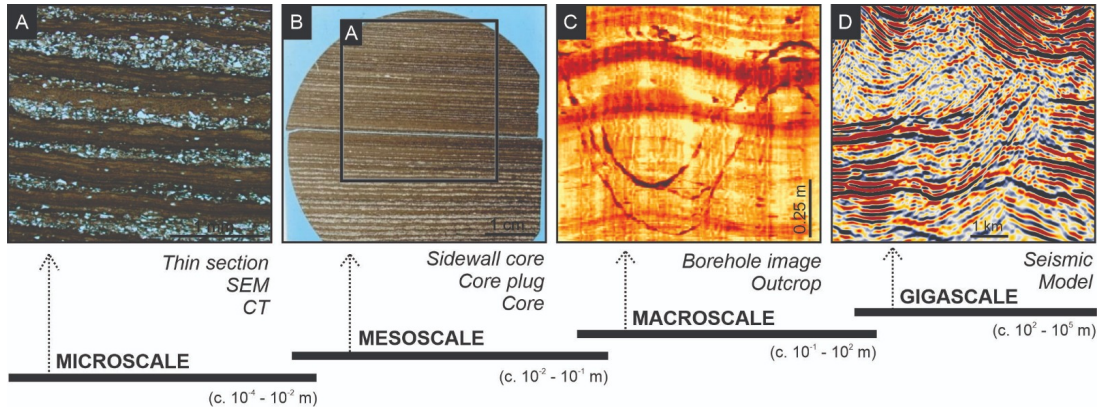
Figure 1.1: Representative examples of geological data types and their scales of analysis.

Consequently, to deal with this large range of data, computer vision emerges, with the image processing and machine learning solutions, in this field, as an excellent tool to help address the problems that arise when dealing with the inherent heterogeneity of geological data.

1.2   Motivations and Challenges

After a detailed analysis of the issue presented in the introduction, fundamental motivations and challenges were identified for research in the field of computer vision and its technologies applied to reservoir characterization.

These aspects underscore the importance of addressing specific issues that directly impact the understanding of the problem. Therefore, this study outlines the main motivations (**M**) and challenges (**C**) driving it:

- (**M**) The computer vision field encompasses techniques that range from the acquisition, processing, analysis and understanding of complex higher-dimensional data

from the environment of research and technical exploration [93]. Its range of applications can be found in different stages of reservoir characterization, mainly because it acts as a tool capable of extracting descriptions of a geological nature through images. According to Sebe [188], the computer vision field has evolved from the traditional pattern recognition and image processing techniques, to more advanced applications that encompass image comprehension, model-based vision, and systems capable of learning.

- (**M**) Understanding and analyzing geological characteristics and their influence on reservoir properties is crucial for the success of hydrocarbon exploration and production. Moreover, automating these processes can result in the production of deliverables that are useful in well planning optimization, reservoir modeling, and risk analysis [260].

- (**C**) The carbonate rocks that make up a significant portion of the pre-salt reservoirs are characterized by different types of porosity and have unimodal, bimodal, and other complex pore size distributions. These variations present high heterogeneity and complexity to the data, and make it difficult to make predictions related to its productivity [217].

- (**C/M**) Manual interpretation has been the most direct and effective approach to characterizing three-dimensional geological surfaces, in which an interpreter visually analyzes seismic reflection patterns, identifies important patterns, and labels them with distinct marks and/or colors. However, the dramatically increasing size of 3D seismic surveys has significantly challenged the efficiency and accuracy of such manual interpretation [48].

- (**C/M**) According to Chang et al. [32], the vast dimension of the Santos Basin, combined with the scarcity of data and information about its geology and petroleum systems, gives it the status of a relatively unknown basin. However, it stands out as a significant and promising oil exploration frontier in Brazil, given the abundant discoveries of oil and gas.

- (**M**) Lastly, every technological advancement enables the exploration of well-established basins. According to Suslick and Schiozer [202], these international exploration/production strategies based on technology combined with new elements, represent important components of a series of investment decisions based on risk analysis and decision models.

1.3 Objectives and Contributions

Machine learning and image processing has been a field of research with significant interdisciplinary character. Its evolution has enabled several areas to use its resources as tools for manipulation and automation of activities where images are the main material. In the geological field, particularly in reservoir characterization, this is no different.

Throughout the reservoir modeling workflow, there are different activities that can be performed to optimize and automate this process. Therefore, the main objective of this thesis is to investigate the use of machine learning and image processing approaches in the reservoir characterization process and, practically, to present solutions through the application of this practices in several aspects of this workflow. To this end, we intend to guide the research with the following specific objectives.

- Present the context of technologies that utilize different types of geological data represented in image form within the field of reservoir characterization, as well as the geological tasks that require greater academic attention.

- Introduce deep learning techniques and image processing methods into the context of reservoir characterization to automate and optimize different tasks, such as fault identification, facies classification, and well image enhancement for the segmentation of pores structures.

- Discuss the benefits of integrating different technologies within the context of reservoir characterization.

By achieving these objectives, we have the following main contributions:

- A detailed study of the state of the art in computer vision methods for reservoir characterization, covering techniques from image processing to machine/deep learning models. Identifying the recurring problems in this task, along with commonly employed solutions, can provide valuable insights for this research field, promoting a direction in the development of new technologies.

- A methodology for noise reduction in well images with low computational cost, optimizing the analysis of geological structures present in the images, such as lithological layers, fractures, and pores.

- A model for fault identification in seismic data using Transformers approaches to abstract the heterogeneities presented by this type of data.

- A model for facies classification through convolutional models can improve the efficiency of identifying different facies in the reservoir. This is essential for understanding the distribution of different types of rocks and fluids in the reservoir. These contributions can have a significant impact on the field of reservoir characterization, providing improvements in accuracy, efficiency, and decision-making.

1.4   Research Questions

Our research was primarily guided by two main questions:

- How can computer vision and its techniques contribute across different stages of reservoir characterization, from data acquisition to final modeling?

- Which computational tools/techniques have been most relevant in the geological context that encompasses the reservoir characterization?

To address these questions, we have defined three practical applications, which were outlined in the objectives of this research, and some specific questions guide the investigation of these activities:

- What are the benefits associated with the use of Transformers in fault identification?

- How can convolutional models enhance facies classification?

- What is the impact of applying image processing techniques on improving the quality of noisy well images?

1.5 Publications

The following papers have been developed throughout the course of our research, listed in chronological order by publication year. Paper 1, published during the doctoral period, is an extension of the master's dissertation. Paper 2 is detailed in Chapter 4, Paper 3 in Chapter 6, and Paper 6 in Chapter 5. Paper 5 is discussed in Chapter 2, providing a literature review. The remaining two papers were co-authored and are not directly addressed in this thesis.

1. L.S. Bomfim, G.D. Avansi, A.C. Vidal, H. Pedrini. *A Computational Tool for Geometric Characterization of Pores and Fractures in Microtomography Rock Images.* Revista Brasileira de Cartografia, v. 75, pp. 1-18, 2023. Available on: `https://seer.ufu.br/index.php/revistabrasileiracartografia/article/view/68352/37161`.

2. L.S. Bomfim, H. Pedrini, A.C. Vidal. *A Combined Noisy Borehole Image Log Segmentation Method.* 30th International Conference on Systems, Signals and Image Processing (IWSSIP), pp. 1-5. IEEE, June 2023. Available on: `https://ieeexplore.ieee.org/stamp/stamp.jsp?tp=&arnumber=10180269`.

3. L.S. Bomfim, O.R. Cunha, M.C.K. Kuroda, A.C. Vidal, H. Pedrini. *Transformer Model for Fault Detection from Brazilian Pre-Salt Seismic Data.* Brazilian Conference on Intelligent Systems, pp. 3-17. Cham: Springer Nature Switzerland, September 2023.

4. M.V.T. Soares, L.S. Bomfim, A.C. Vidal, M.C.K. Avansi, O.R. Cunha, R.G.V. García, R.S.P Medeiros. *Pre-Salt Carbonate Cyclicity and Depositional Environment: NMR Petrophysics and Markov Cyclicity of Lacustrine Acoustic Facies (Santos Basin, Brazil).* Marine and Petroleum Geology, v. 157, p. 106494, 2023. Available on: `https://www.sciencedirect.com/science/article/pii/S0264817223004002`.

5. L.S. Bomfim, M.V.T. Soares, A.C. Vidal, H. Pedrini. *A Review on Computer Vision Techniques for Geological Reservoir Characterization Tasks*. Journal of Petroleum Science and Engineering (Submitted), 2024.

6. L.S. Bomfim, M.V.T. Soares, O.R. Cunha, R.G. Vasconez, M.C.K. Avansi, A.C. Vidal, H. Pedrini. *Seismic Facies Analysis in Reservoir Characterization: Deep Learning Approach for Robust Classification and Data Refinement*. IEEE Transactions on Geoscience and Remote Sensing (Submitted), 2024.

7. R.G.V. Garcia, S. Mohammadizadeh, M.C.K. Avansi, G. Basilici, L.S. Bomfim, O.R. Cunha, M.V.T. Soares, A.F. Mesquita, S.K. Mahjour, A.C. Vidal. *Geological Insights from Porosity Analysis for Sustainable Development of Santos Basin's Pre-Salt Carbonate Reservoir*. Sustainability, v. 16, n. 13, p. 5730, 2024. Available on: `https://www.mdpi.com/2071-1050/16/13/5730`.

1.6   Text Organization

In this chapter, we provide the context for the main problem addressed in this work: the use of computer vision in reservoir characterization. The remaining text is structured as follows. In Chapter 2, we present an extensive literature review on our theme. In Chapter 3, we introduce the datasets and metrics. In the subsequent three chapters, we introduce three practical applications developed to enhance the workflow of reservoir characterization based on Papers 2, 3, and 6 from the previous section. The detailed chapters that follow are presented in order of increasing complexity of the methodologies employed. Chapter 4 describes the proposed methodology for enhancing the quality of noisy well images. Chapter 5 details the work on facies classification in seismic data. Chapter 6 outlines the work on fault identification using Transformers. Finally, we present our concluding remarks in Chapter 7.

Chapter 2

Fundamentals

This chapter serves as the theoretical foundation for the central theme of this research, presenting the concepts and framework of the related literature. It covers the main tasks involved in the characterization of geological reservoirs, the various types of data associated with this activity, as well as the widely employed techniques of computer vision and the tools used in this context. This exploration of the fundamentals is essential for a comprehensive understanding of the methodologies and approaches adopted throughout this study, providing a broad overview of the key elements that shape the characterization of geological reservoirs.

2.1 Geological Tasks

By collecting articles, it was possible to identify topics that have demanded great attention from the academic community on addressing the geological features that characterize the heterogeneities of reservoir rocks. These topics encompass the study of rock structures (for example, pores, matrix, faults, fractures) that make up the reservoirs, parameters that guide the evaluation of the reservoir's properties and activities that control the oil and gas exploration work.

In the search for characterization and understanding of reservoirs, one of the main activities is the analysis of their pore spaces. In this environment, the pore spaces are classified as primary porosity (i.e., rock's original pore structure) and secondary porosity (i.e., faults, fractures, vugs, and caverns) that originate from post-depositional processes (*sensu* [38]). Therefore, understanding the rocks' total porosity volume, their geometry, degree of connection and spatial distribution is crucial not only for identifying their formative geological environment, but also to evaluate the storage and flow capacity of the reservoir. In addition, it facilitates critical processes in the context of water and resources, including recovery of spilled hydrocarbons, enhanced oil recovery, and geological carbon sequestration [244].

As a result, research has shown great interest in the quantitative characterization of this porous space and its complex geometry in different types of unconventional reservoirs, such as coal [79, 98, 255] and shale [55, 77, 100, 256].

Providing the accumulation and migration of hydrocarbons, the faults and fractures

may act as pathways or barriers to the fluid flow estimation since they influence the rock's original properties of porosity and permeability [133]. In carbonate reservoirs, for example, pore spaces may either increase in volume and connectivity (via dissolution and natural fracturing) as well as decrease in porosity and permeability (via pore occlusion through cementation) during post-depositional processes [119]. Therefore, the tasks of detecting or extracting faults and fractures have received continuous attention over time, both due to their importance and the challenge encountered in generalizing the environment in which they are found.

To interpret faults and fractures, several deep learning models are applied. In the literature analyzed several works seeks to provide the use of new methodologies, starting from techniques with Gaussian beams [168] to the use of convolutional networks [52, 165, 191, 243] and adaptive segmentation methods [133] for fault detection proposals. Furthermore, other works seek to provide a characterization of the fracture structure using image processing [12, 79, 164], analyze the behavior of fractures and its implication in the parameters of the reservoirs [59], model their distribution in reservoirs [184] and to highlight fault images [234].

The structures that enable reservoir flow are just one part of the complete picture. The analysis of lithological formation and the distribution of sedimentary facies also play a crucial role in the characterization of reservoirs, as lithology represents the reservoirs' petrophysical characteristics [28] and the facies provide fundamental insights about the formation evaluation to identify and characterize suitable reservoir zones for exploration [138].

Predicting lithology according [250] is the fundamental process, since the properties of the rocks affect the response of every tool used to measure formation properties. For this, deep learning methods have been the main tool for an accurate response in the prediction and classification of lithology, whether using well logs data [246], seismic [248], the combination of both (seismic and well) [250], or even drilling string vibration data [33]. The use of facies has been presented in different approaches. The methodologies analyzed present the use of (i) wavelet transform-based [14] and multiple point geostatistical simulation [81] for facies mapping, (ii) generative models of facies modeling to consider more realistic reservoir models [30, 247] and to generate reliable models with prior geological knowledge [88], (iii) Bayesian deep learning models for classifying complex geological facies through uncertainty quantification [86], and (iv) image processing to analyze reservoir microfacies [236].

When analyzing parameters, one of the most important is permeability, which evaluates the physical properties of the reservoir and its quality [54]. According to Tang et al. [208], permeability analysis plays an important role since it measures the ability of rocks to transmit fluid. This important parameter is generally modeled in laboratory simulations using Darcy's Law [41]. However, due to the difficulties encountered in this process, such as the destruction of the sample and the time spent on the task, alternative methods have been used in estimation of this parameter. Studies show how an optimized tool, for example, the use of convolutional networks fed by rock sample images [208, 209, 264] and the use of Bayesian deep networks using borehole image logs [20] to predict the permeability. Furthermore, research also investigates the association of factors that provide favorable permeability conditions, such as fault zones and fracture networks [72, 218] and

pore tortuosity [54].

Another important activity that involves the reservoir exploration process is monitoring Carbon Capture, Utilization and Storage (CCUS) of carbon dioxide [192] in order to prevent the leakage of this substance into the atmosphere. This process is extremely beneficial to mitigate climate change and, besides that, according to Bryant [27], CO_2 is responsible for more than 64% of the enhanced greenhouse effect. Regarding the use of CO_2 in the exploration process, the analyzed works seek to understand the sandstone fracturing process by supercritical CO_2 [245] and also promote measurements of the CO_2-water-rock system [220] relationship.

Regarding the process of monitoring and carbon sequestration in order to reduce damage to the environment, research focuses on promoting tools to detect CO_2 plumes in overlying aquifers [235, 257] and in the subsurface carbon storage reservoir [73], monitoring CO_2 geological migration and sequestration through the interpretation of 4D seismic [121, 192], and vertical seismic profiling data [109].

In conclusion, the characterization and understanding of reservoirs are crucial, involving the analysis of porous spaces, fractures, faults, and the distribution of sedimentary facies. The primary and secondary porosity of rocks prove to be key elements in assessing the storage and flow capacity of reservoirs, and the faults and fractures show a significantly influence the permeability and porosity of rocks, acting as pathways or barriers to fluid flow.

In terms of lithology, facies are essential for identifying and characterizing suitable exploration zones. Advanced methods such as convolutional neural networks and image processing are widely used for the detection and characterization of all these tasks, being widely used for the detection and characterization of different features. These technologies provide significant benefits, including improved accuracy, efficiency, and the ability to handle large and complex datasets. A summary of these key points and methodologies is provided in Table 2.1.

Table 2.1: Summary of the main geological tasks.

Topic	Main Activities	Methodologies Used
Porous Spaces	Analysis of primary and secondary porosity	Geometric quantification, connectivity studies
Faults and Fractures	Detection and characterization of faults and fractures	Convolutional neural networks, Gaussian beams, image processing
Lithology and Facies	Lithology prediction and facies mapping	Deep learning with well log and seismic data
Permeability	Permeability estimation	Bayesian neural networks, laboratory simulations
CO_2 Monitoring	Monitoring and storage of CO_2	4D seismic interpretation, seismic profiling

2.2 Data Types

In the field of geology, there are different types of data acquisition that make it possible to understand reservoirs and build geological models from different perspectives. This data, as presented by [85], is found on multiple scales, where each one provides a different abstraction through its particles, texture, lithology, etc. On a micro-scale (< mm) the textural and mineralogical characteristics of rock grains, the geometry and arrangement of pores and the behavior of fluids can be analyzed through the various physical phenomena that permeate them. In a laboratory environment, the meso-scale (< m) allows contact with representative samples of rocks, in addition to enabling the determination of thermo- and petrophysical properties of different lithotypes. In a larger context, the macro-scale (> km) makes it possible to study different facies patterns and structural elements.

During the literature research, it was possible to find several data that permeate the different scales discussed previously. Table 2.2 presents a summary of these highlighted methods and shows their main characteristics and applications, providing a comprehensive overview of the available tools. By understanding the capabilities and limitations of each technique, professionals can make more informed decisions about which methods are best suited for their specific geological analysis needs. Therefore, in this section, we present each of these techniques and their particularities.

2.2.1 Rock Thin Sections

Rock thin-section is an important evaluation means of oil and gas exploration and development. The traditional method of thin-section identification relies on experts visually observing rocks through an optical microscope and its application aids in identifying the petrographic characteristics of reservoirs and understanding the pore space structure [126]. However, analysis in digital media allows an even more accurate understanding of its composition, bringing the possibility of a complete description of flow properties, texture and micromorphology [110].

As discussed by Berg et al. [16], it was more common to analyze the digital rocks physics to reconstruct 3D structures from 2D electron microscopy images than to use 3D X-ray tomography images directly due to the access to the structure and quality of the X-ray acquisition. Nevertheless, with the advance of technology and the increase in the quality and availability of this tool, its use is more frequent. However, there are situations in which the other acquisition methods can be preferentially used.

The methods commonly employed for generating image rocks through thin sections are described in the following subsections.

SEM Images

The scanning electron microscope (SEM) has the ability to magnify micro- to nanometric features or objects otherwise unresolvable to the human sight. The images resulting from this technique are obtained by scanning a beam of high-energy electrons on the surface of the sample (e.g., cores, sidewall cores and cutting samples), where, due to their shorter wavelength, the electrons highlight more subtle characteristics and details of the

Table 2.2: Summary of the data types and their applications.

Method	Scale	Main Characteristics	Main Applications
SEM Images	Nano to Micro	- Magnification of micro to nanometric features - Analysis of rock structure and mineralogy at the nanoscale	- Study of the structure of porous rocks - Analysis of fluid flow properties and rock-fluid interactions
Optical Microscopy	Micro	- Visualization of microstructures - Identification and quantification of mineralogy - Analysis of the morphology of grains and pore spaces	- Identification of mineralogy in thin sections of rocks - Study of pore distribution and connectivity
X-ray Images	Micro to Macro	- Three-dimensional visualization of samples - Analysis of the geometry and texture of particles and pores	- Study of rock characteristics in microscopic details - Estimation of permeability and fracture
Borehole Images	Macro	- High-resolution images of borehole walls - Measurement of electrical resistivity or acoustic impedance	- Provide insights into the features present in the formations surrounding the borehole - Description and characterization of modern reservoirs
Seismic Data	Macro to Giga	- Data generation through reflection/refraction of seismic waves - Identification of structures and geological mapping	- Exploration of oil and gas reservoirs - Mapping of geological horizons and structural characteristics

materials, to a much greater extent when compared to the optical light in microscopes. With the current technological capacity provided by a modern SEM, an image can outline characteristics smaller than 1nm in size. Consequently, its utility is focused on material characterization, delivering insights regarding their structure, surface morphology and composition, thus enabling the analysis of material properties [211].

Another type of SEM, commonly used in the geological context, is field emission scanning electron microscopy (FESEM). Compared to the traditional method, FESEM yields clearer, less electrostatically distorted images with spatial resolution down to 1 1/2 nm—three to six times enhanced [136]. Its use is made primarily employed when SEM characterization of a specific sample fails to provide a clear or satisfactory morphology due to its superior resolution [153].

In the literature, the use of these tools is mostly linked to the analysis of porous

medium [97, 100, 155, 255, 256] due to the ability to study their rock structure and mineralogy on a nanoscale and also provide inferences fluid flow properties and rock-fluid interactions [54]. Furthermore, the use of deep learning also makes it possible to segment and extract information from images coming from SEM [19, 35, 71, 230, 244] further improving the results already achieved due to its accuracy and automation.

Optical Microscopy

Optical microscopy is a material characterization tool that allows to visualize microstructures [151] and seeks to: (i) identify and quantify mineral assemblages, (ii) estimate the size and morphology of grains, and (iii) quantify pore spaces, their morphology, distribution and degree of connectivity [67]. Some of these characteristics are visible at a macroscopic level, however, the use of a petrographic microscope, also known as a polarizing microscope, is typically common, where the technique is called transmitted light microscopy or polarized light microscopy (PLM) [162].

According to Cady [29], the petrographic microscope technique differs in two ways from the basic or biological microscope: (i) it incorporates devices for polarizing light, one below the condenser and one above the objective; and (ii) it features a rotating stage, graduated in degrees, for measuring angles. The choice to use a petrographic microscope is motivated by the simple process of creating thin sections from a rock sample (e.g., conventional core and sidewall core) and the examination when compared to other analytical methods, such as X-ray diffraction analysis or scanning electron microscopy. Thus, the focus of optical mineralogy is directed towards analyzing the interaction of materials with light in thin sections, where each identified mineral has unique optics that will allow its characterization [177].

Numerous applications utilizing thin-section petrographic images have been investigated. Image processing techniques have served as a valuable tool for analyzing the information conveyed in these images, including the generation of data for characterizing fluids through fractal models [179]. Moreover, their application extends to deep and machine learning endeavors, as a pre-processing step, given the range of resolution provided by microscopy acquisition, where recent efforts have explored the utilization of artificial intelligence-based techniques for the segmentation and classification of mineralogy in thin sections, as evidenced by studies [126, 129, 144, 177, 186, 207, 236, 242].

X-ray Images

X-ray computed tomography (CT) is an image acquisition technology that enables the study of several important materials in geological characterization work. Its success and wide application is mainly due to its rapid image acquisition process. Furthermore, it also offers an internal view of the analyzed object without causing any damage. The CT enables three-dimensional visualization through the generation of images that depict the changes in X-ray attenuation within objects, which closely correlates with changes in density [104].

As discussed by Ketcham and Carlson [104], the CT scanners can be generally grouped into four categories, based on their spatial resolution and the size of objects, that are:

1. Conventional type, with observation scale of meters and resolution of millimeters.

2. High-resolution type, with observation scale of decimeters and resolution of 100 micrometers.

3. Ultra-high-resolution type, with an observation scale of centimeters and a resolution of 10 micrometers.

4. Microtomography type, with observation scale of millimeters and resolution of 1 micrometer.

Each of these categories allows, for instance, the examination of distinct attributes of the material being analyzed. In the literature, it is possible to find several demonstrations of the usability of these classes. This acquisition method made it possible to begin internal and non-destructive analysis of the rocks using the conventional method [94, 122, 125, 200] and high resolution [201]. However, with the evolution and popularization of technology, it was then possible to undertake an analysis in high detail, promoted by Micro-CT, of a range of characteristics present in these rocks, such as: (i) the geometry and textures of particles and pores [56, 57, 139, 180, 198, 249], (ii) contact angle between surfaces and fluids [220], (iii) fractures and microfractures [59, 72, 218], and (iv) permeability estimation [209].

Therefore, to acquire these images, three elements are generally required: an X-ray source, the object to be imaged and a series of detectors that measure the extent to which the X-ray signal has been attenuated by the object [104]. The difference between conventional CT and micro-CT data acquisition is in the rotational movement. In the case of conventional CT, the object remains stationary while the system rotates around it, as most X-ray CT studies of geological materials are carried out using medical scanners of different generations [137]. In the case of micro-CT systems, the object under investigation is rotated, allowing for better mechanical stability which is required at high resolutions [39]. By these processes, two-dimensional images called slices are created corresponding to the view of the object throughout the scanning process.

2.2.2   Borehole Image Logs

Wirelogging data are a crucial type of reservoir data obtained through the deployment of various imaging tools, enabling the characterization of the physical properties (such as electrical resistivity or acoustic impedance) of a borehole throughout its depth. Specifically, borehole images are a special category of wirelog data, as they capture multidimensional distributions of these properties [115, 212]. Their use plays a central role in the description and characterization of modern reservoirs, upon which successful exploration and production strategies depend [166].

As explained by [68], in generating images that represent resistivity-based properties, specialized tools directly measure the formation's micro-conductivity using an array of resistivity buttons mounted on pads that are pressed against the borehole wall. These tools typically provide the highest-resolution borehole images in conductive (water-based) muds. Notable examples include the Schlumberger Formation MicroScanner (FMS) and

Fullbore Formation MicroImager (FMI). On the other hand, the generation of images using acoustic tools involves sending sound pulses into the formation and measuring both the amplitude and travel time of the returning signals. This method is more successful in resistive (oil-based) muds, where electrical conductivity is poor. A prominent example of this technology is the Schlumberger Ultrasonic Borehole Imager (UBI).

Some of the primary applications for borehole imaging derived from their inherent ability to provide detailed insights into the features present in the formations surrounding the borehole. As analyzed by [167], these applications can be categorized as follows: (1) fracture identification and evaluation (both natural and induced through drilling or formation stimulation), (2) diagnosing completion and production problems, (3) analysis of sedimentology, bedforms, and depositional structures, (4) net pay counts in thinly bedded formations, and (5) identification of wellbore faults such as borehole breakouts, tensile wall cracks, and shear surfaces.

Therefore, image analysis techniques are employed for both the qualitative recognition and quantitative extraction of various of these geological features [167]. The reviewed literature demonstrates the active presence and effectiveness of computational tools in tasks that utilize the BHI, such as: the estimation of uncertainty quantification for permeability and porosity [20], the detection of gravels using semantic segmentation techniques for improved characterization of glutenite reservoirs [101], lithology identification through the extraction of multi-scale feature information [190], the classification of facies in carbonate rocks [239], and the prediction of geological features such as induced fractures, natural fractures, and sedimentary surfaces [80].

2.2.3 Seismic Data

Seismic method is by far the most widely applied method in exploration of oil and gas deposits [6]. This type of data provides support for several activities that involve the characterization of reservoirs and, its methodology, according to [237], permeates three main applications: (i) engineering seismology, for engineering studies to explore features within a depth up to 1 km, (ii) exploration seismology, to explore oil and gas fields up to 10 km deep, and (iii) earthquake seismology, to investigate earth crustal structure within a depth of up to 100 km. Furthermore, the interpretations carried out on seismic data allow the identification of morphological (e.g., shelf, slope, mound, slump, etc.) and structural features (e.g., faults) as also mapping geological horizons [216].

The seismic data is generated through the time course of reflection (or refraction) of seismic waves produced by a mechanical energy source that are emitted through a surface. In the case of the exploration of oil and gas, this acquisition can be carried out by different ways from continental to shore, shallow marine and marine environments. According to [145], the wave generation process is generally formed by putting a source of impulse such as dynamite, air-gun or vibrator that sends acoustic energy into the Earth. Thus, sensors or geophones placed on the surface are capable of capturing the reflected acoustic energy, converting it into an electrical signal that is displayed as a trace seismic signal.

In the specific case of maritime acquisition, the acquisition environment contains the

main tool large ships with air-guns that are located behind this vessel. In this way, the seismic signal is formed by forcing highly pressurized air into the water at a given interval. Marine receivers with piezoelectric hydrophones, also located on the back of the ship and streamers, capture information about the change in pressure in the water. For this acquisition, the vessels follow predetermined patterns of parallel circuits.

In terrestrial acquisition, geophones can be organized in different ways and unlike marine acquisition, the seismic line will rarely be in a straight line. This type of acquisition becomes more complicated due to the nature of the terrestrial environment which contains, in most cases, natural and artificial structures (e.g., lakes, buildings, roads and irregular soil). Thus, as described by Mondol [145], groups of geophones tend to be grouped on a line with shot points at the end or in the middle of the receiver array and to capture the generated waves the shot points are gradually moved along a line of geophones.

After the acquisition process, the processing stage aims to transform the acquired seismic data into a representation of the geology, for which geometric corrections are usually made to generate data consistent with the source reference system. The main objective in this processing stage is to enhance the signal and suppress the coherent and non-coherent noises and multiples. To deal with it, numerical analysis (such as Fourier Analysis, Convolution and Deconvolution, Equalization, Correlation functions) are applied to the input seismic traces [6].

With the seismic data processed and containing information regarding the amplitude of the signal initially propagated, it is also possible to compute attributes that highlight characteristics of the seismic signal. With this it is possible to more easily identify structures as geological layers, faults, caves, horizons, etc. These attributes can be computed by a mathematical manipulation of the original seismic and evaluate the shape or other characteristic of one or more seismic traces and their correlation at specific time intervals [8].

However, it is also important to point out that the processing of seismic data for the most part also depends on the quality of the environment in which the data were acquired. Characteristics of the surface analyzed in this way such as the environment, weather conditions and demographic restrictions have a significant impact on field data quality, this is because these conditions interfere with the generating energy that penetrates into the surface and also during data recording [237]. Likewise, ultradeep reservoirs in the Brazilian pre-salt reservoirs illustrate how the subsurface environment may also decrease the quality of seismic images due to distortion and attenuation on the seismic waves path when crossing thick (i.e., 2 km) and highly-deformed salt layers [146].

2.3   Computer Vision Techniques

Several computer vision techniques are applied to characterize reservoirs, and through a literature review, the type of operations found can be divided into two groups: those based on image processing and those based on deep learning. These methods currently work together, presenting a mutualistic relationship, where deep learning models mostly require pre-processing steps involving traditional image processing techniques, and these

techniques are increasingly adding artificial intelligence concepts to improve the resolution of users' proposals.

As a tool to identify and understand the use of these techniques, we use the word cloud approach that produces a visual representation of a set of words, presenting different sizes according to their frequency or importance [46]. As shown in Figure 2.1, a word cloud was generated with the computer vision methods and targets, used in selected articles for each of the last 10 years. Through it, it was possible to perceive the transition from a purely problem-solving approach through image processing techniques, to 2018, with the beginning of the popularity of neural networks, where deep learning techniques also became a target for the characterization of reservoirs. Therefore, in this section, the main approaches of both groups and their relationship in the geological analysis workflow will be described.

Figure 2.1: Word cloud of computer vision methods and target research areas from the last ten years of selected literature.

2.3.1 Image Processing

As described by Gonzalez and Woods [74], the utilization of image processing methods comes from two main areas of application: Improvement of visual elements for human interpretation and processing of image data for storage, transmission, and representation. Within these areas of application, processes may exist that range from low-level activities involving primitive operations such as pre-processing for noise reduction, surpassing more complex activities such as segmentation and classification of objects, up to high-level activities involving the process of assigning meaning to the elements identified in these images. Thus, in this section, we address which of these tasks are commonly identified in reservoir characterization and how their application process occurs.

Image Denoising

As previously presented, the reservoir characterization process includes the manipulation of different types of images that are acquired by different sensors. During this acquisition

process, it is very common for data to be contaminated with noise, whether due to the quality of the equipment, a problem with the data being analyzed or even interference from the environment in which the data was acquired. Furthermore, noise can be introduced due to transmission errors and compression. Consequently, denoising frequently becomes a crucial step to be taken before the images data is analyzed and compensate any data corruption [147].

It was possible to notice the prominent presence of three main algorithms for this task: (i) the median filter, (ii) the mean filter and (iii) Gaussian smoothing. These filters act locally, as they are restricted to a spatial distance, and makes use of low pass filtering on pixel groups with the statement that the noise occupies a higher region of the frequency spectrum [60]. Therefore, its application differs due to the operation carried out in these filters, the Gaussian filter and the mean filter have linear approaches, while the median filter operates in a non-linear way.

The linear filtering is based on linear combinations of input values, while non-linear filtering allows for more complex and adaptable operations, often being preferable in situations where specific features of the information need to be preserved. The median filter, for example, is a case of a non-linear filter. The medial pixel value among all the neighbors in a window are generally used to reduce noise in an image, preserving the smoothness in the resulting image [23]. On the other hand, the mean filter acts linearly, smoothing the pixels with a weighted average of the neighbors with the specified parameters. For this set of neighbor pixels, the new spatial center is calculated and it will serve as the center for the next iteration until the values stop changing or the maximum number of iterations is achieved.

In the same class, the linear one, the Gaussian filter can be consider as a non-uniform low-pass filter that preserves low spatial frequency and reduces image noise and unnecessary details in an image. The Gaussian function assigns higher weights to the pixels closest to the center pixel, gradually decreasing the weights as the distance increases. This is commonly achieved through the convolution of an image with a Gaussian kernel. The 2D form of this Gaussian kernel is expressed as:

$$G_{\text{2D}}(x, y, \sigma) = \frac{1}{2\pi\sigma^2} e^{-\frac{x^2 + y^2}{2\sigma^2}} \tag{2.1}$$

where σ is the standard deviation of the distribution and x and y are the locations indices and controls the variance around a mean value of the Gaussian distribution, which influences the degree of blurring around a pixel [230].

Image Segmentation

Image segmentation is one of the preponderant tasks in the area of visual computing given its relevance in feature extraction, object localization and image classification. In the specific context of reservoir characterization, its use is highly linked to work on identifying and extracting regions of interest in rock images (e.g., pore spaces, fractures and seismic data (e.g., seismic facies, faults, fractures, caverns) [19, 35, 52, 86, 132, 133, 186, 207, 220]. This information, when extracted, plays a significant role in analyzing the data present

in the images, providing insights into rock mineralogy, porosity, permeability, fluid flow, location and geometry of pores and fractures.

A great variety of segmentation algorithms have been developed in the last few decades and this number continually increases each year [254]. Their approaches can be divided into three main groups: (i) those based on the principle of similarity, which groups image pixels based on a common property, (ii) those based on the principle of discontinuity, which extracts regions that differ, in properties such as intensity, color, texture or other statistics [113] and (iii) the neural network based, that combine both approaches. Among these categories, the technique that stands out in the group of similarity between the works evaluated are thresholding methods. This method is one of the most used for image segmentation and is useful in discriminating between foreground and background by the selection of a suitable T (threshold) value. The gray tones in an image can be converted to binary values, where the choice of T can be made by manually, choosing an arbitrary value, or by analyzing the histogram of the image to be segmented. In the case of histogram analysis, the ideal case is presented when there is a bimodal distribution of the data and the T value can be defined as the valley point between the two regions, however in more complex regions other image characteristics can be taken into account [3].

In discontinuity-based techniques, we have methodologies based on edges and contours that identify discontinuities in the image and highlight abrupt transitions in intensity, color or texture. There are three different types of discontinuities in the grey level: point, lines and edges. In these cases, spatial masks can be used to detect all the three types of discontinuities in an image. They are based on 1st order derivative operations (Prewitt operator, Sobel operator, Test operator) and second-order derivative operations (e.g., Laplacian operator, zero-crossings) [181]. Another method in this category is the watershed segmentation; this technique is based on a "flooding" and segments an image into regions that can be interpreted as "height fields" and "landscapes". As discussed by Szeliski [204] computing such regions involves initiating a flooding process across all local minimum in the landscape and marking ridges wherever differently evolving components meet, which are points of higher intensity or gradient where different components of the image meet. This results in a partitioning of the image into distinct areas based on the intensity or gradient characteristics, with watershed lines marking the boundaries between these regions.

Finally, we have neural networks that, with their emergence, made it possible to build complex models for segmenting images that have a deviation from the normal situation, also reducing the requirements of expert intervention during the image segmentation process [113]. In this methodology, features are initially extracted from images and then the image is segmented based on this features.

Data Augmentation

The use of data augmentation is quite common as a data pre-processing step for machine learning models. This constantly occurs due to insufficient data or cases of sample imbalance. The first case mainly becomes common in the geological study of reservoirs due to privacy concerns of the oil and gas industries that acquire this information. The second

case is directly related to the population of the datasets, where a sample and/or group that will be extracted or classified has less representation.

In both cases, the majority of transformations applied are geometric, following by color transformations and based on Generative Adversarial Networks (GANs) [75]. In geometric transformations, affine operations are applied to manipulate the input data. Thus, for each image, its duplication is generated through operations such as flipping, distortion, zoom in/out, shift, or shading with a hue [161]. However, in geometric operations, it is necessary to analyze the characteristic of the data to avoid applying an operation that creates an erroneous representation of the information. This is particularly crucial in seismic images where the orientation of the image is of paramount importance for its conceptualization.

Given that seismic images are always interpreted horizontally, any operation that distorts this characteristic, such as rotation or horizontal flipping, will introduce errors into the model's learning. Therefore, in this specific case, it is common to use only the vertical flipping operation. In color space transformation, simple operations involving the R, G, B channels can be applied to enhance the images. For example, an image can quickly be converted into a representation of a single color channel by isolating one color channel and nullifying the content of the others. Additionally, RGB values can be manipulated through matrix operations that can increase or decrease the brightness of an image. In the case of more complex operations, the image histogram can be assessed and altered to produce transformations with variations in brightness [194].

With the GANs, the strategy is creating synthetic images, enabling the expansion and enhancement of datasets through artificial instances. These instances are generated based on original data, with features extracted to serve as a foundation for generating new images [75]. This approach allows for enriching and diversifying datasets, promoting greater robustness and variety in analyses and model training. In addition to these methods, the literature also presents more sophisticated data augmentation applications, which use traditional techniques (such as those mentioned above) with more advanced ones (CutOut and CutMix). Koeshidayatullah [111], for example, applied this combination to deal with class imbalance in its database. The developed workflow applied methods such as flip, zoom and add Gaussian blur and also the CutOut method, where black squares are added to the images, and CutMix, where the input image of a given class is superimposed with a small image of a different class. Thus, the association of these methods improves the model's robustness against input corruption and its out-of-distribution detection performances.

Geometry Analysis

The use of visual computing is present through the application of image processing techniques for the geometric characterization of two important structures: pores and fractures. These structures, as previously discussed, are of utmost importance in defining reservoir modeling. Thus, quantifying their presence in this environment has proven to be a fundamental task in the study of reservoirs, which involves several steps, including the imaging techniques already described previously.

To carry out this analysis of geometry, researchers use different approaches and tools. In the work developed by Wu et al. [231], the effect of micropore geometry on pore systems was discussed, where through image processing, parameters such as the pore radius, throat (i.e., small interpores linkage) and shape were measured to also create a pore network model.

Jia et al. [98] sought in their work to analyze different aspects of the pore structure through SEM images using MATLAB programs; for this, these images were binarized through an adaptive threshold and through language functions, such as "label", "region-props" and "bwlabel", the pores are identified and divided into units that will be measured. With information about the distribution of pixels in each unit relative to the pores and functions such as "area" and "sum", the measurements of porosity, radius, pore-throat radius, the pore network and the location are calculated.

Similar characteristics were previously studied by Jiao et al. [100]. However, the analysis carried out on the nanopores was guided by the use of the PCAS software (Pores (Particles) and Cracks Analysis System) in FESEM image, in which a threshold was defined for the segmentation of the images and various geometric parameters of the pores including their perimeter, area, length, width, and form factor, as well as statistical parameters of the pore system, including probability entropy and fractal dimension were also measured.

In the work described by Pal et al. [155], the main tool used was ImageJ; through it, FESEM images are smoothed and segmented by the Otsu threshold and only then can porosity and permeability be calculated through well-defined pore structures based on characteristic length, constriction, and tortuosity, measurements that are extracted through the skeletonization technique and the calculation of the Euclidean distance between extremes. Other approaches analyzed also make use of more than one tool, such as in [180], which in addition to using the Avizo software, also used the Python programming language. With this, filtering and segmentation (by the software) were applied so that, through Skeletonization, a distance map was calculated and the diameter of the pores was extracted (by Python). Using these image processing techniques to extract the morphology of these structures also allows machine learning models to be used to automate the classification of these structures.

In the work developed by Mollajan et al. [144], geological parameters (such as roundness, diameter, rectangularity, solidity, among others) were extracted from rock sections segmented images to feed a pore type classification model. This type of hybrid workflow, with image processing and machine learning model, was also proposed by Li et al. [122] for the classification of rock types through the extraction of some key characteristic parameters as area, perimeter, effective length, equivalent width, equivalent circle diameter, and azimuth. Finally, in research that seeks to purely analyze faults and fractures, it is possible to note the importance of quantitative characterization of the fractal dimension of a rock fracture network system [12, 79, 164]. In these works, techniques such as Canny edge detection, box- counting methodology and segmentation tools guide the main task of its extraction so that its dimensions are calculated.

2.3.2 Deep Learning

With the advance of technology and the increase in the complexity of problems presented in the field of visual computing, the use of deep learning has been applied as a powerful tool to deal with tasks involving segmentation, classification and image generation. This technological tool known as Deep Learning (DL) acts as a subset of machine learning characterized by a series of operations that systematically extract complex features by utilizing the results of previous operations as input [76], and its principals keys components are the training set, network architectures and the parameter optimization.

Over time, the DL use have increasingly been applied in geological analysis applications, primarily in tasks for reservoir characterization that require a powerful ability to extract deep features and manipulate complex data. In this section, it will be presented in details the mostly used deep learning architectures resulting from the literature research, namely (i) Convolutional Neural Networks and the deep generative models, more specifically, (ii) the Generative Adversarial Networks.

Convolutional Neural Networks

The Convolutional Neural Networks (CNNs) have proven to be one of the most famous and powerful deep neural networks, especially in the field of image data linked to challenges encountered in the field of computer vision. The input data for this model usually has a matrix format and can be presented as time-series data (1D data), grayscale images (as the rock thin sections), color images (three-channel data with 2D inputs), and multidimensional time-varying data (as 3D seismic data) [206].

The CNN takes this name based on the mathematical linear operations between matrices, namely convolution [4] and, it is composed of three types of layers: (i) convolutional layers, (ii) pooling layers, and (iii) fully connected layers, where each one has a different objective.

In the convolutional layers, the CNN uses the concept of kernels, which is a matrix used in the convolution operation. The kernel is always smaller in size than the image and has values that are learned during network training. Its application to an image acts as filtering, which seeks to extract information such as edges, textures or more complex patterns. The convolution operation is constituted by the multiplication of the kernel by the elements of the same position that overlap in the image (input), where the result of the multiplication is added in order to produce a single value in an output image (also known as a feature map). Generally in convolutional layers there is more than one filter, and each of them traverses the image based on a stride that controls the distance between the path of its application, and generates a series of feature maps. In this process there is also a need to pay attention to the information present at the edges of the images, for this, another parameter used is the padding, which when used adds a border of zeros in order to control the spatial size of the output. At the end, an activation function performs the nonlinear transformation to extract this features.

In the pooling layers, the main objective is to reduce the spatial dimension of the input volume in order to extract key features for the next convolutional layer. This process is known as downsampling and can be applied through operations such as max pooling,

that reports the maximum output within a rectangular neighborhood or average pooling, that calculates the average of this neighborhood. Thus, this layer seeks to make the representation invariant to small translations in the input and be able to preserve the locality of a feature [76].

At the end of the process, the fully-connected layers aim to understand and utilize the extracted high-level features. Neurons within a fully connected layer establish complete connections with all activations in the preceding layer where their activation can hence be computed with a matrix multiplication followed by a bias offset converting the 2D feature maps into a 1D feature vector to complete the reasoning tasks, such as regression or classification [206, 219].

When building a typical convolutional network architecture, the initial layers will mainly consist of convolution and pooling layers. At the output of a convolutional layer, an activation function such as sigmoid or hyperbolic tangent will be applied to introduce non-linearity to the data and adjust or limit the generated output. Subsequently, the fully connected layers will consolidate the extracted features for final decision making.

The network training process occurs through backpropagation, a technique that uses gradient descent to adjust the network weights present in the kernel. During training, the input data along with the corresponding desired outputs (labels) are fed to the network. The difference between the outputs predicted by the network and the actual outputs is calculated using a loss function. This error is then back-propagated through the network, adjusting the weights for a set number of epochs to minimize loss until the network reaches acceptable performance.

CNNs have played an important role in reservoir characterization, their applications mainly play a role in the segmentation and classification of geological structures. Table 2.3 summarizes the different convolutional networks, in addition to the conventional ones, identified in the analyzed state of the art. Through it, it is possible to perceive the wide variety of data types that feed different convolutional models used in reservoir characterization, as well as the diversity of tasks that can be solved through this type of network.

Generative Adversarial Networks

The Generative Adversarial Networks (GANs) [75] belongs to the class of generative models, in which through training data the main objective is to generate similar data. For this, GANs consist of two neural networks: one is the generator G, that has to learn to generate fake sample distributions, and the other is the discriminator D, that needs to learn how to distinguish the real and fake distribution generated by the Generator [43].

As explained by Wu et al. [226], G will capture the distribution of the input sample data, and an image will be generated using a noise z that obeys a certain distribution; The discriminative model D works estimating the probability of a sample which came from the training data rather than G, in the training process and this probability is used as the error metric to improve the generator capability. Over the epochs the generator and the discriminator tries to compete against each other in a process of optimization based on the minimax game problem, giving meaning to the term "adversarial", and its parameters

Table 2.3: CNN-based methods for reservoir characterization tasks and their approaches.

Models	Data Types	Objectives	References
Multiscale Convolutional Neural Network model (MsNet)	Simulated Images	- Predict the equivalent permeability	[264]
Super Resolution Convolutional Neural Network model (SR-CNN)	Seismic Data	- A method for fault enhancement	[243]
Continuous Wavelet Transforms CNN (CWT-CNN)	Seismic Data	- Seismic lithology prediction	[248]
3D Scattering Wavelet Transform Convolutional Neural Network (3-D SCWT)	Seismic Data	- Fault detection through SCWT multiscale and multidirection characteristics	[191]
PoreFlow-Net	3D Digital Rock Images	- Fluid flow predictions	[183]
AlexNet	SEM Images	- Characterizing clay textures	[71]
Active Attention Module (AAM U-Net)	Seismic Data	- Attention module based on the characteristics of seismic faults for faults detection	[52]
ConvNet	Laser Scanning Fluorescence Microscopy (LSFM)	- Automated characterization of pore-scale wettability	[244]
CNN Phys	3D digital rock images	- Predicting permeability	[208]
LGCNN	Micro-CT Images	- Reconstruction of the porous media	[249]
Theory-guided Convolutional Neural Network (TgCNN)	Permeability map	- Well placement optimization.	[221]
Spectral Decomposition via Inversion Strategies (ISD-CNN)	Seismic Data	- Calculate the probability distribution of occurrence of lithology/fluid	[250]
Mask R-CNN	Digital photos (Outcrops) and Rock Thin Sections	- Intelligent image recognition technology to study the microscopic remaining oil occurrence into four categories - Determination of pore space characteristics - Construct a particle segmentation model	[126, 222, 227]
U-Net	Rock Thin Sections, Seismic Data, GPR data, SEM Images	- Inversion of surface gravity data to predict 2-D high-resolution subsurface CO_2 distribution - Grain segmentation - CO_2 Interpretation From 4D Sleipner Seismic Images - Classify the rock types - Salt domes and faults identification - Mapping of karstified zones imaged through GPR surveys - Effective discrimination of clay aggregates mixed with matrix mineral particles and organic matter	[5, 35, 92, 121, 132, 207, 235]
CNNs	Rock Thin Sections, Seismic Data, Permeability map, X-ray Micro-CT	- Lithology classification models - Automatic classification of subsurface hydrocarbon regions from 2D seismic images - Carbonate petrography characterization - Determining the placement of an oil production well - Facies classification - Characterizing Paleokarst Collapse Features - Detect and classify intact and non-intact cores - Estimating the permeability of complex carbonate	[7, 112, 114, 157, 197, 209, 229]

will be updated by the back propagation process. At the end the generator must be able to generate realistic looking images while the Discriminator aims to continually improve its ability to distinguish between generated fake images and real ones [43].

Reservoir characterization work that involves the use of GANs is mostly linked to the generation of synthetic image datasets for model training. However, in Table 2.4, it is also possible to see the variety of models and simulations process that can be developed by the use of generative models.

Table 2.4: GAN-based methods for reservoir characterization tasks and their approaches.

Models	Objectives	References
Conditional Deep Convolutional Generative Neural Network (cDC-GAN)	- Predict the reservoir fluid distribution at any time by considering reservoir properties	[261]
Wasserstein GAN with Gradient Penalty (WGAN-GP)	- Seismic inverse modeling	[232]
Conditional Generative Adversarial Networks (CGAN)	- Simulate multiple geological models generating realizations that respect spatial observations	[88]
Generative Adversarial Network-based Geomodeling Simulation Approach (GANSim)	- Stochastic Conditional Geomodeling	[196]
Deep Convolutional Generative Adversarial Networks (DCGAN)	- Model regeneration scheme for reliable uncertainty quantification of channel reservoirs without conventional model inversion methods	[120]
Relativistic Average GANs (RAGANs)	- Enhance the resolution of thin sections images	[129]
Spatially Assembled GANs (SAGANs)	- Fast and scalable earth texture synthesis	[107]
U-Net GAN	- Create unconditional and conditional facies models.	[247]
Generative Adversarial Network based on a Single Image (SinGAN)	- Simulation of Complex Geological Architectures	[128]

2.4 Computational Tools

Several tools have been used to manipulate the different types of images involved in the reservoir characterization process, depending on the type of analysis carried out with the image or the computational domain. Three main tools were identified in the literature papers that are used in this domain: (i) Python programming language, (ii) Matlab, and (iii) ImageJ, which are briefly described as follows.

2.4.1 Python Programming Language

Python [214] is a high-level, open source, object-oriented language, with an extensive library of pre-built modules. Its user-friendly nature, and the growing of users community have contributed to its popularity and continuous improvement. Furthermore, Python has proven to be an excellent tool when it comes to massive data processing improved by the advent of machine and deep learning, forming part of several works identified in the literature.

There are many applications involving Python in terms of visual computing, ranging from modules that work in image processing to the implementation of deep learning models. Regarding the first field, image processing, one of the main modules used is the OpenCV library, which has powerful image manipulation capabilities. This library can help explore solutions to the needs presented through standardized data format that is interoperable with scientific libraries such as NumPy and SciPy [87]. Furthermore, its use can be linked to different types of functions, such as image processing, structure analysis, movement and object analysis, pattern recognition and camera calibration and 3D reconstruction.

In the field of artificial intelligence, Python scripts have increasingly enabled research to advance. This is mainly due to the development of Theano and then TensorFlow [1], two symbolic tensor manipulation frameworks that support autodifferentiation, greatly simplifying the process of implementing new models, and by the rise of libraries such as Keras [36] and PyTorch [158], that enables the straightforward construction of deep learning models [37].

2.4.2 Matlab

Matlab [135] is also a high-level language with control flow statements, functions, data structures, input/output, and object-oriented programming features. This language includes commands for 2D and 3D data visualization, image processing, animations and graphic presentations, in addition to having a vast collection of computational algorithms that implement everything from basic mathematics to complex arithmetic and transformed functions.

In the literature, it is possible to find its use mainly linked to the activity of characterizing geological structures such as pores and fractures, where its application involves the analysis of images to measure the geometry of such structures and provide mathematical analysis [98, 178, 255, 256], in addition, it also enables analyzes of the textures present in the images [71].

2.4.3 ImageJ

ImageJ [2] is a public domain Java image processing and analysis program that can read many image formats including TIFF, GIF, JPEG, BMP, DICOM, FITS and 'raw'. Its processing power and multi-threaded capacity allows the execution of a series of tasks with excellent performance, being able to support several application open simultaneously and perform time-consuming tasks in parallel with other operations. Through this tool, it

is possible to extract statistical analysis of pixels, measure distance and angles, create density graphs, apply geometric transformations (e.g., scaling, rotating and flipping), manipulate contrast, apply filters and several other image processing functions.

ImageJ exhibits numerous attributes that make it an outstanding tool for acquiring proficiency in computational techniques aimed at extracting information from images in the context of reservoir characterization. Its use can be seen in the works developed by Pal et al. [155], Ellamey and Attia [56], and Strzelecki et al. [198] that extract information through pixels, such as porosity from high-resolution images.

Chapter 3

Materials

This chapter provides an overview of the materials used in this study, including databases, evaluation metrics, and computational resources. Understanding these components is crucial for comprehending the methodologies and results presented in the following chapters.

3.1 Database

For the research development, our study area is located in the Santos Basin. In this region, six wells have been drilled, of which three are the focus of our research due to their formation and location. These wells are identified as X, Y, and Z. Extracted from this region, we have a seismic amplitude cube in depth with dimensions of $1480 \times 1080 \times 301$ pixels, with resolution of $12.5 \times 12.5 \times 5$ meters (inline/crossline/depth) representing an area of approximately 240 km^2.

For the creation of the datasets used in Chapters 6 and 5, two different seismic volumes representing the mapping of faults and facies were also generated. These volumes were modeled by geologists with expertise in classifying these geological structures. Thus, the models can be trained with reliable information, allowing for their refinement based on the results obtained from deep neural networks.
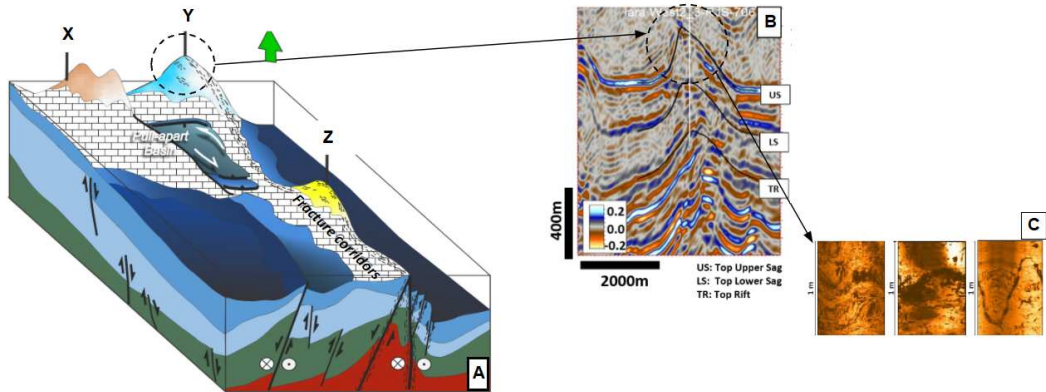

Figure 3.1: Illustration of the field at three different levels: (A) field representation, (B) seismic scale, and (C) well scale.

The borehole logs data provides detailed visual information of the well's interior and it has a scale corresponding to an area of 500 meters. The regions depicted in these images are also present in the seismic data, as evidenced in Figure 3.1, which illustrates the transition from the broader scale of the field to the more detailed scale of the well images.

3.2   Metrics

A poorly defined metric can lead to inaccurate conclusions, such as selecting suboptimal models when comparing the effectiveness of classifiers [70]. Therefore, we will describe two classes of metrics below that seek to provide a more precise evaluation of our results within their respective contexts.

3.2.1   Metrics Based on Classification

Since semantic segmentation can also be understood as pixel-wise classification, some metrics used in this task can also be applied in our context. These metrics focus on evaluating the prediction performance of positive samples, based on the concept of confusion matrix, which provides a representation to measure the effectiveness of the classification model by presenting the predictions made for each class. For example, in the application of identifying geological faults, positive samples indicate faults and their locations in a seismic volume [89].

Table 3.1: Structure of a confusion matrix.

		True Classes	
		Positive	Negative
Predicted Values	**Positive**	TP	FP
	Negative	FN	TN

An illustration of the confusion matrix structure is presented in Table 3.1. From it, we can describe the following metrics:

1. Precision: It can be defined as the ratio of true positives to the sum of true positives and false positives, analyzing among all positive classifications made by the model, how many are correct.

$$P = \frac{TP}{TP + FP} \tag{3.1}$$

2. Recall: Defined as the ratio of true positives to the sum of true positives and false negatives, analyzing among all situations of positive class as the expected value, how many are correct.

$$R = \frac{TP}{TP + FN} \tag{3.2}$$

3. Accuracy: Consists of the quantity of elements that were correctly predicted, positively or negatively, divided by the total number of samples. Accuracy aims to indicate how often the classifier is correct.

$$A = \frac{TP + TN}{Total} \tag{3.3}$$

4. F1 Score: Consists of the combination (harmonic mean) between precision and recall, which measures the effectiveness of the analysis when considering both precision and recall in a single metric.

$$F1 = 2 \cdot \left(\frac{P \cdot R}{P + R}\right) \tag{3.4}$$

3.2.2 Metrics Based on Semantic Segmentation

For a segmentation system to be useful and produce efficient contributions, its effectiveness must be rigorously evaluated. Thus, we selected two functions for evaluating semantic segmentation methods, which is the main task of our objectives.

1. The Intersection over Union (IoU) metric, also known as the Jaccard index [193], quantifies the percentage overlap between the input mask (i.e., the segmentation target) and the predicted output. It calculates a ratio by comparing the intersection and union of two sets (ground truth and prediction). This ratio can be expressed as the number of true positives (intersection) divided by the sum of true positives, false negatives, and false positives (union). In multi class problems the IoU is calculated individually for each class and then averaged across all classes.

$$IoU = \frac{TP}{TP + FP + FN} \tag{3.5}$$

2. Dice Coefficient: This metric is widely used in the computer vision community to calculate the similarity between two images A and B [40] and is very similar to IoU. Its value is calculated as twice the overlap area divided by the total number of pixels in both images.

$$Dice = \frac{2\,|A \cap B|}{|A| + |B|} \tag{3.6}$$

3.3 Computational Resources

For conducting this research, we utilized the Python programming language version 3. Python is widely adopted in the academic community and boasts numerous libraries that provide access to various resources. Therefore, we will describe the environment used for implementing and executing the research both with this language and additional resources.

3.3.1 Libraries

Among the libraries used in this work, we can divide their applications into four categories. For data manipulation, NumPy [152] is used for reading and mathematical manipulation of the data, while segyio [58] version 1.9.7 facilitates interaction with seismic data formatted in the SEG-Y standard. For image manipulation, the OpenCV library [24] (Open Source Computer Vision Library) version 2 is employed for object identification and manipulation in images, while Scikit-Image [213] is used for image pre-processing and segmentation.

For developing deep learning-based solutions, the TensorFlow package [1] version 2 is one of the main open-source libraries for developing and creating machine learning models. Another widely used library, in conjunction with TensorFlow, is Keras, an open-source neural network library written in Python and designed to enable rapid experimentation with deep neural networks [36]. Finally, for image visualization, the Matplotlib library [91] is primarily focused on displaying images and 2D graphics.

3.3.2 Equipment

The experiments in this work were conducted locally on a personal machine equipped with an AMD Ryzen Threadripper PRO 5975WX CPU (32 cores, 3600 MHz), an NVIDIA GeForce RTX 4090 graphics card, and the Windows 11 Pro operating system. Additionally, Google Colab Pro was utilized, a paid cloud service that enables the implementation of Python code via the browser using notebooks. Colab Pro provides access to two types of graphics processing units, T4 or P100, with 25GB of memory each.

Chapter 4

A Combined Noisy Borehole Image Log Segmentation Method

In this chapter, a methodology was developed for segmenting noisy well images [42]. This type of data are a valuable tool for studying and characterizing reservoirs. However, the quality of these images is often compromised by various types of noise due to the environment in which they are acquired. Additionally, extracting the relevant information from these images can be a challenging task, as the existing noise can impede data segmentation even after improvement. Therefore, we investigate the best combined strategy for enhancing these images using Equalization and Retinex methods, as well as segmenting them using threshold and quantization techniques to achieve better extraction of regions of interest.

4.1   Contextualization

Borehole image logs are widely used in the geological context to understand and characterize the reservoir environment in oil and gas wells [44, 117, 149, 187, 205, 241, 252, 265]. These images provide crucial data for extracting sedimentary and structural information in a millimeter scale, offering important insights into structural, fracture, and depositional features [21, 61, 116, 167].

Machine learning models and image processing algorithms can be applied to these images to assist in the characterization process of the attributes present in the logs [63, 64, 80, 95, 99, 189, 225, 240]. Obtaining good-quality and high-resolution images has become a crucial step in utilizing these resources in technology, as well as their segmentation to generate datasets and enable more detailed analysis of their geological components.

However, as these images are generated at the bottom of wells, several problems can occur in their acquisition process, such as the noise generated in the images due to obstacles in the operating environment and hardware restrictions that result in images with little contrast and color distortion. The loss of details makes it difficult to identify important attributes for a precise geological characterization.

To address this problem, efforts have been made to eliminate noise in these images using convolutional networks [124], contrast enhancement approaches [65], or defogging [50]

and super-resolution [170] algorithms. However, segmentation is also important for identifying geological structures, and conventional approaches may not provide a satisfactory result.

In this work, we aim to identify the best approach for enhancing and segmenting these images to extract information effectively. Based on the type of noise found in the images, we analyze the effectiveness of combining contrast and defogging enhancement with conventional image segmentation and quantization methods.

Our approach contributes to efficient segmentation of noised borehole log images, providing a more accurate evaluation of the pore geometry present in the log samples, as well as allowing for labeling of these images to apply to machine learning models.

4.2   Background

This section presents and discusses each step of the proposed borehole image log segmentation method.

4.2.1   Histogram Equalization

The purpose of an image histogram is to provide a graphical representation of the probability occurrences of intensity values versus their intensity levels in the image. Histogram equalization (HE) is a method used to equalize the probability distribution of intensity occurrence values in an image [159].

HE is one of the simplest and most widely used methods for enhancing contrast in images. There are two types of HE methods: global and local. The global method takes into account the overall appearance of the image, distributing the pixels over the entire dynamic intensity range by calculating a linear cumulative histogram of the original image and spreading the intensity values over its dynamic intensity range. The local method, on the other hand, considers the histogram intensity statistics of neighboring pixels [47].

However, HE can introduce undesirable visual artifacts and over-enhancement caused by large peaks in the histogram. Adaptive methods seek to avoid these issues, such as block-based processing of histogram equalization, which performs the equalization on each sub-image or block of the original image. One well-known method that uses this approach is Contrast Limited Adaptive Histogram Equalization (CLAHE) [266], which limits the amplification by clipping the histogram at a predefined value before computing the cumulative distribution function (CDF) [140].

4.2.2   Retinex Algorithm

The Retinex theory, originally proposed by Land and McCann [118], is centered around human perception of objects with regard to color and brightness. Its goal is to develop a model of the human visual system that can recognize and match colors across a diverse range of lighting conditions. The core of the Retinex algorithm leverages this property to separate the illumination image, $L(x, y)$, from the reflected image, $R(x, y)$, as both

together form an image, $S(x, y)$, expressed in Equation 4.1.

$$S(x, y) = L(x, y) * R(x, y) \tag{4.1}$$

The complexity of the multiplication in Equation 4.1 can be simplified into a basic addition operation from a mathematical standpoint. Thus, the first step in most Retinex algorithms is to convert the input image into the logarithmic domain, as shown in Equation 4.2.

$$\log S(x, y) = \log L(x, y) + \log R(x, y) \tag{4.2}$$

By applying this equation, the logarithm of the reflectance can be computed by subtracting the logarithm of the illumination from the logarithm of the image, as shown in Equation 4.3.

$$\log R = \log S - \log L \tag{4.3}$$

The reflectance, in comparison to the illumination, has a low-frequency component. To estimate this illumination, the Retinex algorithm uses a Gaussian low-pass filter. Therefore, to obtain the estimated value of the high frequency information in the reflected image, the illumination image $L(x, y)$ is first obtained by Gaussian filtering, expressed in Equation 4.4.

$$L(x, y) = F(x, y) * S(x, y) \tag{4.4}$$

The Single-Scale Retinex (SSR) approach estimates the illumination by convolving the original image with a Gaussian filter and then subtracting it from the original image to obtain an illumination-invariant description, expressed in Equation 4.5.

$$R_{ssr}(x, y) = \log(S(x, y))) - \log(S(x, y) \circledast G(x, y)) \tag{4.5}$$

where $G(x, y)$ is the Gaussian filter and the symbol $\circledast$ denotes the convolution.

In contrast, the Multi-Scale Retinex (MSR) [103] method is calculated as a weighted sum of different SSR outputs at multiple scales, which can be expressed in Equation 4.6.

$$R_{msr}(x, y) = \sum_{n=1}^{N} \omega_n R_{ssr_n} \tag{4.6}$$

In this formula, N denotes the number of scales, R_{ssr_n} represents the output of the n-th scale component, ω_n denotes the weighting factor for the n-th scale, where $\omega_1 + \omega_2 + \ldots + \omega_n = 1$, and R_{msr} represents the output of the MSR algorithm.

4.2.3 Image Quantization

According to Heckbert [83], color image quantization involves selecting a set of colors to represent the color gamut of an image, along with computing the appropriate mapping of the color space.

Typically, this process involves two phases: first, selecting a small set of colors that represent the original image, and second, mapping each pixel of the image to one of the colors in this palette [134].

Therefore, segmentation of images using this method can be achieved by defining a color sample of the region of interest, represented by the "average" color value to be segmented. The objective of this segmentation is to classify the RGB pixels of an image as belonging or not to a particular class. This determination can be mathematically expressed through a similarity metric, with one of the simplest being the Euclidean distance [74].

Thus, considering $p(R, G, B)$ as an arbitrary pixel composed of RGB values, it is similar to the point $a(R, G, B)$ if the distance between them is less than a specified threshold, as demonstrated by Equation 4.7.

$$d(p, a) = ((R_p - R_a)^2 + (G_p - G_a)^2 + (B_p - B_a)^2)^{\frac{1}{2}}) \tag{4.7}$$

where (R_p, G_p, B_p) refers to the RGB value of pixel p and (R_a, G_a, B_a) to pixel a. The set of points p that satisfy $d(p, a) \leq d_0$ forms a solid sphere of radius d_0, where the points contained in it are those that satisfy the specified color criterion, while the points outside do not. The coding of the image points in binary form is performed by assigning black and white to these two classes.

4.3   Experimental Results

We began our experiments on the segmentation problem of noisy borehole images by applying traditional algorithms from the field of image segmentation. We used two types of approaches: algorithms for uniform background images (minimum [108], local [17] and Otsu [154] Threshold) and non-uniform (Niblack [150] and Sauvola [185]).

However, as shown in Figure 4.1, we found that even after applying several approaches to address the problem of this type of image, none of them were able to provide satisfactory results for the feature extraction task. Therefore, it was necessary to investigate the origin of the noise and explore alternative approaches to deal with the situation.

After analyzing the characteristics of the acquisition process of images in high-temperature, high-pressure environments under oil wells, we found that the noise present in these images is mostly due to effects such as blurring and fogging. Histogram Equalization algorithms are a well-known method for enhancing blurred images, and are often used as the first step in pre-processing tasks in this domain. Therefore, we evaluated the effectiveness of these methods by applying HE and CLAHE, followed by an efficient approach for the defogging problem found in the literature, the Retinex algorithms: Multi-Scale Retinex with Color Preservation (MSRCP) and Multi-Scale Retinex with Color Restoration (MSRCR).

According to Zhang et al. [251], both MSRCR and MSRCP amplify noise as enhancing images, and the noise will affect the efficiency of image retrieval or target recognition. The MSRCR [103] estimates the illuminance of the image using Gaussian filters of different scales and conduct enhancement by multiplying it by a color restoration function of the chromaticity, and the MSRCP [163] will perform color preservation by applying Multi-scale Retinex on intensity image-channel.

To assess the quality of the enhanced images by means of the concepts discussed
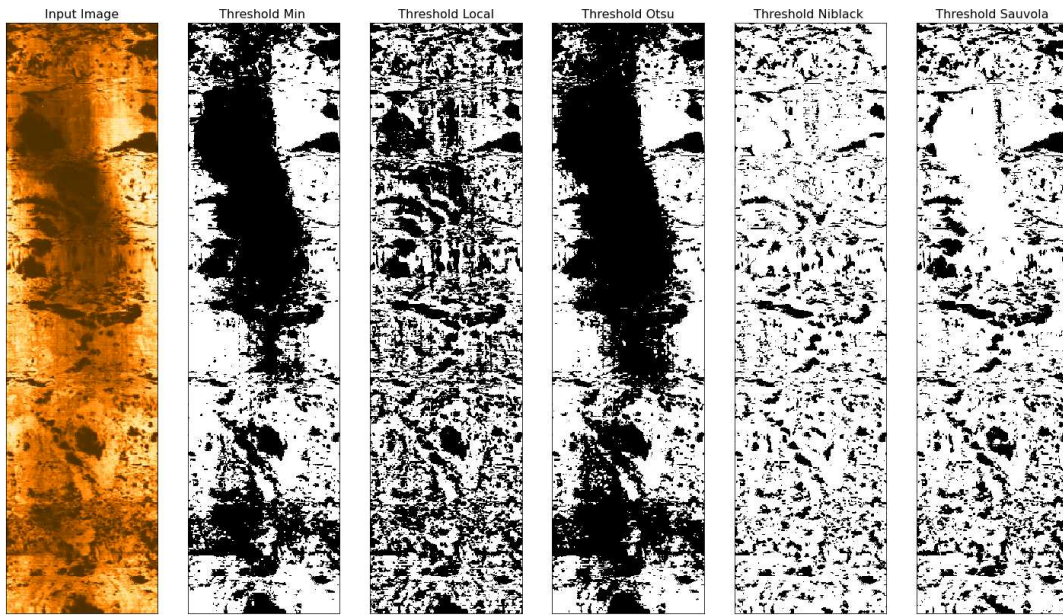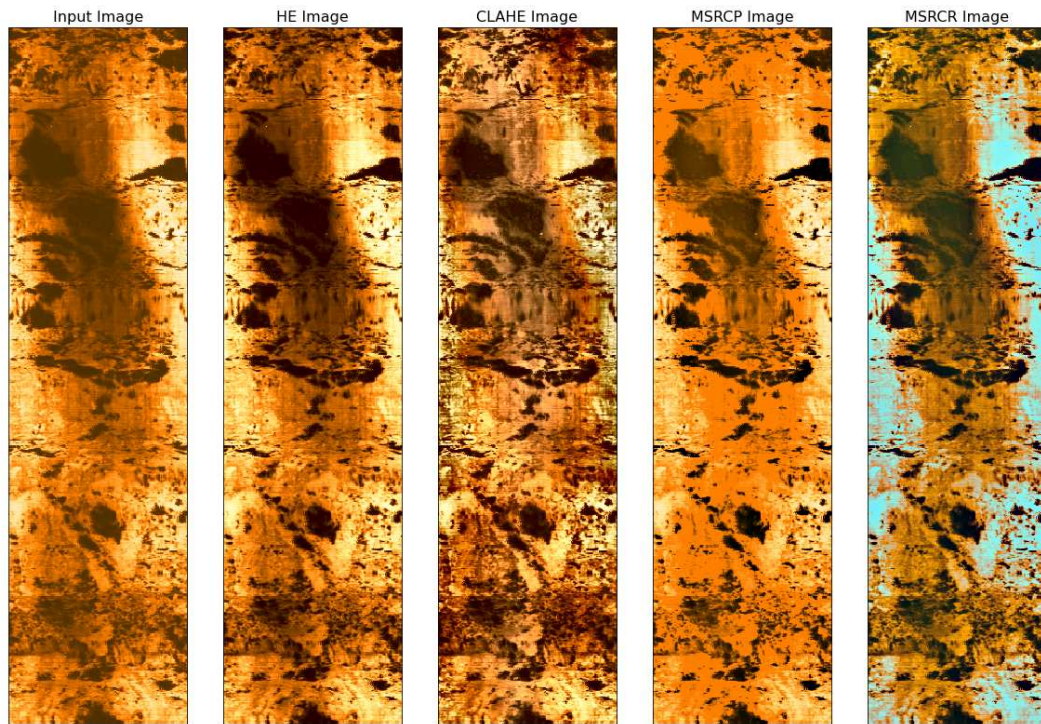
Figure 4.1: Description of seismic facies classes.

Figure 4.2: Result of applying enhancement algorithms.

previously, we analyzed the results illustrated in Figure 4.2. In addition to subjective evaluation, we applied three Image Quality Assessment (IQA) metrics: (i) mean square error (MSE), which provides a quantitative measure of similarity between the reference and distorted images (lower values indicate higher similarity), (ii) structural similarity index measure (SSIM), which measures the similarity between two images in the human visual system (SSIM index varies between -1 and 1, with 1 indicating perfect similarity and 0 indicating no similarity), and (iii) peak signal to noise ratio (PSNR), which measures

the power of peak signal (higher values indicate better quality) [182]. The results are reported in Table 4.1.

Table 4.1: Quantitative results for image enhancement.

Methods	Metrics		
	PSNR	SSIM	MSE
HE	23.99	0.90	259.45
CLAHE	16.03	0.62	1620.05
MSRCP	14.68	0.58	2208.43
MSRCR	19.57	0.84	717.73

The results obtained from applying the HE and MSRCP methods showed a better qualitative response. However, upon further visual analysis, it became apparent that the MSRCP method was able to preserve the original colors and textures of the image better than the HE method. This provided better conditions for the application of segmentation algorithms, which were applied again to evaluate their effectiveness after the data improvement.

In Figure 4.3, the segmentation results for both the HE and MSRCP images are shown. It is evident that the MSRCP approach led to better performance in feature extraction, particularly with the minimum threshold algorithm, which was able to extract regions such as pores and fractures (empty spaces in black) more accurately.

Despite the good results shown by the minimum threshold method compared to the other methods, there is still noise present around some structures with greater shading. Therefore, considering the presence of this noise and the contrast between the pore tone and the orange tone of the background, we decided to apply RGB image quantization (RGBQ) as a means of segmenting the images, aiming to extract only the pixels close to the black value that indicates the actual region of interest.

To obtain the quantized image, we used the RGB tone corresponding to black $(0, 0, 0)$ as the target for quantization, and set the threshold at 127 to allow for color approximation that corresponds to half of the RGB values $(0 - 255)$. Figure 4.4 presents a comparison between the segmentation obtained by the minimum threshold and RGBQ methods.

In this image, it is noticeable that image quantization was able to effectively segment the structures of interest by capturing both the overexplored regions and the regions ignored by the minimum threshold. This was possible by combining it with the enhancement provided by the MSRCP algorithm. Figure 4.5 illustrates the definition of the best model analyzed for the segmentation of these images.

4.4   Considerations

We proposed a combined method for extracting information from borehole log images using image enhancement and quantization. The investigation into the best approach for this task was guided by the origin of noise in the image acquisition process, which led to lighting problems such as shading and fogging. Thus, through the research carried out, two algorithms were used as the primary approach for image processing: the Multi-Scale
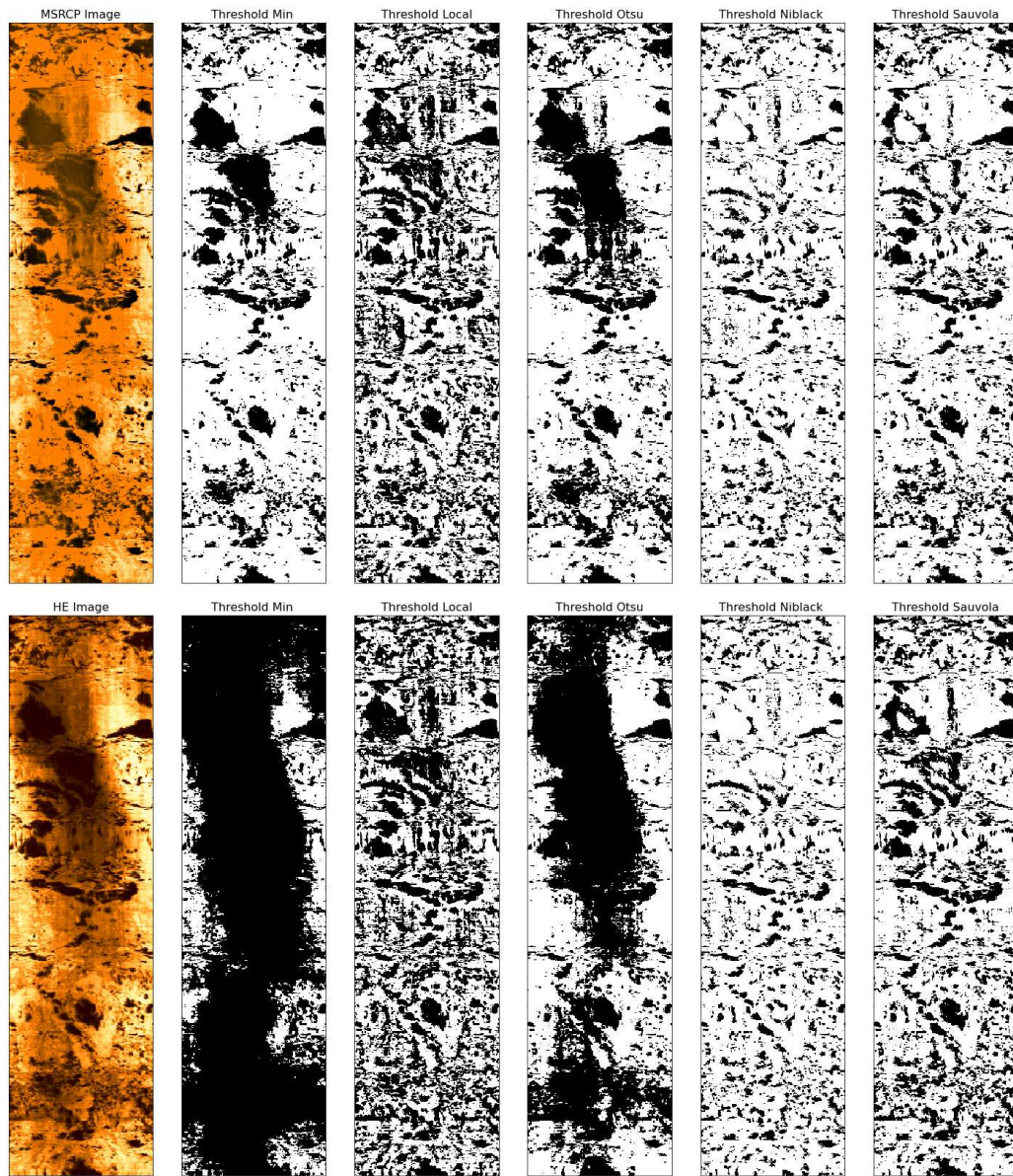
Figure 4.3: Result of applying segmentation algorithms to HE and MSRCP images.

Retinex with Color Preservation and RGB image quantization. These methods enabled the defogging of the image by preserving the structure present in the predominant texture of the data, and the extraction of the region of interest by analyzing the distance between the tones of its pixels.

Compared to other approaches presented in this work, the combination of these techniques resulted in an efficient solution to the problem. This approach enables accurate and improved analysis of the geological structures of interest and labeling of these structures, facilitating their application in machine learning models.
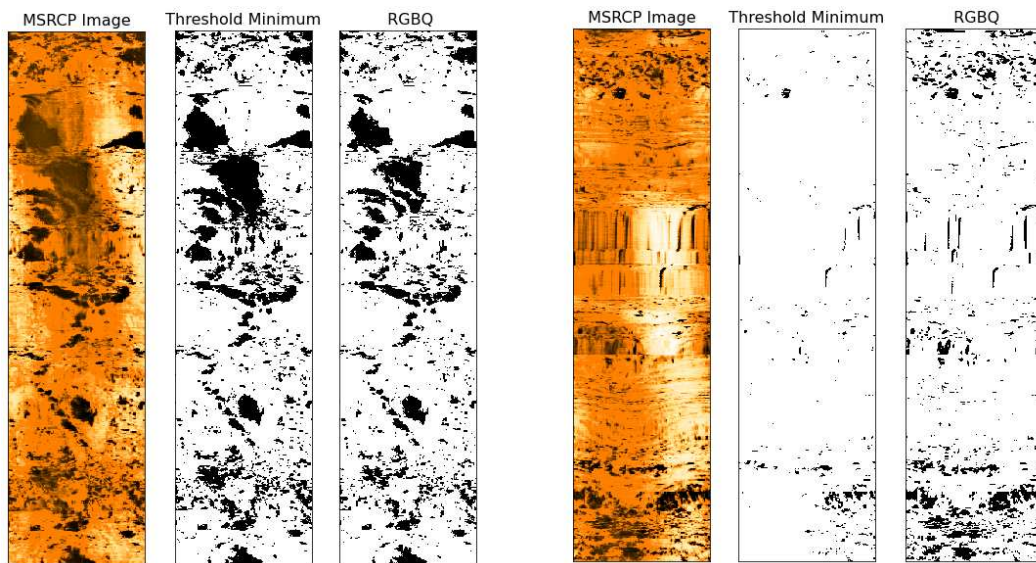
Figure 4.4: Comparisons between two samples segmented by the RGBQ method and the minimum threshold.
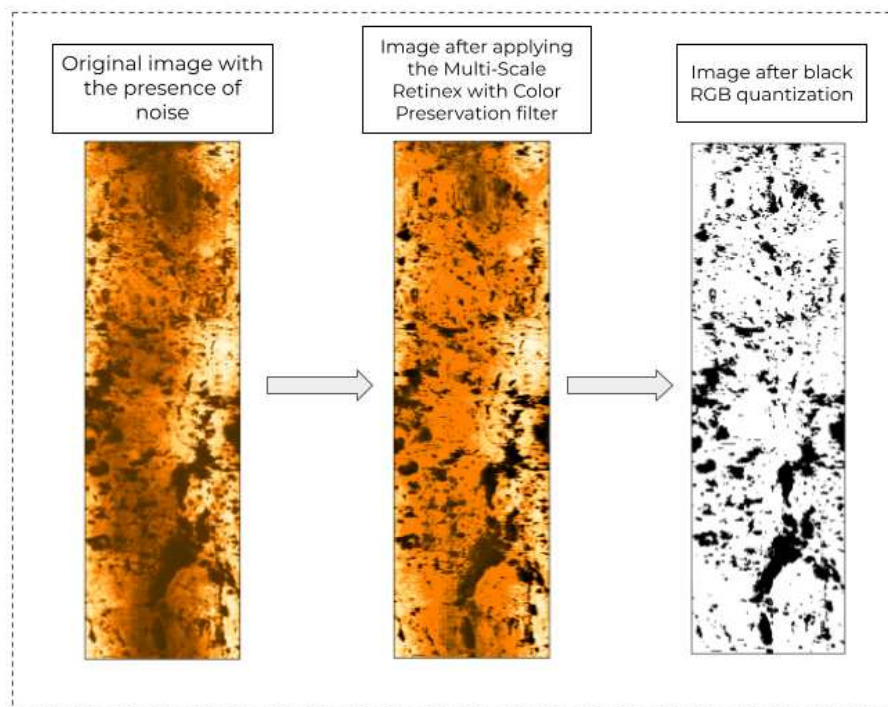

Figure 4.5: Definition of the final methodology for extracting features from noisy borehole log images.

Chapter 5

Deep Learning Method for Classification and Refinement of Seismic Facies

In this chapter, we present a method for classifying and refining facies in seismic data. The seismic facies analysis is a crucial task in the process of reservoir characterization. Traditional seismic facies labeling often require exhaustive manual analysis and rely heavily on the expertise of professionals to classify extremely complex data. With the emergence of deep learning techniques, several applications have been developed to assist and automate manual and repetitive tasks. In order to construct a refined seismic facies model for pre-salt carbonates of the Barra Velha Formation (Santos Basin, Brazil), we developed a seismic facies model consisting of 5 classes (Mounds 1 and 2, Trough, Wedge, and Chaotic) by mapping the amplitude present in seismic data. We then applied a convolutional neural network based on the U-Net architecture to refine the results and provide a robust classification model for the heterogeneous context of the pre-salt carbonate reservoirs.

5.1   Contextualization

In geology, the term facies (sensu lato) is applied to categorize rock units presenting similar geological characteristics (e.g., lithology, sedimentary features, biological content, genesis, seismic patterns) that are defined according to the specific goal. In this regard, the goal of seismic facies analysis (sensu stricto) is to identify units of similar seismic reflection patterns that are distinguishable from adjacent units and carry petrophysical (e.g., reservoir interval), depositional (e.g., depositional environment, system tract) or post-depositional (e.g., hydrothermal vent, karst) significance [26, 175, 233]. Therefore, the interpretation of the seismic facies aims at understanding not only the stratigraphic organization of the rock record (e.g., lithology, stratification patterns, depositional bodies) and its potential reservoirs, but also at providing valuable insights about the paleoenvironment and formative depositional processes throughout the geological evolution. In this approach, each seismic facies is characterized in terms of its geometry (e.g., external and internal reflectors morphology), reflectors configuration (e.g., smoothness, lateral

continuity), reflectors termination (e.g., onlap, downlap, toplap, offlap), and their stacking patterns (e.g., progradation, retrogradation, aggradation), as also the properties of seismic waves (e.g., dominant amplitude and frequency) (*sensu* [31, 142, 143, 233]).

However, interpreting large amounts of data, as seismic volumes usually present themselves, is a time-consuming and laborious task. When performed manually, the interpreter identifies seismic reflection patterns and delimit the regions with color marker labels [49].

The manual labeling is usually conducted at regularly-spaced control seismic images (e.g., cross-line or in-lines) using straight polyline segments. In this process, the intermediary seismic slices between labelled images are left uninterpreted or with unprecise correlation between adjacent labeled slices, producing either gaps or geologically inaccurate label boundaries (e.g., serrated outlines) in the interpretation dataset.

Several works have been following the advancement of computer vision techniques and make use of them throughout their evolution. When applied, these methods can enhance the visibility of features that characterize significant structures within seismic data, facilitating the comprehension of structures and patterns that might otherwise go unnoticed by interpreters in the mapping task.

The literature on technologies that assist in this characterization illustrates how various approaches and tools can be employed in this endeavor. In recent years, with the advancement of machine learning methods, there has been a noticeable evolution in technology's domain and its application in the task of classifying seismic facies. Initially, the facies analysis process could be approached through the concept of a self-organizing map, one of the most widely used algorithms for seismic facies analysis, to cluster classes effectively [53, 259].

Therefore, with the demonstrated power of machine learning-based methods, recent works have explored semi-supervised, unsupervised, and supervised approaches. In the first case, methodologies employ pseudo-labeling techniques to predict seismic facies, especially when obtaining a significant amount of labeled data is not feasible [10, 123, 127, 169, 199]. When no labeled data is available, unsupervised methods are applied, such as those mentioned in the work developed by Ferreira et al. [62], which perform the classification of seismic facies in a specific region of the Santos Basin using the k-means clustering method. However, the methods that have been receiving more attention are convolutional networks based on supervised learning, which, through a dataset with labels, seek to map regions of interest in seismic data. The pre-processing of these data is shown to be a fundamental part for the network's performance, requiring refinement of labels [253] and diversification of techniques involving dataset construction [102] before the network application.

Linked to the training process, explainability techniques have proven to be a new and effective tool in understanding the behavior of networks in this automatic classification task [92, 172, 238]. In addition to the established use of CNNs, new lines of research are also exploring the potential of Transformers and their self-attention mechanism to optimize the facies segmentation process [223], as well as automatically optimizing the development of network architecture [69].

Therefore, the present research aims to create a robust model, with low complexity and high efficiency, trained with a large amount of data to classify 5 different types of

facies that are deposited in a region of Santos Basin in the Brazilian Pre-Salt. This region is extremely important in the context of Brazilian oil and gas exploration, as it emerges as one of the main oil producing basins. However, its heterogeneous and particular formation, since it represents the largest nonmarine carbonate reservoirs in the world [203], introduces complexities to the task of modeling and classifying attributes, such as facies, within fields having such a structure.

To deal with it, we developed a massive database derived from a seismic volume, originating from a region of the Santos Basin, which was entirely labeled with the main geological facies found. Consequently, the automatic classification of this target can be done using deep learning resources, such as convolutional networks, through the use of the segmentation technique based on U-Net. By training this network, it is possible to: (i) produce more accurate and precise prediction of uninterpreted seismic images between manually-labelled slices, (ii) correct gaps and outline artifacts of labels to better depict lateral and vertical boundaries between facies, and (iii) optimize the time on future seismic facies analysis in highly heterogeneous reservoirs.

5.2 Methodology

To achieve the creation of a model capable of refining and classifying data pertaining to seismic facies within a pre-salt region, a systematic approach was undertaken. This encompassed a step-by-step process, beginning with the assembly of a original dataset and concluding with a comprehensive assessment of the model's efficacy. In Figure 5.1, there is a representation of a detailed workflow describing the stages of this process, which will be elaborated on in the subsequent sections.
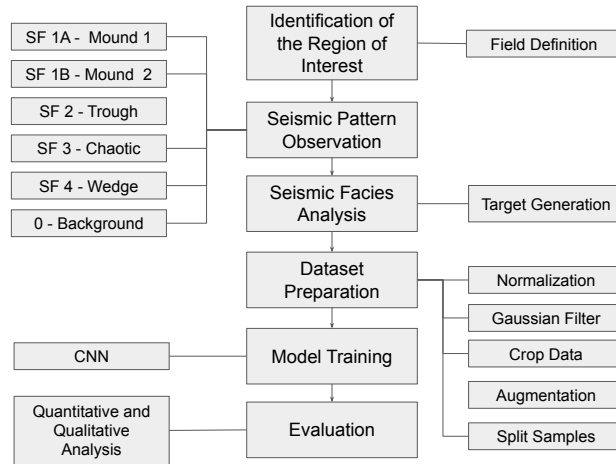

Figure 5.1: Detailed workflow for building a seismic facies classification model.

These stages include: (i) the definition of a region of interest, where the geological formation of interest was delimited, as well as its reservoirs, (ii) the observation of the seismic patterns of greatest influence and importance in the present lithology and geology, (iii) the analysis of facies in the seismic data through the 3D mapping of the defined facies, aiming at creating the target of the model, (iv) preparation of the seismic data to feed the network; for this purpose, image processing techniques were used to improve

the quality of the seismic data, normalize its values, and select the sections for training, validation, and testing, (v) training the network using a convolutional neural network model, and (vi) the evaluation of the results through classification and similarity metrics for a quantitative analysis and the comparison of the obtained prediction results for a final qualitative analysis.

5.2.1 Seismic Facies Analysis

In this work, we conducted a seismic facies analysis using a seismic volume (20.5×12.5×0.9 km) of pre-salt carbonate reservoirs of the Barra Velha Formation in the Santos Basin, Brazil. A total of five seismic facies were mapped and classified as: (i) chaotic, (ii) mound type 1, (iii) mound type 2, (iv) wedge, and (v) trough seismic facies, as illustrated in Figure 5.2.
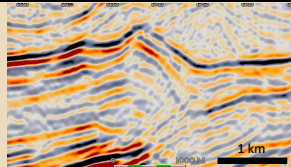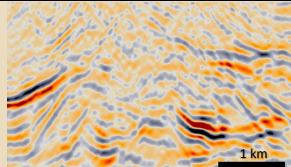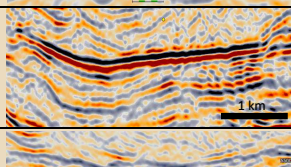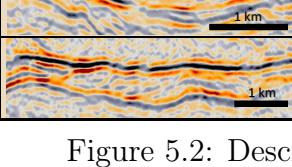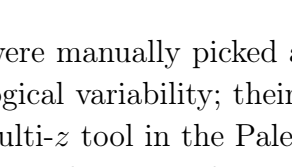

SF	SEISMIC FACIES EXAMPLE	EXTERNAL GEOMETRY	REFLECTOR PATTERNS	OCCURRENCE
Mound type 1 (SF 1A)		Mound-shaped body with convex-upward base and top	**Amplitude**: low to medium. **Geometry**: continuous to discontinuous reflectors with concave-upwards geometry that converge outward and downward.	Structural highs (large-scale inverse faults)
Mound type 2 (SF 1B)			**Amplitude**: low to medium. **Geometry**: discontinuous reflectors with concave-upwards geometry	
Trough (SF 2)		Tabular with concave-upward base and top	**Amplitude**: high. **Geometry**: Smooth parallel reflectors that are laterally continuous and onlap towards structural highs.	Large-scale structural lows
Chaotic (SF 3)		Tabular with irregular base and top boundaries	**Amplitude**: low. **Geometry**: chaotic discontinuous reflectors.	Structural highs (shallow normal faults)
Wedge (SF 4)		Lens-shaped bodies with flat top and concave-upward base	**Amplitude**: low to medium. **Geometry**: progradational reflectors that downlap atop the concave-upward base.	Small-scale structural lows

Figure 5.2: Description of seismic facies classes.

The facies were manually picked along seismic cross-lines oriented in the direction of maximum geological variability; their mapping followed regular (5 or 10 steps) intervals. By using the multi-z tool in the PaleoScan software (version 2023 1.0), the intermediary cross-lines between the mapped images were automatically mapped and merged to compose three-dimensional geobodies containing seismic facies volumes. Finally, each seismic facies geobody was assigned to an integer value (from 1 to 5) to produce the classificatory facies mask of the original seismic volume, leaving unclassified volumes with null value.

The chaotic seismic facies display flat and irregular base and top, composing an approximately 4.82 km^3 plateau positioned at high stratigraphic intervals (lower seismic depth) with a 0.004 average seismic amplitude. Internally, the seismic facies show chaotic pattern with laterally discontinuous subhorizontal reflectors due to the presence of pairs of subvertical small-scale normal faults marked by bright spot cores. The chaotic facies is laterally bounded by the trough and the mound type 1 seismic facies.

Types 1 and 2 mound seismic facies resemble ridges enclosed by an irregular flat base and a convex-upward top that laterally tappers the bottom horizon, occupying volumes of approximately 1.85 km^3 and 12.8 km^3, respectively. Both mound types are characterized by the presence of large-scale inverse faults. However, they differ in terms of internal seismic reflectors configuration and lateral boundaries. Type 1 mound facies displays an internal seismic pattern of small-scale chaotic reflectors that are laterally discontinuous, with random angular orientation, and approximately 0.0042 in average seismic amplitude. Moreover, the mound type 1 is bounded by the chaotic and the trough seismic facies on opposite sides. Alternatively, Type 2 mound is internally organized into conformable and parallel convex-upward reflectors with an approximately -0.04 average seismic amplitude. Finally, the type 2 mound is bounded by the trough and the wedge seismic facies.

The wedge seismic facies occurs partially enclosed between the type 2 mound seismic facies. It resembles an approximately 2.2 km^3 wedge-shaped body limited by a concave-up base and a flat and horizontal top horizon. Its major axis is aligned with the mound type 2 ridges at both sides. Internally, the seismic reflectors (approximately -0.0027 average amplitude) are organized into clinoforms that downlap the concave-up lower horizon parallel to the wedge's major axis. Furthermore, the wedge seismic facies is bounded on both sides by type 2 mound facies.

The trough seismic facies appear as a bowl-shaped geobody limited at the base and the top by concave-upward horizons; it displays a major axis parallel to the mound ridges and occupies a total volume of approximately 17.2 km^3. Internally, the trough facies is composed of high-amplitude (approximately 0.0027) conformable and parallel seismic reflectors displaying concave-up geometry. Additionally, large-scale normal faults are depicted at both margins of the geobody. The trough seismic facies is laterally bounded and onlaps the mound (types 1 and 2) and the chaotic seismic facies.

From the mapping of the previously defined seismic characteristics, a seismic cube was built to serve as the basis for creating the seismic facies dataset. In this cube, as illustrated in Figure 5.3, there are the presence of the 5 seismic facies and a background region that surrounds the region of interest.
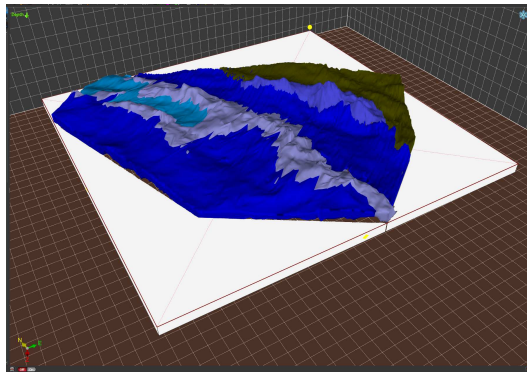

Figure 5.3: Seismic cube containing the results of mapping the seismic facies of interest.

5.2.2   Dataset Preparation

From the mapping of the facies defined in the previous section, a seismic cube of dimension 1050×1073×194 pixels, which refers to the dimensions of inlines, crosslines, and depth, was generated to feed the machine learning model for facies prediction. This wealth of data can facilitate the incorporation of heterogeneity within the model, enabling an investigation into its learning capabilities across a diverse carbonate reservoir scenarios.

For the classification task, this target cube presents five distinct geological facies and a background region. Figure 5.4 illustrates a seismic inline containing labels denoting its presence. As discussed, the geological facies were categorized to represent regions sharing similar characteristics, whether attributed to their chaotic shapes, generally associated with non-reservoir areas, or from their mound-like geometries, indicative of their association with reservoir regions.
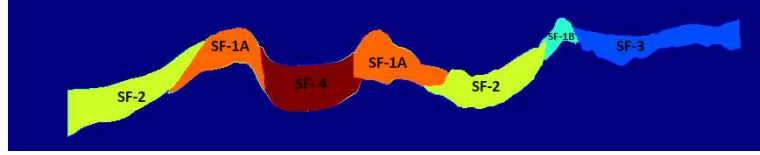

Figure 5.4: Example of a mask section with class labeling.

To train the model, the data preparation process begins with the pre-processing of the data that will be used as input for the network, which in this case will be a seismic cube related to the seismic amplitude of the same facies region. Given the wide range of amplitudes, the initial step involved data normalization to improve input consistency and prevent errors during gradient updating and other training processes. Subsequently, a Gaussian filter it was also utilized with a 5×5 kernel to reduce noise and enhance details.

As the model needs to be fed with images of specific sizes to perform convolutions and upsampling processes, both input and target were cropped, as shown in Figure 5.5 (A), into data slices of 194×194 pixels extracted by a sliding window of size 194 with no overlaps, traversing each 1050 inline, creating a dataset of 3987 pairs of images.
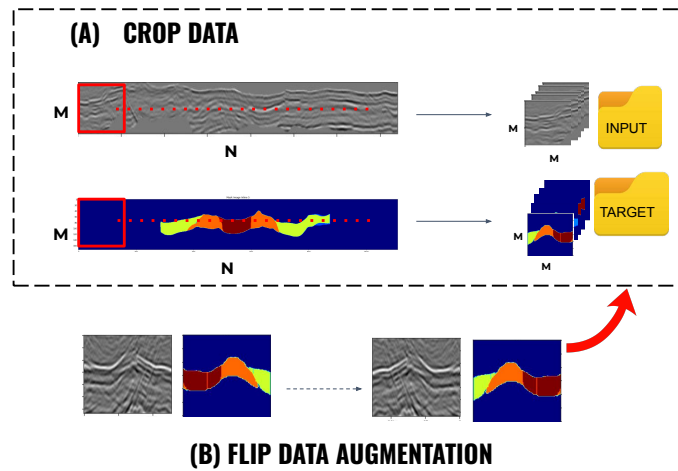

Figure 5.5: Process of dataset building through the crop and augmentation steps.

For a proper evaluation of the model, we divided the dataset into 75% for training and

15% for blind testing. However, as shown in the graph in Figure 5.6, the complete dataset exhibits an imbalance in the number of pixels representing each facies class. Therefore, to increase the presence of the classes with fewer instances (SF 1B, SF 3, SF 4) and to improve the quality of the training dataset, a vertical flip operation was applied, as shown in Figure 5.5 (B), to all slices containing these classes. This approach augmented the number of images composing the training process, and we further divided them to obtain 15% of this data for the validation process. This validation set serves as an independent sample to assess the model's performance on unseen data, ensuring that the learning process can generalize beyond the training set.
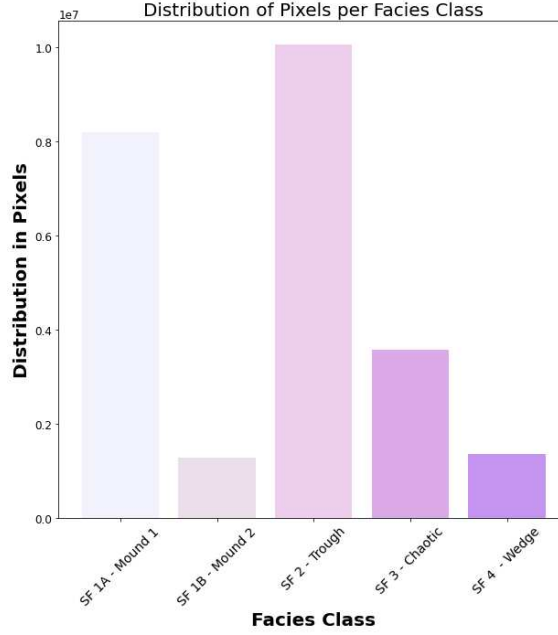

Figure 5.6: Distribution of pixel quantity for each facies class.

5.2.3 Model Architecture

The constructed model, as illustrated in Figure 5.7, was developed based on the encoder-decoder architecture of the U-Net network. This architecture is particularly suited for tasks such as image segmentation, where the goal is to assign a class label to each pixel in an input image. In this specific implementation:

- Encoder: The encoder portion of the network consists of several layers, each composed of two convolutional layers with a 3×3 kernel, followed by a ReLU activation function, and a 2×2 max-pooling operation for downsampling. This architecture allows for the extraction of hierarchical features from the input seismic image.

- Decoder: The decoder portion of the network performs the upsampling of the feature maps to reconstruct the segmentation map. At each upsampling step, the upsampled output from the previous layer (obtained through 2×2 transposed convolution) is concatenated with the corresponding cropped feature maps copied from the encoder path. This mechanism helps in recovering spatial information lost during the

downsampling process. Subsequently, two convolutional layers with a 5×5 kernel are applied to refine the feature representation before producing the final output.

Overall, this architecture facilitates the translation of the input seismic image into a class map representing different facies at each sampling point, leveraging both local and global contextual information captured through the encoder-decoder framework.
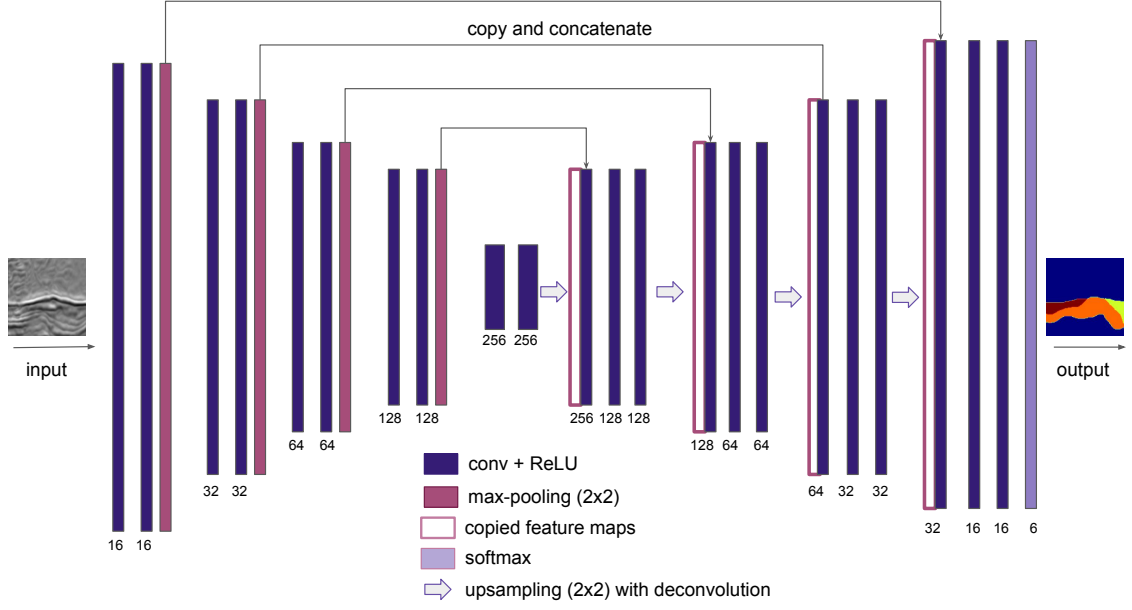

Figure 5.7: Network architecture. Purple blocks represent multichannel feature maps with the number of input channels for each layer at the bottom of the block.

5.3   Results and Discussion

After implementing the aforementioned methodology, the network underwent training for 100 epochs, during which its performance was evaluated using key metrics: dice coefficient, accuracy, precision, and recall.

In the training phase, the model achieved a dice coefficient of 0.9935, an accuracy of 0.9955, a precision score of 0.9955, and a recall of 0.9954. Subsequently, during validation, these metrics were slightly lower but still impressive, with a dice coefficient of 0.9924, an accuracy of 0.9941, a precision of 0.9942, and a recall of 0.9941. These results indicate the robustness and effectiveness of the trained model across both training and validation datasets. Additionally, Figure 5.8 presents a graphical representation of the model's performance in terms of its gain and error throughout the training process.

Following these initial results, the next step was the application of the final model to the test set, consisting of 598 images of the same dimensions as the training. In this dataset, the model achieved an accuracy of 99.24% and a Mean Intersection over Union (MIoU) value of 95.48%. Furthermore, we analyzed the IoU value for each class, obtaining 99.42% for the background class, 94.83% for the Chaotic class, 92.84% for Mound 1, 96.03% for the Trough class, 95.21% for Mound 2, and 94.54% for the Wedge class. To understand the values presented in the IoU metric, which acts as a metric measuring the
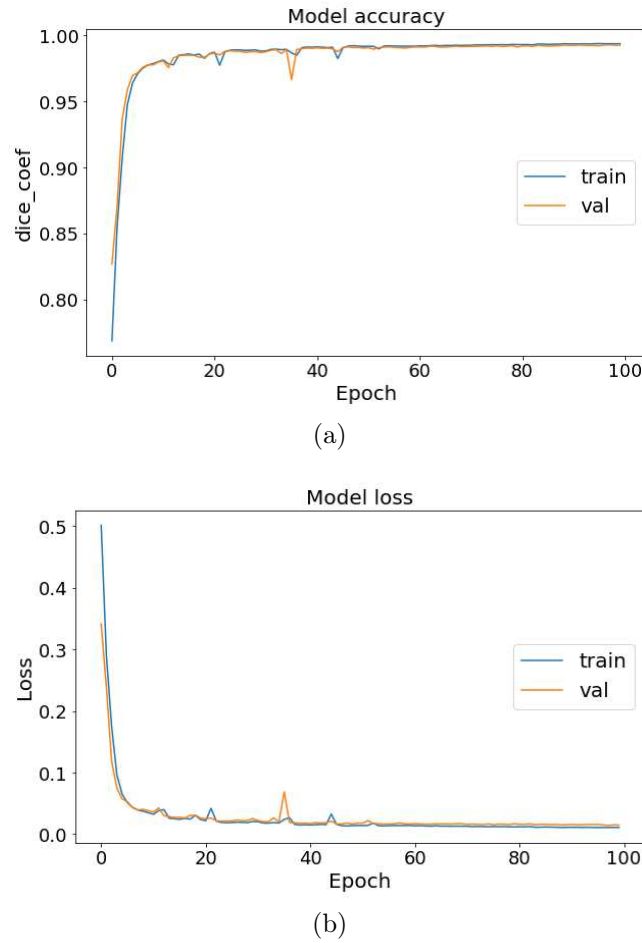
Figure 5.8: Progress of the evaluation metrics comparing the values on the training and validation datasets throughout the learning process. Learning performance through (a) dice loss metrics and (b) error rate representation.

proportion of overlap between the prediction and its ground truth, we plot the confusion matrix to understand how the model is performing in different classes.

The confusion matrix (Figure 5.9) discloses how the pixels were labeled and which classes were mismatched by the model. From the observed outcome, it is evident that the majority of confusion between classes is associated with boundary regions between the classes and the background (according to line 0 in Figure 9), and to a minor extent, between neighboring classes. The high value observed in this relation to other classes suggests a transition between the background and the beginning of the facies, which, as visually perceived, does not represent a drastic difference. Naturally, boundary confusions are also expected due to the degree of similarity shared between adjacent seismic facies (e.g., similar seismic patterns or amplitude values). It is important to note, however, that the boundary confusions depicted in the model do not necessarily imply significant distortions in the facies region, especially when analyzing the predicted images.

Because the goal of the model's prediction extends beyond the sole classification of amplitude data values, the prediction outcomes require validation not only through quantitative approach (i.e., metrics), but also through the qualitative visual analysis to grasp the geological significance of the predicted seismic facies.
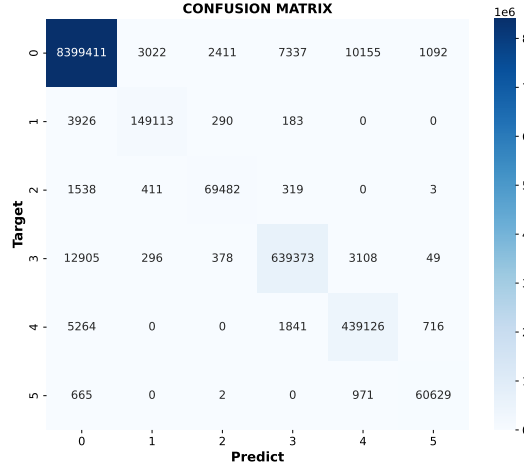
Figure 5.9: Confusion matrix resulting from the prediction in the blind test set.

In fact, the blind test predictions (Figure 5.10 (a)) demonstrates that the model not only offered effective classification of the seismic facies, but further refined their outline by: (i) correctly filling the gaps in the original labels, (ii) smoothed serrated boundaries to become geologically more accurate, (iii) and preserved geologically complex lateral boundaries between seismic facies (e.g., concave, convex, and embedded boundaries) (Figure 5.10 (b)). Therefore, the few observed boundary confusions in the model can be partially accounted to enhancements performed by the model on ensuring coherent continuity at places of target discontinuities due to inherent morphological limitations in the labeling process.
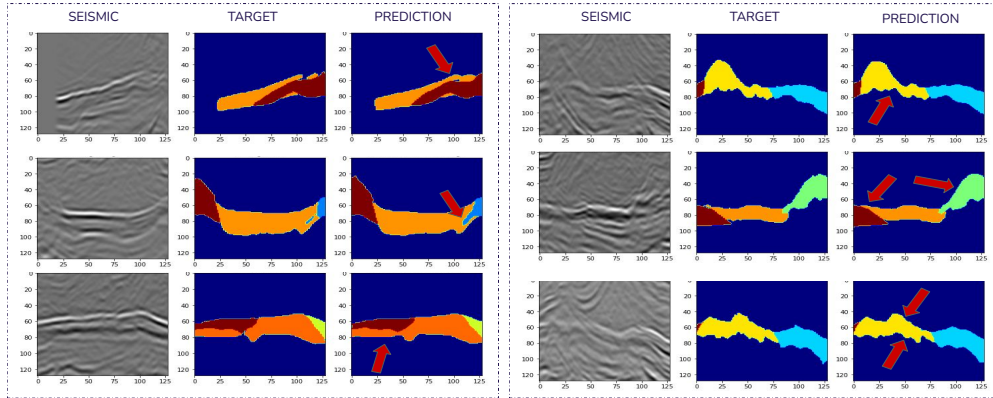
Figure 5.10: Results of facies classification and refinement in test data. (a) Improvement in facies classification; (b) Improvement and smoothing of edges.

After testing the model's performance on the blind test set, we applied the trained model to the entire seismic dataset to truly assess its ability to refine the data generated through manual labeling. In Figure 5.11, it is possible to see, through the reconstruction of predicted sections in inlines, that the model has developed the capacity for generalization in its learning, predicting the region in line with the ground truth, providing a suitable delineation of the structures, and improving contact relationships. Furthermore, the results obtained also demonstrate the effectiveness of less complex convolutional net-

works for accurate data classification. The depth and number of filters in the layers of the networks used were sufficient to promote an understanding of the data characteristics.

Figure 5.11: Samples of seismic inlines resulting from the application of the trained model across the entire seismic volume.

5.4   Considerations

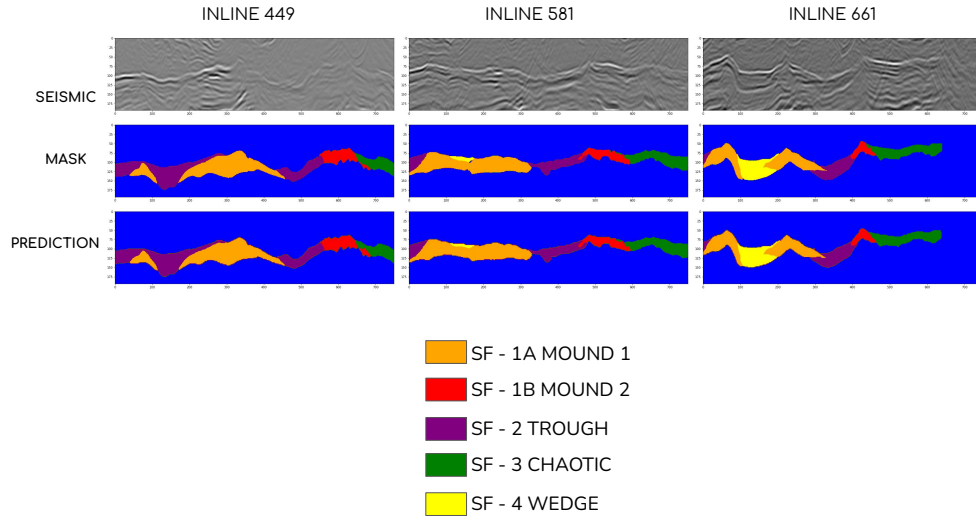Mapping seismic data has long been a challenging task, requiring both meticulous attention to detail and software performance to generate accurate final surfaces. The expertise of the professional conducting the task also plays a crucial role in the quality of the mapping results. In such scenarios, deep learning architectures such as CNNs prove to be among the most effective tools for semantic segmentation tasks, dividing images into classes with distinct meanings.

In this framework, we utilized amplitude seismic data to create a dataset comprising 5 distinct seismic facies from pre-salt reservoir intervals of the Barra Velha Formation in the Santos Basin, Brazil. This region, known for its geological complexity and importance in hydrocarbon exploration, presents a unique set of challenges for facies classification.

To enhance the results of the manual labeling process, we also applied a U-Net-based convolutional neural network, which has been widely recognized as an excellent tool for semantic segmentation tasks in complex geological settings. This powerful architecture is particularly well-suited for capturing intricate patterns and features within seismic data, allowing for more precise and efficient facies classification. By integrating the capabilities of the U-Net model with our manual labeling efforts, we aimed to improve the accuracy and reliability of the seismic facies analysis process in this challenging geological context.

Chapter 6

Transformer Model for Fault Detection From Brazilian Pre-Salt Seismic Data

In this chapter, we present a methodology for identifying faults in seismic data [22]. The Brazilian reservoirs are formed mostly in highly faulted and fractured carbonate rocks, which can increase hydrocarbon transport and storage capacity. Strategies that permit the identification of these structures allow the optimization in the exploration of a reservoir. To fulfill this task, machine learning models have been able to provide an understanding of these environments through the use of data obtained by seismic method. The use of convolutional neural networks has shown to be able to provide excellent abstractions in the field of semantic segmentation, including its use in seismic data. However, due to the highly heterogeneous formation of this type of data, the work of extracting information from these images remains challenging. From this, we investigate the potential of using Transformer models in this geological context focusing on the faults identification.

6.1   Background

The analysis of seismic data is crucial for the progress of hydrocarbon exploration, and it is commonly done through the study of geological structures. Various techniques have been employed to analyze seismic data, including machine learning and image processing, which aim to automate and facilitate the interpretation process, using seismic data in the form of an image.

Pepper and Bejarano [160], for example, presented case studies on automatic fault interpretation using only seismic attributes that highlight faults. These attributes work similarly to filtering techniques used in image processing, and two of them, dip and azimuth, showed the best results in identifying fault regions that were extracted as connected components. Zhao and Mukhopadhyay [258] explored the task of fault detection in synthetic and field data by using convolutional neural networks to develop prediction models. In particular, Zhao and Mukhopadhyay [258] improved the final result by adding image processing algorithms, such as smoothing and sharpening, after the prediction step.

As the need for more robust models for seismic interpretation has become evident, researchers have turned to deep machine learning models for performing these tasks. Wu

et al. [228] developed several models with a primary focus on fault prediction, including FaultNet3D and FaultSeg3D. Using a single CNN, the FaultNet3D model aimed to estimate the probability of faults, cracks, and dips. Meanwhile, the FaultSeg3D model focused on fault delineation, with its output being a binary mask representing the seismic data, where 1 denotes the presence of faults and 0 represents the absence of faults.

Research on fault identification remains crucial in the geological context, as seismic data acquisition has significantly increased and deep convolutional neural networks have been successfully applied. Recent approaches, including [9], have created a large database labeled by experts to supplement synthetic data. A deep CNN based on edge detection has been proposed, producing a pixel-by-pixel binary classification of faults with superior results compared to commonly used CNNs.

6.2 Data Preparation

The dataset utilized in this study comprises two seismic volumes: the input and the target. The dimensions of both volumes are 1401×1481×241 pixels, and they cover an area of approximately 240 km^2, encompassing two pre-salt Santos basin fields. The vertical limit of the volumes is around 2000 m within the area of interest.

The input volume represents the amplitude seismic values of the area, while the target volume contains the faults interpreted from the amplitude seismic. The target volume was generated from 94 interpreted faults, as depicted in Figure 6.1, and used to create a binary model of fault (1) and no-fault (0) scenarios, based on the proximity to faults.
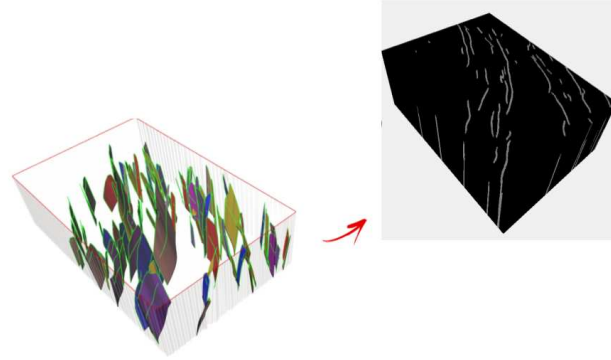
Figure 6.1: Target seismic definition.

From these data, a process of preparing the seismic volumes is carried out. Figure 6.2 shows the four main parts of this phase: data section, data split, data augmentation, and data normalization. Initially, two seismic cubes representing the input and target will be used to generate subsamples that will be augmented to provide the model with a diverse set of inputs.

6.2.1 Pre-Processing

We start by converting the seismic cube and mask into a NumPy array, which are structured in a three-dimensional form. Then, the data is manipulated in 2D sections to
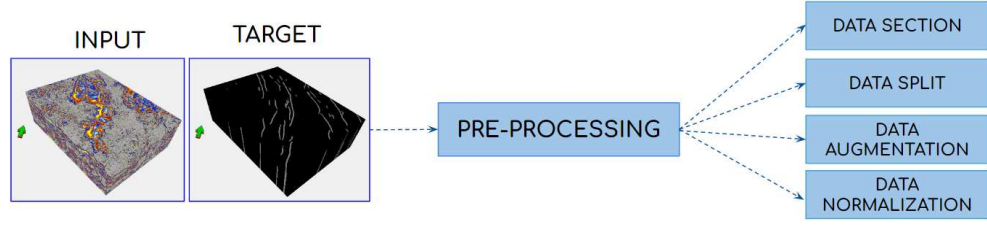
Figure 6.2: Pre-processing diagram.

generate 2D sub-images that can be used to train the model. For this purpose, we extract smaller patches with dimensions $p \times p$ pixels from the seismic inlines, where $p = M$. This method provides a large image dataset with samples that have a conventional square dimensionality suitable for convolutional models.

To avoid repetition of information, the inline region is sectioned into subimages with a $stride = M$, without overlapping, as shown in Figure 6.3. This process generates $\lfloor (n/p) \rfloor$ subimages from each of the treated inline images.
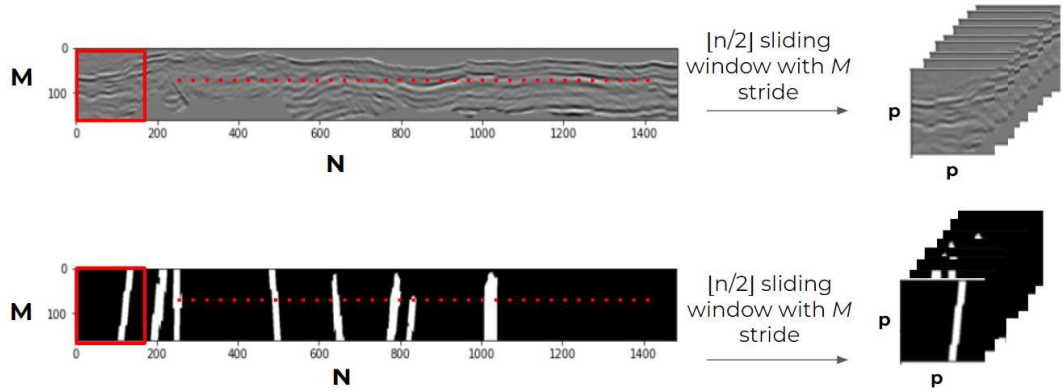
Figure 6.3: Process of data sectioning.

Once the seismic data, input, and target have been prepared, the entire image dataset is randomized and divided into three separate sets: training, validation, and testing. These subsets are partitioned into a ratio of 75%, 15%, and 15% accordingly.

The correspondence between the original seismic and the fault mask is maintained throughout the entire process. Therefore, once the data had been cropped and separated, we opted to apply data augmentation to the images that displayed fault presence. This was necessary since, in this type of task, the majority of the dataset contains images without faults, and classifying pixels one by one tends to be more unbalanced, with more pixels labeled as 0 than as 1 (non-fault/fault) [224].

The augmentation technique applied to the database was the flip transformation. Although there are various geometric transformations that can be used for augmentation, it's important to consider the data domain to ensure that the operations do not introduce errors in the learning process. In this case, flipping was chosen as it preserves the original orientation of faults, which is typically subvertical. By rotating on the vertical axis, the flip operation doubles the number of images, as illustrated in Figure 6.4.

Using the described procedure, we initially generated a database of 9369 sub-images from our seismic dataset, which had a dimension of 1401×1481×160 pixels (in-
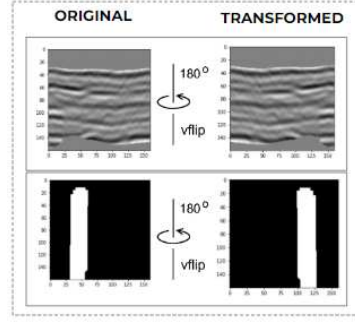
Figure 6.4: Vertical flipping transformation.

line/xlines/crossline). This was achieved by generating $\lfloor (n/p) \rfloor = 9$ images per inline, where $p = 160$. The resulting images were split into 6558 for training, 1405 for validation, and 1406 for testing.

To increase the training and validation sets, data augmentation was applied to all images containing faults, resulting in a 29% increase in the training data and a 36% increase in the test data. As a result, the total number of images in the respective groups became 9242 and 1914.

Finally, all 2D image sections referring to seismic are normalized between -1 and 1, using the following equation:

$$img = 2 \cdot \frac{img[:,:] - \min}{\max - \min} - 1 \qquad (6.1)$$

where img is the 2D image resulting from the normalization, min is the minimum image value, and max is the maximum image value.

6.3 Methods

The TransUNet model, which uses Transformers, is utilized in this work. Given the success of this architecture in the realm of visual computing, our aim is to evaluate its efficacy for fault extraction in heterogeneous seismic fields and compare it with traditional models such as convolutional neural networks. Figure 6.5 shows the training input and the models used in this process.

Figure 6.5: Models used in the training process.

6.3.1 CNN Models

Image classification, a fundamental problem in computer vision, involves categorizing images into predefined classes and serves as the basis for other tasks such as region localization, detection, and segmentation.

The CNNs are one of the most commonly used deep learning networks for this task, named after the linear mathematical operati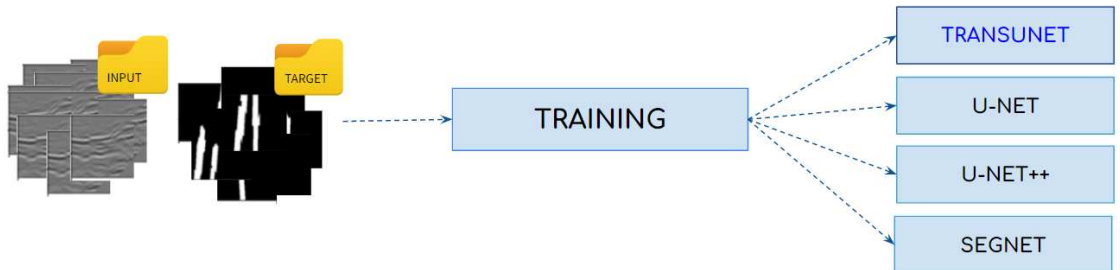on called convolution between matrices [4]. CNNs are a type of feedforward neural networks, meaning that the information flows only in one direction, from the input to the output. Inspired by biological neural networks [171], CNNs differ from regular neural networks in that each unit in a CNN layer is a two-dimensional filter that is convolved with the input of that layer, enabling them to extract local features from images [105].

The convolutional layer of a CNN consists of a two-dimensional filter that convolves with the input feature map. The filter is an array of discrete numbers, where each element is a weight, learned during the training phase. In the beginning, these weights are randomly assigned until the learning process updates them. The CNN architecture includes layers for convolution, pooling to reduce the feature map size, and fully connected layers where each neuron is directly connected to the neurons in the previous and next layers. To gain an understanding of how convolutional networks can be constructed, we will explore three models from the U-Net family and subsequently utilize them to draw comparisons with the Transformer architecture.

U-Net

The original purpose of the U-Net network was to perform segmentation of medical images, and its architecture was an update and extension of the fully connected network. U-Net aimed to improve segmentation accuracy while minimizing the required amount of data [130].

The U-Net architecture, proposed by Ronneberger et al. [176], consists of a contraction path (left side) and an expanding path (right side) for accurate segmentation of medical images. The contraction path has a typical convolutional network architecture, comprising two 3×3 convolutions, each followed by a rectified linear unit (ReLU), and a max-pooling operation with a 2×2 filter and stride 2 for downsampling.

The number of feature channels is doubled at each downsampling step. The expansive path, on the other hand, involves increasing the resolution of the feature map, followed by a 2×2 convolution (half the number of channels), concatenation with the corresponding feature map of the contraction path, and two 3×3 convolutions (each followed by a ReLU). The last layer uses a 1×1 convolution to map the output to the desired number of classes.

U-Net++

[262] developed the U-Net++ architecture with the goal of improving the accuracy of medical image segmentation. This architecture is based on dense and nested skip connections, which provide a new approach to the segmentation task. The U-Net++ architecture was developed to enhance the performance of medical image segmentation by addressing

limitations in previous models.

Zhou et al. [263] proposed an approach that employs multiple U-Nets with different depths, where the encoders and decoders are connected by dense and nested skip connections. The U-Net models share an encoder, while their decoders are interconnected, and deep supervision is used during training to simultaneously train all the constituent U-Nets while benefiting from a shared image representation. The redesigned skip connections in U-Net++ allow for variable-scale feature maps at a decoder node, enabling the aggregation layer to decide how attribute maps carried over the skip connections should be merged with the decoder feature maps.

SegNet

The SegNet [11] is a convolutional neural network architecture designed for semantic pixel segmentation, comprising of an encoder network, a corresponding decoder network, and a pixel-wise classification layer.

The encoder network architecture is similar to that of VGG-16 with 13 convolutional layers. The decoder network also has 13 layers, each corresponding to an encoder layer. The final output of the decoder is fed into a multiclass softmax classifier to generate class probabilities for each pixel. Unlike U-Net, SegNet does not reuse pooling indices but transfers the entire attribute map to the corresponding decoder and concatenates them into upsampled decoder feature maps through deconvolution.

6.3.2 Transformer Models

The Transformer [106, 215] is a recent neural network that utilizes attention operations and was originally developed for Natural Language Processing (NLP), where it has demonstrated remarkable success [90]. In the field of computer vision, the Transformer has been increasingly employed to replace traditional techniques, resulting in various advantages [18].

The Transformer architecture includes an encoder and a decoder, both containing multiple attention blocks with the same architecture. The encoder produces encodings of the input, while the decoder takes these encodings and utilizes its contextual information to generate the output sequence [82]. Specifically, the Transformer encoder is composed of L layers of Multihead Self-Attention (MSA) and Multi-Layer Perceptron (MLP) blocks, alternating between the two. Before each block, Layer Normalization (LN) is applied, and residual connections are used after every block. Finally, the encoded feature representation is upsampled to full resolution to predict the dense output.

The success of the transformer in NLP has encouraged researchers to explore its potential in other areas. Consequently, similar models have been developed to learn useful image representations using the Transformer's concept. The Vision Transformer (ViT) [51], for instance, has proven to be highly effective in several benchmarks, drawing inspiration from the self-attention mechanism in NLP, where word embeddings are substituted by patch embeddings [66].

ViT has paved the way for the development of several other models based on attention mechanisms, which have brought about significant advances in various fields of

computer vision. Surveys conducted by Guo et al. [78] and Han et al. [82] have shown that attention-based methods have been beneficial for tasks such as image classification, semantic segmentation, face recognition, few-shot learning, medical image processing, image resolution, 3D vision, among others.

TransUNet [34] is a model that harnesses the power of Transformers for medical image segmentation. By combining CNN architectures, such as U-Net, which can extract low-level visual features to preserve fine spatial details, and Transformers, which excel in modeling global context, TransUNet creates a powerful hybrid architecture for accurate and efficient medical image segmentation.

TransUNet Architecture

TransUNet combines CNN and Transformer architectures to leverage the spatial details of CNN features and the global context captured by Transformers for medical image segmentation. The model follows a U-shape design, where Transformers establish self-attention mechanisms to encode the features in a sequence-by-sequence prediction perspective. The resulting self-attentive feature is upsampled and combined with high-resolution CNN features that were skipped during encoding, enabling precise localization.

Transformer is used as an encoder by transforming the input image into a sequence of flattened 2D patches through tokenization. To achieve this, the input image x is reshaped into N patches of size $P \times P$, where N is determined by the image's height and width (H and W) and the patch size (P), such that $N = \frac{HW}{P^2}$. A unique marker is assigned to each patch to preserve its positional information in the sequence, and the resulting sequence is fed as input to the encoder.

To recover the spatial order during upsampling, the encoded feature size is reshaped from $\frac{HW}{P^2}$ to $\frac{H}{P} \times \frac{W}{P}$, while the number of channels is reduced to the number of classes using 1×1 convolutions. Finally, the feature map is bilinearly upsampled to the full resolution of $H \times W$ to generate the final segmentation output.

To address the issue of partial information loss resulting from using Transformer solely as an encoder, TransUNet utilizes a hybrid CNN-Transformer architecture that first leverages CNN to extract features from the input, followed by patch embedding of 1×1 patches extracted from the CNN feature map instead of the raw images. Therefore, the sequence of hidden features is reshaped to achieve full resolution from $\frac{H}{P} \times \frac{W}{P}$ to $H \times W$ by applying multiple cascades of upsampling blocks. Each block includes a $2 \times$ upsampling operator, a 3×3 convolution layer, and a ReLU layer in sequence. This enables the aggregation of features at different resolution levels through skip connections.

6.4   Results and Discussions

The presentation and discussion of the results obtained from the trained models, seismic areas reconstruction, and performance metrics are presented using the previously described model.

6.4.1 Experiments

To assess the effectiveness of applying Transformer on seismic data, we utilized the TransUNet model on the database outlined in Section 6.3. Moreover, we employed three additional models that employ the convolutional neural network approach to compare the attained results.

The architectures used were parameterized with identical settings for the loss function, learning rate, and number of epochs to enable comparison of outcomes with the same initialization. An empirical value of $1e-4$ was chosen for the learning rate based on previous evaluations of different values. For the loss function, binary cross-entropy was chosen as it is commonly used for classification purposes and semantic segmentation is a pixel-level classification task. The number of epochs was set to 100 for all models, except for TransUNet where the batch size was reduced to 16 due to its higher memory complexity compared to the other networks.

The results obtained from the execution of all methods are presented in Table 6.1, where it can be observed that the TransUNet network surpasses the other architectures (U-Net, U-Net++, and SegNet) by 2.35%, 4.93%, and 5.03%, respectively, achieving an overall Dice score of 88.34%. Considering the IoU metric, this difference increases to 4.86%, 6.73%, and 7.23%, with TransUNet obtaining a value of 84.34%.

Table 6.1: Quantitative comparison of the segmentation performance in fault detection task.

Models	Metrics					
	Dice	IoU	Accuracy	Precision	Recall	F1-Score
U-Net	0.8599	0.7948	0.9781	0.9258	0.9204	0.9230
U-Net++	0.8341	0.7761	0.9682	0.8852	0.8934	0.8892
SegNet	0.8331	0.7711	0.9570	0.9266	0.8312	0.8763
TransUNet	**0.8834**	**0.8434**	**0.9785**	**0.9303**	**0.9174**	**0.9238**

It is worth noting that the difference between the values obtained by these two metrics is mainly due to the high penalty imposed by the IoU in cases where the classification results are poor. The evaluation of the other metrics confirms the superior performance of the TransUNet network.

The comparisons between the predictions made by the previously presented models are illustrated in Figure 6.6. The results indicate that U-Net and TransUNet produced images that are more similar to the target, while SegNet and U-Net++ exhibit a considerable amount of noise in their outputs. When comparing U-Net and TransUNet, a slightly more accurate border delimitation can be observed in U-Net. This may be due to the greater abstraction of global context extraction in the initial layers of TransUNet.

To conduct a more comprehensive analysis of the performance of the two networks, we reconstructed the slices that were formed by each predicted sub-image. This reconstruction was made possible by the fact that each input image to the network has a corresponding nomenclature that corresponds to the seismic inline and its cut order. Consequently, the training images were predicted in sequential order and their results were concatenated, as illustrated in an example shown in Figure 6.7.
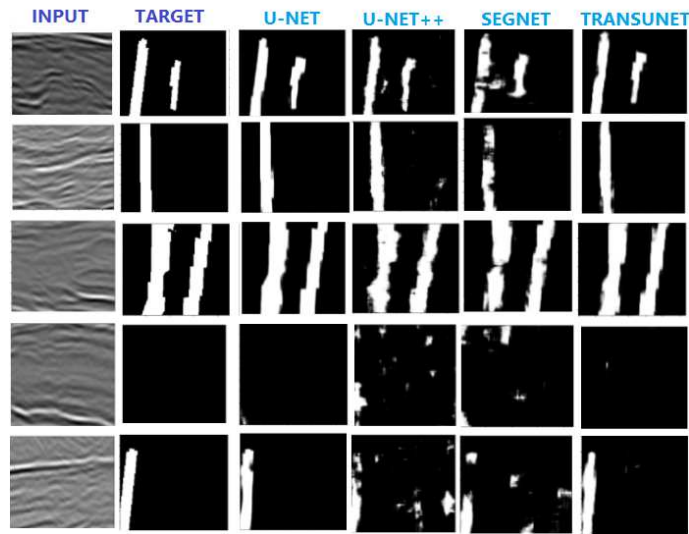
Figure 6.6: Qualitative comparison of different models applied to seismic segmentation.
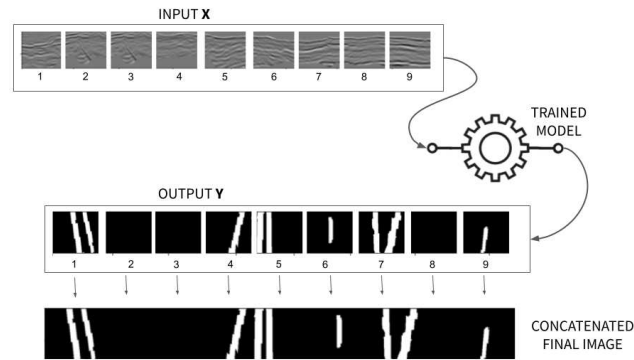
Figure 6.7: Image prediction and concatenation process.

By applying this approach, we can reconstruct the entire seismic volume and examine the output of the two models. Figure 6.8 presents a comparison of the predictions made for two different slices, indicating that both models were able to detect the structures highlighted in the target, as well as some smaller regions, with TransUNet providing a more significant representation of them.
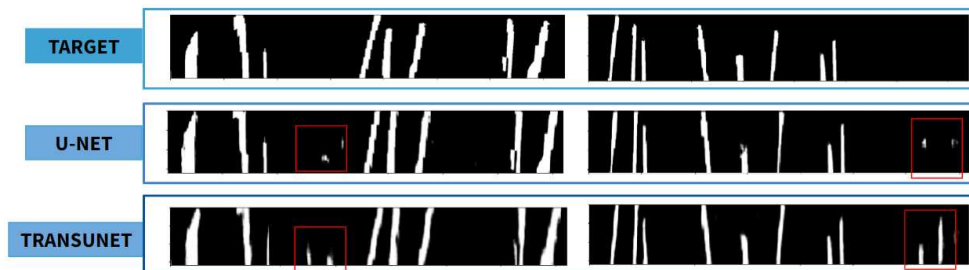
Figure 6.8: Comparison between U-Net and TransUNet predictions.

Upon analyzing the overall result by visualizing the seismic cube prediction, as presented in Figure 6.9, it is evident that both models were able to identify most of the structures present in the target. However, some additional small regions were also detected, which require detailed analysis when viewed in two dimensions, as depicted in

Figure 6.10.
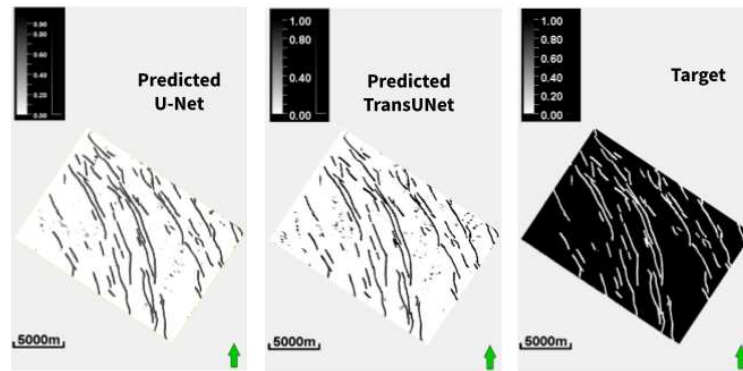
Figure 6.9: Comparison between U-Net and TransUNet prediction in full 3D field.
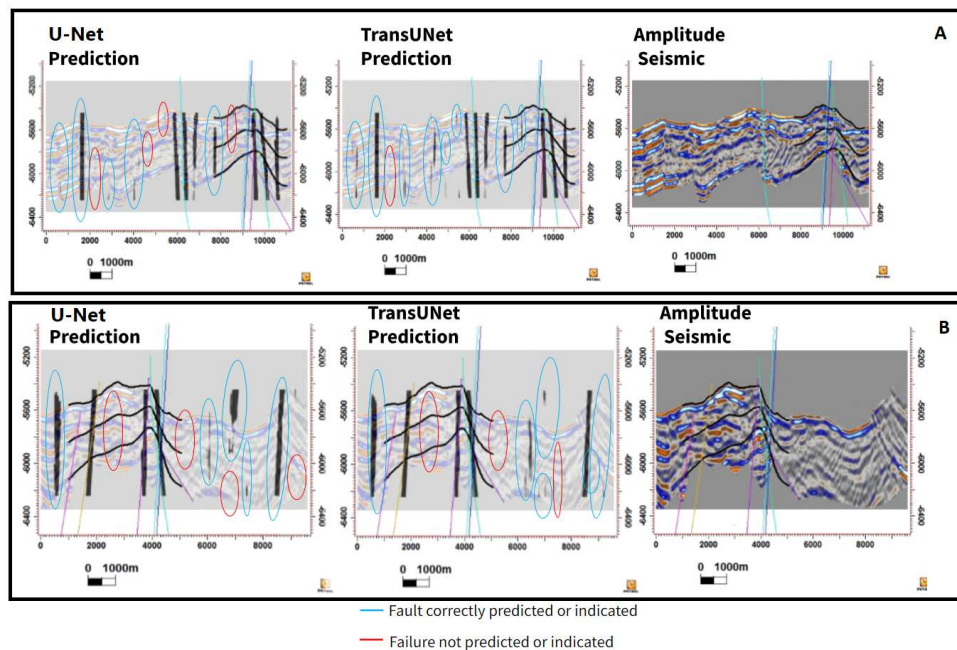
Figure 6.10: Analysis of predicted failures in two different regions, A and B.

The TransUNet prediction achieved slightly better results, with more indicated faults and greater vertical continuity of faults outside the regions present in the target binary cube. Nevertheless, the overall difference between the two methods was minimal.

6.5 Final Considerations

We investigated the use of a hybrid model, TransUNet, which combines the strengths of convolutional networks and Transformer's content abstraction in the geological context. The results demonstrate the effectiveness of this approach in segmenting seismic images from a heterogeneous environment, such as the pre-salt layer, indicating potential applications of this architecture in various configurations for identifying and extracting geological structures in the field of seismic imaging.

The effectiveness of TransUNet in fault identification on seismic data was demonstrated by comparing it to conventional state-of-the-art methods. This study concludes

that the incorporation of Transformer in this context has the potential to extract valuable information from seismic databases. The evaluation included both qualitative and quantitative approaches, suggesting that this new type of architecture could serve as a benchmark for other databases considering the use of TransUNet in the field of visual computing.

Chapter 7

Conclusions and Future Work

The increasing prevalence of computer vision techniques, in specific machine learning and image processing, in reservoir characterization is a response to the manifold challenges inherent in manual analysis. The efficiency and agility afforded by these techniques have proven to be valuable allies to analyses previously conducted in laboratories.

Through this research, it was possible to perceive the various difficulties that researchers faced, such as: the large amount of data to be analyzed, the difficulty of distinguishing structures in rocks, obstructions in the sample preventing the replication of experiments and also the generation of a subjective result given the interpreter experience. In this way, the use of images has enabled a new approach to research, where the computer vision field serves as the means of interaction with this data, facilitating the provision of effective tools to handle diverse information across various data scales.

In this research, we contextualize both, computer techniques and the challenges associated with reservoir characterization, providing an overview of the state of the art in this field. Additionally, we present practical methodologies developed to address some of the key challenges encountered in the routine of geological analysis and interpretation. In this way, through the work carried out, it was possible to answer the research questions listed in Chapter 1:

- **How can computer vision and its techniques contribute across different stages of reservoir characterization, from data acquisition to final modeling?**

  The use of computer vision in reservoir characterization brings, as its main contribution, the possibility of optimizing and automating various activities of the geological workflow. As demonstrated in the extensive literature review presented in Chapter 2, computational methods promote the manipulation of different types of data where the required complexity can be adapted to the available resources, making it possible to gain efficiency through the application of simple image processing algorithms to elaborate deep learning models. Furthermore, its use enables the manipulation of large volumes of data, the identification of complex patterns, and the reduction of the time required for analysis.

- **Which computational tools/techniques have been most relevant in the geological context that encompasses the characterization of reservoirs?**

During the course of the research, it became evident that the Python programming language has emerged as a fundamental tool in some computational tasks of the characterization of geological reservoirs. Python offers a wide range of libraries for data manipulation, such as Pandas and NumPy, and for image processing, such as OpenCV and Pillow. Additionally, Python facilitates the construction and training of machine learning models through libraries like TensorFlow, Keras, and PyTorch.

Besides that, one technique that particularly stands out in the analysis of geological images is the convolutional neural networks. These networks have shown great versatility and effectiveness. For example, models based on U-Net are widely used due to their ability to perform precise segmentations, which are essential for identifying specific geological features, and, models like ResNet have been successfully applied to the classification of different types of rocks and structures. Furthermore, other architectures that incorporate advanced techniques such as attention, transformers, and GANs have been developed to enhance the abstraction and understanding of complex geological data.

In Chapters 6 and 5, we used convolutional neural networks to address two critical problems in reservoir characterization: fault detection and facies classification. We made use of transformers and a U-Net based architecture, known for their advanced semantic understanding capabilities. The application of these techniques demonstrated high effectiveness in the analysis and interpretation of geological data, underscoring the importance of modern computational tools in the field of geology.

- **What are the benefits associated with the use of Transformers in fault identification?**

Through the results presented in Chapter 6, it was possible to perceive that the insertion of Transformers in convolutional networks enabled a step forward in the identification of complex structures due to its ability to capture long-range relationships between data and dynamically adapt to the context of the problem.

- **How can convolutional models enhance facies classification?**

Convolutional networks already have a great recognition in their ability to abstract data and segment images. In the multi-class classification task presented in Chapter 5, the power of this technology proved capable of providing an accurate facies model, further enhancing the manual labeling performed for dataset construction even with fewer filters and depth architecture, allowing the objective to be achieved quickly and still effectively.

- **What is the impact of applying image processing techniques on improving the quality of noisy well images?**

A high-quality image enables a more precise evaluation of metrics such as porosity and permeability, and facilitates accurate mapping of features such as pores, caverns, and fractures. Consequently, enhancing image quality empowers professionals to conduct analyses with greater speed and accuracy. Furthermore, these improved

images can serve as input for intelligent models capable of extracting valuable insights from well-processed data.

In summary, the applications outlined here play a pivotal role in the comprehensive lifecycle of image utilization – from capturing by diverse sources, to enhancing their quality, extracting features, analyzing parameters, estimating properties, generating information, and classifying attributes. All these steps were distributed across two major pillars of visual computing: image processing and deep learning models.

The integration of these techniques represents a substantial leap forward in geological research, providing a comprehensive approach to reservoir characterization, but also highlights the importance of computational techniques as a tool for optimizing the processes described here. The persistent challenges and the evolving collaboration between these two major fields underscore the continual significance and vast potential of computer vision techniques, where this progression continues to reshape our understanding and management of geological reservoirs.

In the future, this work can be extended in several ways. In the following, we outline some potential directions for future research:

- Investigation of a way to integrate data from different sources, such as seismic data, well data, and surface images, to obtain a more comprehensive and accurate view of reservoirs.

- Transformation of the developed practical applications into software tools for application in other datasets.

- Development and enhancement of computer vision algorithms to handle more complex and heterogeneous geological data, enabling transfer learning to other geological systems such as basins from other formations.

- Incorporation of machine learning applications into other routines of reservoir characterization.

Bibliography

[1] M. Abadi, P. Barham, J. Chen, Z. Chen, A. Davis, J. Dean, M. Devin, S. Ghemawat, G. Irving, and M. Isard. Tensorflow: A system for large-scale machine learning. In *12th USENIX Symposium on Operating Systems Design and Implementation*, pages 265–283, 2016. 39, 44

[2] M. D. Abràmoff, P. J. Magalhães, and S. J. Ram. Image processing with ImageJ. *Biophotonics International*, 11(7):36–42, 2004. 39

[3] S. S. Al-amri, N. Kalyankar, and S. Khamitkar. Image Segmentation by Using Thershod Techniques, 2010. 32

[4] S. Albawi, T. A. Mohammed, and S. Al-Zawi. Understanding of a convolutional neural network. In *International Conference on Engineering and Technology*, pages 1–6. IEEE, 2017. 35, 68

[5] M. Alfarhan, M. Deriche, and A. Maalej. Robust concurrent detection of salt domes and faults in seismic surveys using an improved UNet architecture. *IEEE Access*, 10:39424–39435, 2020. 37

[6] H. N. Alsadi. *Seismic Hydrocarbon Exploration*. Springer, 2017. 28, 29

[7] F. Alzubaidi, P. Mostaghimi, G. Si, P. Swietojanski, and R. T. Armstrong. Automated rock quality designation using convolutional neural networks. *Rock Mechanics and Rock Engineering*, 55(6):3719–3734, 2022. 37

[8] F. Aminzadeh and S. N. Dasgupta. *Geophysics for Petroleum Engineers*. Newnes, 2013. 29

[9] Y. An, J. Guo, Q. Ye, C. Childs, J. Walsh, and R. Dong. Deep convolutional neural network for automatic fault recognition from 3D seismic datasets. *Computers & Geosciences*, 153:104776, 2021. 65

[10] S. Asghar, J. Choi, D. Yoon, and J. Byun. Spatial pseudo-labeling for semi-supervised facies classification. *Journal of Petroleum Science and Engineering*, 195: 107834, 2020. 54

[11] V. Badrinarayanan, A. Kendall, and R. Cipolla. SegNet: A deep convolutional encoder-decoder architecture for image segmentation. *IEEE Transactions on Pattern Analysis and Machine Intelligence*, 39(12):2481–2495, 2017. 69

[12] R. Basirat, K. Goshtasbi, and M. Ahmadi. Determination of the fractal dimension of the fracture network system using image processing technique. *Fractal and Fractional*, 3(2):17, 2019. 22, 34

[13] M. Basso, J. P. P. Souza, B. C. Z. Honório, L. H. Melani, G. F. Chinelatto, A. M. P. Belila, and A. C. Vidal. Acoustic image log facies and well log petrophysical evaluation of the Barra Velha Formation carbonate reservoir from the Santos Basin, offshore Brazil. *Carbonates and Evaporites*, 37(3):50, 2022. 16

[14] K. Bauer, B. Norden, A. Ivanova, M. Stiller, and C. M. Krawczyk. Wavelet transform-based seismic facies classification and modelling: application to a geothermal target horizon in the NE German Basin. *Geophysical Prospecting*, 68(2):466–482, 2020. 22

[15] A. M. P. Belila, M. Basso, G. F. Chinelatto, M. C. Kuroda, and A. C. Vidal. Pore typing using nuclear magnetic resonance, an example with samples from cretaceous pre-salt lacustrine carbonates in the Santos Basin, Brazil. *Journal of Petroleum Science and Engineering*, 190:107079, 2020. 16

[16] C. F. Berg, O. Lopez, and H. Berland. Industrial applications of digital rock technology. *Journal of Petroleum Science and Engineering*, 157:131–147, 2017. 24

[17] J. Bernse. Dynamic thresholding of grey-level images. In *8th International Conference on Pattern Recognition*, pages 1251–1255, 1986. 48

[18] J. Bi, Z. Zhu, and Q. Meng. Transformer in computer vision. In *IEEE International Conference on Computer Science, Electronic Information Engineering and Intelligent Control Technology*, pages 178–188. IEEE, 2021. 69

[19] A. Bihani, H. Daigle, J. E. Santos, C. Landry, M. Prodanović, and K. Milliken. MudrockNet: Semantic segmentation of mudrock SEM images through deep learning. *Computers & Geosciences*, 158:104952, 2022. 26, 31

[20] C. R. Bom, M. B. Valentín, B. M. Fraga, J. Campos, B. Coutinho, L. O. Dias, E. L. Faria, M. P. de Albuquerque, M. P. de Albuquerque, and M. D. Correia. Bayesian deep networks for absolute permeability and porosity uncertainty prediction from image borehole logs from Brazilian carbonate reservoirs. *Journal of Petroleum Science and Engineering*, 201:108361, 2021. 22, 28

[21] L. Bomfim and H. Pedrini. Characterization of Fracture Geometry with Computed Microtomography Rock Images. In *XXIII Brazilian Symposium on GeoInformatics*, Nov. 2022. 45

[22] L. Bomfim, O. Cunha, M. Kuroda, A. Vidal, and H. Pedrini. Transformer Model for Fault Detection from Brazilian Pre-salt Seismic Data. In *Brazilian Conference on Intelligent Systems*, pages 3–17. Springer, 2023. 64

[23] A. Boyat and B. K. Joshi. Image denoising using wavelet transform and median filtering. In *Nirma University International Conference on Engineering (NUiCONE)*, pages 1–6. IEEE, 2013. 31

[24] G. Bradski. The openCV library. *Dr. Dobb's Journal: Software Tools for the Professional Programmer*, 25(11):120–123, 2000. 44

[25] L. V. Branets, S. S. Ghai, S. L. Lyons, and X.-H. Wu. Challenges and technologies in reservoir modeling. *Communications in Computational Physics*, 6(1):1, 2009. 16

[26] L. Brown Jr and W. Fisher. Seismic-stratigraphic interpretation of depositional systems: examples from Brazilian rift and pull-apart basins: Section 2. Application of seismic reflection configuration to stratigraphic interpretation. *AAPG Special Volumes*, 26:51–53, 1977. 53

[27] E. Bryant. *Climate Process and Change.* Cambridge University Press, 1997. 23

[28] L. Buryakovsky, G. V. Chilingar, H. H. Rieke, and S. Shin. *Fundamentals of the Petrophysics of Oil and Gas Reservoirs.* John Wiley & Sons, 2012. 22

[29] J. G. Cady. Petrographic microscope techniques. *Methods of Soil Analysis: Part 1 Physical and Mineralogical Properties, Including Statistics of Measurement and Sampling*, 9:604–631, 1965. 26

[30] S. W. Canchumuni, A. A. Emerick, and M. A. C. Pacheco. History matching geological facies models based on ensemble smoother and deep generative models. *Journal of Petroleum Science and Engineering*, 177:941–958, 2019. 22

[31] O. Catuneanu. *Principles of Sequence Stratigraphy.* Newnes, 2022. 54

[32] H. K. Chang, M. L. Assine, F. S. Corrêa, J. S. Tinen, A. C. Vidal, and L. Koike. Sistemas petrolíferos e modelos de acumulação de hidrocarbonetos na Bacia de Santos. *Revista Brasileira de Geociências*, 38(2 suppl):29–46, 2008. 17

[33] G. Chen, M. Chen, G. Hong, Y. Lu, B. Zhou, and Y. Gao. A new method of lithology classification based on convolutional neural network algorithm by utilizing drilling string vibration data. *Energies*, 13(4):888, 2020. 22

[34] J. Chen, Y. Lu, Q. Yu, X. Luo, E. Adeli, Y. Wang, L. Lu, A. L. Yuille, and Y. Zhou. Trans-UNet: Transformers make strong encoders for medical image segmentation. *arXiv preprint arXiv:2102.04306*, 2021. 70

[35] Z. Chen, X. Liu, J. Yang, E. Little, and Y. Zhou. Deep learning-based method for SEM image segmentation in mineral characterization, an example from Duvernay Shale samples in Western Canada Sedimentary Basin. *Computers & Geosciences*, 138:104450, 2020. 26, 31, 37

[36] F. Chollet. Keras, 2015. `https://github.com/fchollet/keras`. 39, 44

[37] F. Chollet. *Deep Learning with Python.* Simon and Schuster, 2021. 39

[38] P. W. Choquette and L. C. Pray. Geologic nomenclature and classification of porosity in sedimentary carbonates. *AAPG Bulletin*, 54(2):207–250, 1970. 21

[39] V. Cnudde and M. N. Boone. High-resolution X-ray computed tomography in geosciences: A review of the current technology and applications. *Earth-Science Reviews*, 123:1–17, 2013. 27

[40] W. R. Crum, O. Camara, and D. L. Hill. Generalized overlap measures for evaluation and validation in medical image analysis. *IEEE Transactions on Medical Imaging*, 25(11):1451–1461, 2006. 43

[41] X. Cui, A. Bustin, and R. M. Bustin. Measurements of gas permeability and diffusivity of tight reservoir rocks: different approaches and their applications. *Geofluids*, 9(3):208–223, 2009. 22

[42] L. da Silva Bomfim, H. Pedrini, and A. C. Vidal. A Combined Noisy Borehole Image Log Segmentation Method. In *International Conference on Systems, Signals and Image Processing*, volume 30, pages 1–5, Ohrid, North Macedonia, 2023. 45

[43] A. Dash, J. Ye, and G. Wang. A review of Generative Adversarial Networks (GANs) and its applications in a wide variety of disciplines–From Medical to Remote Sensing. *arXiv preprint arXiv:2110.01442*, 2021. 36, 38

[44] R. Dashti and H. Rahimpour-Bonab. The effect of mechanical stratigraphy on natural fractures morphology and distribution in carbonate reservoirs. *Journal of Petroleum Science and Engineering*, 217:110915, 2022. 45

[45] L. S. de Souza and G. N. C. Sgarbi. Bacia de Santos no Brasil: geologia, exploração e produção de petróleo e gás natural. *Boletín de Geología*, 41(1):175–195, 2019. 15

[46] C. A. DePaolo and K. Wilkinson. Get your head into the clouds: Using word clouds for analyzing qualitative assessment data. *TechTrends*, 58(3):38–4, 2014. 30

[47] K. G. Dhal, A. Das, S. Ray, J. Gálvez, and S. Das. Histogram equalization variants as optimization problems: A review. *Archives of Computational Methods in Engineering*, 28:1471–1496, 2021. 46

[48] H. Di. Developing a seismic pattern interpretation network (SpiNet) for automated seismic interpretation. *arXiv preprint arXiv:1810.08517*, 2018. 17

[49] H. Di, D. Gao, and G. AlRegib. Developing a seismic texture analysis neural network for machine-aided seismic pattern recognition and classification. *Geophysical Journal International*, 218(2):1262–1275, 2019. 54

[50] H. Dong and R. Ma. Application and Research of Dark Channel Defogging Algorithm in Video Logging Image Enhancement. In *6th International Conference on Intelligent Computing and Signal Processing*, pages 162–165. IEEE, 2021. 45

[51] A. Dosovitskiy, L. Beyer, A. Kolesnikov, D. Weissenborn, X. Zhai, T. Unterthiner, M. Dehghani, M. Minderer, G. Heigold, and S. Gelly. An image is worth 16×16 words: Transformers for image recognition at scale. *arXiv preprint arXiv:2010.11929*, 2020. 69

[52] Y. Dou, K. Li, J. Zhu, X. Li, and Y. Xi. Attention-based 3-D seismic fault segmentation training by a few 2-D slice labels. *IEEE Transactions on Geoscience and Remote Sensing*, 60:1–15, 2021. 22, 31, 37

[53] H.-k. Du, J.-x. Cao, Y.-j. Xue, and X.-j. Wang. Seismic facies analysis based on self-organizing map and empirical mode decomposition. *Journal of Applied Geophysics*, 112:52–61, 2015. 54

[54] S. Du. Prediction of permeability and its anisotropy of tight oil reservoir via precise pore-throat tortuosity characterization and "umbrella deconstruction" method. *Journal of Petroleum Science and Engineering*, 178:1018–1028, 2019. 22, 23, 26

[55] S. Du. Pore characterization of unconventional reservoirs. *Natural Gas Industry B*, 9(4):365–375, 2022. 21

[56] C. M. Ellamey and A. M. Attia. Enhanced Reservoir Characterization Using Petrographic Image Analysis. *Petroleum & Coal*, 64(3), 2022. 27, 40

[57] A. Elrahmani, R. I. Al-Raoush, H. Abugazia, and T. Seers. Pore-scale simulation of fine particles migration in porous media using coupled CFD-DEM. *Powder Technology*, 398:117130, 2022. 27

[58] Equinor. Segyio, 2018. https://segyio.readthedocs.io/en/latest/. 44

[59] D. N. Espinoza, I. Shovkun, O. Makni, and N. Lenoir. Natural and induced fractures in coal cores imaged through X-ray computed microtomography—Impact on desorption time. *International Journal of Coal Geology*, 154:165–175, 2016. 22, 27

[60] L. Fan, F. Zhang, H. Fan, and C. Zhang. Brief review of image denoising techniques. *Visual Computing for Industry, Biomedicine, and Art*, 2:1–12, 2019. 31

[61] F. Fernández-Ibáñez, J. DeGraff, and F. Ibrayev. Integrating borehole image logs with core: A method to enhance subsurface fracture characterization. *AAPG Bulletin*, 102(6):1067–1090, 2018. 45

[62] D. J. A. Ferreira, W. M. Lupinacci, I. de Andrade Neves, J. P. R. Zambrini, A. L. Ferrari, L. A. P. Gamboa, and M. O. Azul. Unsupervised seismic facies classification applied to a presalt carbonate reservoir, Santos Basin, offshore Brazil. *AAPG Bulletin*, 103(4):997–1012, 2019. 54

[63] A. I. Fischetti and A. Andrade. Porosity images from well logs. *Journal of Petroleum Science and Engineering*, 36(3-4):149–158, 2002. 45

[64] E. M. FitzGerald, C. J. Bean, and R. Reilly. Fracture-frequency prediction from borehole wireline logs using artificial neural networks. *Geophysical Prospecting*, 47 (6):1031–1044, 1999. 45

[65] Q. Fu, Z. Zhang, M. Celenk, and A. Wu. A POSHE-based optimum clip-limit contrast enhancement method for ultrasonic logging images. *Sensors*, 18(11):3954, 2018. 45

[66] Z. Fu. Vision Transformer: ViT and its Derivatives. *arXiv e-prints*, pages arXiv–2205, 2022. 69

[67] F. Fueten. A computer-controlled rotating polarizer stage for the petrographic microscope. *Computers & Geosciences*, 23(2):203–208, 1997. 26

[68] P. Gaillot, T. Brewer, P. Pezard, and E.-C. Yeh. Borehole imaging tools-principles and applications. *Scientific Drilling*, 5(5):1–5, 2007. 27

[69] Z. Gao, K. Wang, Z. Wang, and J. Gao. Optimizing seismic facies classification through differentiable network architecture search. *IEEE Transactions on Geoscience and Remote Sensing*, 2024. 54

[70] A. Garcia-Garcia, S. Orts-Escolano, S. Oprea, V. Villena-Martinez, P. Martinez-Gonzalez, and J. Garcia-Rodriguez. A survey on deep learning techniques for image and video semantic segmentation. *Applied Soft Computing*, 70:41–65, 2018. 42

[71] N. Golsanami, M. N. Jayasuriya, W. Yan, S. G. Fernando, X. Liu, L. Cui, X. Zhang, Q. Yasin, H. Dong, and X. Dong. Characterizing clay textures and their impact on the reservoir using deep learning and Lattice-Boltzmann simulation applied to SEM images. *Energy*, 240:122599, 2022. 26, 37, 39

[72] R. Gomila, G. Arancibia, D. Mery, M. Nehler, R. Bracke, and D. Morata. Palaeopermeability anisotropy and geometrical properties of sealed-microfractures from micro-CT analyses: An open-source implementation. *Micron*, 117:29–39, 2019. 22, 27

[73] K. Gonzalez and S. Misra. Unsupervised learning monitors the carbon-dioxide plume in the subsurface carbon storage reservoir. *Expert Systems with Applications*, 201: 117216, 2022. 23

[74] R. C. Gonzalez and R. E. Woods. *Digital Image Processing*. Pearson Education, 2007. 30, 48

[75] I. Goodfellow, J. Pouget-Abadie, M. Mirza, B. Xu, D. Warde-Farley, S. Ozair, A. Courville, and Y. Bengio. Generative Adversarial Nets. *Advances in Neural Information Processing Systems*, 27, 2014. 33, 36

[76] I. Goodfellow, Y. Bengio, and A. Courville. *Deep Learning*. MIT Press, 2016. 35, 36

[77] J. Goral, M. Andrew, T. Olson, and M. Deo. Correlative core-to pore-scale imaging of shales. *Marine and Petroleum Geology*, 111:886–904, 2020. 21

[78] M.-H. Guo, T.-X. Xu, J.-J. Liu, Z.-N. Liu, P.-T. Jiang, T.-J. Mu, S.-H. Zhang, R. R. Martin, M.-M. Cheng, and S.-M. Hu. Attention mechanisms in computer vision: A survey. *Computational Visual Media*, pages 1–38, 2022. 70

[79] C. Guoxi, J. Bo, L. Ming, L. Fengli, and X. Shaochun. Quantitative characterization of fracture structure in coal based on image processing and multifractal theory. *International Journal of Coal Geology*, 228:103566, 2020. 21, 22, 34

[80] K. D. Gupta, V. Vallega, H. Maniar, P. Marza, H. Xie, K. Ito, and A. Abubakar. A deep-learning approach for borehole image interpretation. In *SPWLA 60th Annual Logging Symposium*. OnePetro, 2019. 28, 45

[81] F. Han, H. Zhang, J. Rui, K. Wei, D. Zhang, and W. Xiao. Multiple point geostatistical simulation with adaptive filter derived from neural network for sedimentary facies classification. *Marine and Petroleum Geology*, 118:104406, 2020. 22

[82] K. Han, Y. Wang, H. Chen, X. Chen, J. Guo, Z. Liu, Y. Tang, A. Xiao, C. Xu, and Y. Xu. A Survey on Vision Transformer. *IEEE Transactions on Pattern Analysis and Machine Intelligence*, abs/2012.12556:1–20, 2022. 69, 70

[83] P. Heckbert. Color image quantization for frame buffer display. *ACM Siggraph Computer Graphics*, 16(3):297–307, 1982. 47

[84] R. Herlinger Jr, L. F. De Ros, R. Surmas, and A. Vidal. Residual oil saturation investigation in Barra Velha Formation reservoirs from the Santos Basin, Offshore Brazil: A sedimentological approach. *Sedimentary Geology*, 448:106372, 2023. 16

[85] S. Homuth, A. E. Götz, and I. Sass. Physical properties of the geothermal carbonate reservoirs of the Molasse Basin, Germany—outcrop analogue vs. reservoir data. In *World Geothermal Congress*, pages 19–24, 2015. 24

[86] E. Hosseini-Fard, A. Roshandel-Kahoo, M. Soleimani-Monfared, K. Khayer, and A. R. Ahmadi-Fard. Automatic seismic image segmentation by introducing a novel strategy in histogram of oriented gradients. *Journal of Petroleum Science and Engineering*, 209:109971, 2022. 22, 31

[87] J. Howse. *OpenCV Computer Vision with Python*, volume 27. Packt Publishing Birmingham, 2013. 39

[88] F. Hu, C. Wu, J. Shang, Y. Yan, L. Wang, and H. Zhang. Multi-condition controlled sedimentary facies modeling based on generative adversarial network. *Computers & Geosciences*, 171:105290, 2023. 22, 38

[89] L. Huang, X. Dong, and T. E. Clee. A scalable deep learning platform for identifying geologic features from seismic attributes. *The Leading Edge*, 36(3):249–256, 2017. 42

[90] M. Huang, X. Zhu, and J. Gao. Challenges in building intelligent open-domain dialog systems. *ACM Transactions on Information Systems*, 38(3):1–32, 2020. 69

[91] J. D. Hunter. Matplotlib: A 2D graphics environment. *Computing in Science & Engineering*, 9(03):90–95, 2007. 44

[92] M. V. Jacinto, A. D. D. Neto, D. L. de Castro, and F. H. Bezerra. Karstified zone interpretation using deep learning algorithms: Convolutional neural networks applications and model interpretability with explainable AI. *Computers & Geosciences*, 171:105281, 2023. 37, 54

[93] B. Jähne and H. Haußecker. *Computer Vision and Applications*. Academic Press, 2000. 17

[94] M. Jardine, J. Miller, and M. Becker. Coupled X-ray computed tomography and grey level co-occurrence matrices as a method for quantification of mineralogy and texture in 3D. *Computers & Geosciences*, 111:105–117, 2018. 27

[95] J. Jeong, E. Park, I. Emelyanova, M. Pervukhina, L. Esteban, and S.-T. Yun. Interpreting the subsurface lithofacies at high lithological resolution by integrating information from well-log data and rock-core digital images. *Journal of Geophysical Research: Solid Earth*, 125(2), 2020. 45

[96] A. Jia, D. He, and C. Jia. Advances and challenges of reservoir characterization: A review of the current state-of-the-art. *Earth Sciences*, 1, 2012. 15, 16

[97] M. Jia, W. Huang, and Y. Li. Quantitative Characterization of Pore Structure Parameters in Coal Based on Image Processing and SEM Technology. *Energies*, 16 (4):1663, 2023. 26

[98] M. Jia, W. Huang, and Y. Li. Quantitative Characterization of Pore Structure Parameters in Coal Based on Image Processing and SEM Technology. *Energies*, 16 (4):1663, 2023. 21, 34, 39

[99] J. Jiang, R. Xu, S. C. James, and C. Xu. Deep-Learning-based Vuggy Facies Identification from borehole images. *SPE Reservoir Evaluation & Engineering*, 24(01): 250–261, 2021. 45

[100] K. Jiao, S. Yao, C. Liu, Y. Gao, H. Wu, M. Li, and Z. Tang. The characterization and quantitative analysis of nanopores in unconventional gas reservoirs utilizing FESEM–FIB and image processing: An example from the lower Silurian Longmaxi Shale, upper Yangtze region, China. *International Journal of Coal Geology*, 128: 1–11, 2014. 21, 26, 34

[101] Z. Jiao, Q. Xing, J. Zhang, J. Wang, and Y. Wang. Gravel Extraction from FMI Based on DSAM-DeepLabV3+ Network. In *16th IEEE International Conference on Signal Processing*, volume 1, pages 405–410. IEEE, 2022. 28

[102] X. Jin, K. Zhang, J. Pan, J. Gu, H. Zheng, and J. Zeng. Improving seismic facies classification and estimating uncertainty through Label Refinery. In *3rd International Conference on Electronic Information Engineering and Computer (EIECT)*, pages 284–287. IEEE, 2023. 54

[103] D. J. Jobson, Z.-u. Rahman, and G. A. Woodell. A multiscale retinex for bridging the gap between color images and the human observation of scenes. *IEEE Transactions on Image Processing*, 6(7):965–976, 1997. 47, 48

[104] R. A. Ketcham and W. D. Carlson. Acquisition, optimization and interpretation of X-ray computed tomographic imagery: applications to the geosciences. *Computers & Geosciences*, 27(4):381–400, 2001. 26, 27

[105] S. Khan, H. Rahmani, S. A. A. Shah, and M. Bennamoun. A guide to convolutional neural networks for computer vision. *Synthesis Lectures on Computer Vision*, 8(1): 1–207, 2018. 68

[106] S. Khan, M. Naseer, M. Hayat, S. W. Zamir, F. S. Khan, and M. Shah. Transformers in Vision: A Survey. *ACM Computing Surveys*, 54(10s):1–41, 2022. 69

[107] S. E. Kim, H. Yoon, and J. Lee. Fast and scalable earth texture synthesis using spatially assembled generative adversarial neural networks. *Journal of Contaminant Hydrology*, 243:103867, 2021. 38

[108] J. Kittler and J. Illingworth. Minimum error thresholding. *Pattern Recognition*, 19 (1):41–47, 1986. 48

[109] A. Klokov and B. Hardage. Seismic characterization and monitoring of a deep CO_2 storage reservoir with 3D VSP using direct shear waves. *Journal of Petroleum Science and Engineering*, 155:109–119, 2017. 23

[110] M. A. Knackstedt, S. Latham, M. Madadi, A. Sheppard, T. Varslot, and C. Arns. Digital rock physics: 3D imaging of core material and correlations to acoustic and flow properties. *The Leading Edge*, 28(1):28–33, 2009. 24

[111] A. Koeshidayatullah. Optimizing image-based deep learning for energy geoscience via an effortless end-to-end approach. *Journal of Petroleum Science and Engineering*, 215:110681, 2022. 33

[112] A. Koeshidayatullah, M. Morsilli, D. J. Lehrmann, K. Al-Ramadan, and J. L. Payne. Fully automated carbonate petrography using deep convolutional neural networks. *Marine and Petroleum Geology*, 122:104687, 2020. 37

[113] M. J. Kumar, D. G. R. Kumar, and R. V. K. Reddy. Review on image segmentation techniques. *International Journal of Scientific Research Engineering & Technology*, 3(6):993–997, 2014. 32

[114] S. Kwon, G. Park, Y. Jang, J. Cho, M.-g. Chu, and B. Min. Determination of oil well placement using convolutional neural network coupled with robust optimization under geological uncertainty. *Journal of Petroleum Science and Engineering*, 201: 108118, 2021. 37

[115] J. Lai, G. Wang, Z. Fan, J. Chen, S. Wang, and X. Fan. Sedimentary characterization of a braided delta using well logs: the upper triassic xujiahe formation in central sichuan basin, china. *Journal of Petroleum Science and Engineering*, 154: 172–193, 2017. 27

[116] J. Lai, G. Wang, S. Wang, J. Cao, M. Li, X. Pang, C. Han, X. Fan, L. Yang, Z. He, et al. A review on the applications of image logs in structural analysis and sedimentary characterization. *Marine and Petroleum Geology*, 95:139–166, 2018. 45

[117] J. Lai, X. Pang, Q. Xiao, Y. Shi, H. Zhang, T. Zhao, J. Chen, G. Wang, and Z. Qin. Prediction of Reservoir Quality in Carbonates via Porosity Spectrum from Image Logs. *Journal of Petroleum Science and Engineering*, 173:197–208, 2019. 45

[118] E. H. Land and J. J. McCann. Lightness and Retinex Theory. *Josa*, 61(1):1–11, 1971. 46

[119] K. Larssen, K. Senger, and S.-A. Grundvåg. Fracture characterization in Upper Permian carbonates in Spitsbergen: A workflow from digital outcrop to geo-model. *Marine and Petroleum Geology*, 122:104703, 2020. 22

[120] Y. Lee, B. Kang, J. Kim, and J. Choe. Model Regeneration Scheme Using a Deep Learning Algorithm for Reliable Uncertainty Quantification of Channel Reservoirs. *Journal of Energy Resources Technology*, 144(9):093004, 2022. 38

[121] B. Li and Y. E. Li. Neural network-based CO_2 interpretation from 4D sleipner seismic images. *Journal of Geophysical Research: Solid Earth*, 126(12):e2021JB022524, 2021. 23, 37

[122] B. Li, X. Tan, F. Wang, P. Lian, W. Gao, and Y. Li. Fracture and vug characterization and carbonate rock type automatic classification using X-ray CT images. *Journal of Petroleum Science and Engineering*, 153:88–96, 2017. 27, 34

[123] K. Li, W. Liu, Y. Dou, Z. Xu, H. Duan, and R. Jing. CONSS: Contrastive Learning Method for Semi-Supervised Seismic Facies Classification. *IEEE Journal of Selected Topics in Applied Earth Observations and Remote Sensing*, 16:7838–7849, 2023. 54

[124] S. Li, B. Fu, J. Wei, Y. Lv, Q. Wang, and J. Tu. Ultrasonic Logging Image Denoising Based on CNN and Feature Attention. *IEEE Access*, 9:116845–116856, 2021. 45

[125] X. Li, Y. Lu, X. Zhang, W. Fan, Y. Lu, and W. Pan. Quantification of macropores of Malan loess and the hydraulic significance on slope stability by X-ray computed tomography. *Environmental Earth Sciences*, 78:1–19, 2019. 27

[126] H. Liu, Y.-L. Ren, X. Li, Y.-X. Hu, J.-P. Wu, B. Li, L. Luo, Z. Tao, X. Liu, and J. Liang. Rock thin-section analysis and identification based on artificial intelligent technique. *Petroleum Science*, 19(4):1605–1621, 2022. 24, 26, 37

[127] X. Liu, B. Li, J. Li, X. Chen, Q. Li, and Y. Chen. Semi-supervised deep autoencoder for seismic facies classification. *Geophysical Prospecting*, 69(6):1295–1315, 2021. 54

[128] X. Liu, X. Chen, J. Cheng, L. Zhou, L. Chen, C. Li, and S. Zu. Simulation of complex geological architectures based on multi-stage generative adversarial networks integrating with attention mechanism and spectral normalization. *IEEE Transactions on Geoscience and Remote Sensing*, 2023. 38

[129] Y. Liu, Q. Zhang, N. Zhang, J. Lv, M. Gong, and J. Cao. Enhancement of thin-section image using super-resolution method with application to the mineral segmentation and classification in tight sandstone reservoir. *Journal of Petroleum Science and Engineering*, 216:110774, 2022. 26, 38

[130] J. Long, E. Shelhamer, and T. Darrell. Fully convolutional networks for semantic segmentation. In *IEEE Conference on Computer Vision and Pattern Recognition*, pages 3431–3440, 2015. 68

[131] F. J. Lucia, C. Kerans, and J. W. Jennings Jr. Carbonate Reservoir Characterization. *Journal of Petroleum Technology*, 55(6):70–72, 2003. 15

[132] O. A. Malik, I. Puasa, and D. T. C. Lai. Segmentation for Multi-Rock Types on Digital Outcrop Photographs Using Deep Learning Techniques. *Sensors*, 22(21): 8086, 2022. 31, 37

[133] A. Marques, G. Racolte, D. C. Zanotta, E. Menezes, C. L. Cazarin, L. Gonzaga, and M. R. Veronez. Adaptive segmentation for discontinuity detection on karstified carbonate outcrop images from UAV-SfM acquisition and detection bias analysis. *IEEE Access*, 10:20514–20526, 2022. 22, 31

[134] S. Marshall and M. E. Celebi. Comparison of Conventional and Bisecting k-means algorithms on color quantization. In *14th IASTED International Conference on Signal and Image Processing*, 2012. 47

[135] S. Matlab. Matlab. *The MathWorks, Natick, MA*, 2012. 39

[136] A. Mayeen, L. K. Shaji, A. K. Nair, and N. Kalarikkal. Morphological Characterization of Nanomaterials. In S. Mohan Bhagyaraj, O. S. Oluwafemi, N. Kalarikkal, and S. Thomas, editors, *Characterization of Nanomaterials*, Micro and Nano Technologies, pages 335–364. Woodhead Publishing, 2018. 25

[137] F. Mees, R. Swennen, M. V. Geet, and P. Jacobs. Applications of X-ray computed tomography in the geosciences. *Geological Society, London, Special Publications*, 215(1):1–6, 2003. 27

[138] A. D. Miall. *Principles of Sedimentary Basin Analysis*. Springer Science & Business Media, 2013. 22

[139] M. Miarelli and A. Della Torre. Workflow development to scale up petrophysical properties from digital rock physics scale to laboratory scale. *Transport in Porous Media*, pages 1–34, 2021. 27

[140] B. S. Min, D. K. Lim, S. J. Kim, and J. H. Lee. A novel method of determining parameters of CLAHE based on image entropy. *International Journal of Software Engineering and Its Applications*, 7(5):113–120, 2013. 46

[141] M. Minzoni, A. Cantelli, J. Thornton, and B. Wignall. Seismic-scale geometries and sequence-stratigraphic architecture of Early Cretaceous syn-post rift carbonate systems, Presalt Section, Brazil. *Special Publications*, 509:105 – 126, 2020. 16

[142] R. Mitchum Jr, P. R. Vail, and S. Thompson III. Seismic stratigraphy and global changes of sea level: Part 2. The depositional sequence as a basic unit for stratigraphic analysis: Section 2. Application of seismic reflection configuration to stratigraphic interpretation. *AAPG Special Volumes*, 26:53–63, 1977. 54

[143] R. M. Mitchum Jr, P. R. Vail, and J. B. Sangree. Seismic stratigraphy and global changes of sea level: Part 6. Stratigraphic interpretation of seismic reflection patterns in depositional sequences: Section 2. Application of seismic reflection configuration to stratigraphic interpretation. *AAPG Special Volumes*, 26:117–135, 1977. 54

[144] A. Mollajan, J. Ghiasi-Freez, and H. Memarian. Improving pore type identification from thin section images using an integrated fuzzy fusion of multiple classifiers. *Journal of Natural Gas Science and Engineering*, 31:396–404, 2016. 26, 34

[145] N. H. Mondol. Seismic Exploration. *Petroleum Geoscience*, 1:375–402, 2010. 28, 29

[146] J. L. P. Moreira, C. V. Madeira, J. A. Gil, and M. A. P. Machado. Bacia de Santos. *Boletim de Geociencias da Petrobras*, 15(2):531–549, 2007. 29

[147] M. C. Motwani, M. C. Gadiya, R. C. Motwani, and F. C. Harris. Survey of image denoising techniques. In *Proceedings of GSPX*, volume 27, pages 27–30, 2004. 31

[148] M. Muniz and D. Bosence. Pre-salt microbialites from the Campos Basin (offshore Brazil): image log facies, facies model and cyclicity in lacustrine carbonates. *Geological Society, London, Special Publications*, 418(1):221–242, 2015. 16

[149] T. Nagalakshimi and A. Sivasakthi. Advances in the investigation on behaviour of carbonate reservoir rocks. *IOSR Journal of Applied Geology and Geophysics*, 5: 54–58, 2017. 45

[150] W. Niblack. *An Introduction to Digital Image Processing*. Strandberg Publishing Company, 1985. 48

[151] B. O. Obondo and B. O. Nyangoye. Microscopy simple or advance technique of material characterization. *Open Science Journal*, 4(1), 2019. 26

[152] T. E. Oliphant. *A guide to NumPy*, volume 1. Trelgol Publishing USA, 2006. 44

[153] J. T. Orasugh, S. K. Ghosh, and D. Chattopadhyay. Nanofiber-Reinforced Biocomposites. In B. Han, S. Sharma, T. A. Nguyen, L. Longbiao, and K. S. Bhat, editors, *Fiber-Reinforced Nanocomposites: Fundamentals and Applications*, Micro and Nano Technologies, pages 199–233. Elsevier, 2020. 25

[154] N. Otsu. A threshold selection method from gray-level histograms. *IEEE Transactions on Systems, Man, and Cybernetics*, 9(1):62–66, 1979. 48

[155] A. K. Pal, S. Garia, K. Ravi, and A. M. Nair. Pore scale image analysis for petrophysical modelling. *Micron*, 154:103195, 2022. 26, 34, 40

[156] L. Palombo, C. Ulsen, D. Uliana, F. R. Costa, M. Yamamoto, and H. Kahn. Caracterização de rochas reservatório por microtomografia de raios X. *HOLOS*, 5:65–72, 2015. 15

[157] J. Park and J. Jeong. Assessment of the effectiveness of a convolutional autoencoder for digital image-based automated core logging. *Geoenergy Science and Engineering*, 227:211802, 2023. 37

[158] A. Paszke, S. Gross, S. Chintala, G. Chanan, E. Yang, Z. DeVito, Z. Lin, A. Desmaison, L. Antiga, and A. Lerer. Automatic Differentiation in PyTorch. In *31st Conference on Neural Information Processing Systems*, pages 1–4, Long Beach, CA, USA, 2017. 39

[159] S. Patel and M. Goswami. Comparative analysis of Histogram Equalization techniques. In *International Conference on Contemporary Computing and Informatics*, pages 167–168. IEEE, 2014. 46

[160] R. E. F. Pepper and G. Bejarano. PS Advances in Seismic Fault Interpretation Automation. In *AAPG Annual Convention*, 2005. 64

[161] L. Perez and J. Wang. The effectiveness of data augmentation in image classification using deep learning. *arXiv preprint arXiv:1712.04621*, 2017. 33

[162] D. Perkins. Mineralogy. *Begin*, 17:17–38, 1998. 26

[163] A. B. Petro, C. Sbert, and J.-M. Morel. Multiscale Retinex. *Image Processing On Line*, pages 71–88, 2014. 48

[164] Z. Pi, Z. Zhou, X. Li, and S. Wang. Digital image processing method for characterization of fractures, fragments, and particles of soil/rock-like materials. *Mathematics*, 9(8):815, 2021. 22, 34

[165] A. Pochet, P. H. Diniz, H. Lopes, and M. Gattass. Seismic fault detection using convolutional neural networks trained on synthetic poststacked amplitude maps. *IEEE Geoscience and Remote Sensing Letters*, 16(3):352–356, 2018. 22

[166] S. E. Prensky. A survey of recent developments and emerging technology in well logging and rock characterization. *The Log Analyst*, 35(02):1–30, 1994. 27

[167] S. E. Prensky. Advances in borehole imaging technology and applications. *Geological Society, London, Special Publications*, 159(1):1–43, 1999. 28, 45

[168] M. Protasov, G. Reshetova, and V. Tcheverda. Fracture detection by Gaussian beam imaging of seismic data and image spectrum analysis. *Geophysical Prospecting*, 64 (1):68–82, 2015. 22

[169] J. Qi, T. Lin, T. Zhao, F. Li, and K. Marfurt. Semisupervised multiattribute seismic facies analysis: Interpretation. *SB91–SB106*, 2016. 54

[170] A. Qiu, Y. Shi, X. Luo, Z. Li, and W. Zhang. Superresolution Reconstruction Algorithm of Ultrasonic Logging Images Based on High-Frequency Enhancement. *Journal of Sensors*, 2022:1–12, 11 2022. 46

[171] W. Rawat and Z. Wang. Deep convolutional neural networks for image classification: A comprehensive review. *Neural Computation*, 29(9):2352–2449, 2017. 68

[172] Q. Ren, H. Zhang, D. Zhang, X. Zhao, and X. Yu. Enhancing Seismic Facies Classification Using Interpretable Feature Selection and Time Series Ensemble Learning Model with Uncertainty Assessment. *IEEE Transactions on Geoscience and Remote Sensing*, pages 1–13, 2023. 54

[173] C. Riccomini, L. Sant'Anna, and C. Tassinari. Pré-sal: Geologia e Exploração. *Revista USP*, page 33, Nov. 2012. 15

[174] J. Roberts. Introdução ao Petróleo. *Reportando o Petróleo: Um Guia Jornalístico sobre Energia e Desenvolvimento. New York: Open Society Institute*, 2005. 15

[175] M. Roksandić. Seismic Facies Analysis Concepts. *Geophysical Prospecting*, 26(2): 383–398, 1978. 53

[176] O. Ronneberger, P. Fischer, and T. Brox. U-Net: Convolutional Networks for Biomedical Image Segmentation. In *International Conference on Medical Image Computing and Computer-Assisted Intervention*, pages 234–241. Springer, 2015. 68

[177] R. A. Rubo, C. de Carvalho Carneiro, M. F. Michelon, and R. dos Santos Gioria. Digital petrography: Mineralogy and porosity identification using machine learning algorithms in petrographic thin section images. *Journal of Petroleum Science and Engineering*, 183:106382, 2019. 26

[178] M. Saafan and T. Ganat. Inferring capillary pressure curve from 2D rock images based on fractal theory in low-permeability sandstone: a new integrated approach. *Fractals*, 29(06):2150149, 2021. 39

[179] M. Saafan, T. Ganat, M. Mohyaldinn, and X. Chen. A fractal model for obtaining spontaneous imbibition capillary pressure curves based on 2D image analysis of low-permeability sandstone. *Journal of Petroleum Science and Engineering*, 208:109747, 2022. 26

[180] H. Safari, B. J. Balcom, and A. Afrough. Characterization of pore and grain size distributions in porous geological samples–An image processing workflow. *Computers & Geosciences*, 156:104895, 2021. 27, 34

[181] S. Saini and K. Arora. A study analysis on the different image segmentation techniques. *International Journal of Information & Computation Technology*, 4(14): 1445–1452, 2014. 32

[182] T. Samajdar and M. I. Quraishi. Analysis and evaluation of image quality metrics. In *Information Systems Design and Intelligent Applications: Proceedings of Second International Conference*, volume 2, pages 369–378. Springer, 2015. 50

[183] J. E. Santos, D. Xu, H. Jo, C. J. Landry, M. Prodanović, and M. J. Pyrcz. PoreFlow-Net: A 3D convolutional neural network to predict fluid flow through porous media. *Advances in Water Resources*, 138:103539, 2020. 37

[184] H. Sarkheil, H. Hassani, and F. Alinia. Fractures distribution modeling using fractal and multi-fractal–neural network analysis in Tabnak hydrocarbon field, Fars, Iran. *Arabian Journal of Geosciences*, 6:945–956, 2013. 22

[185] J. Sauvola and M. Pietikäinen. Adaptive document image binarization. *Pattern Recognition*, 33(2):225–236, 2000. 48

[186] N. Saxena, R. J. Day-Stirrat, A. Hows, and R. Hofmann. Application of deep learning for semantic segmentation of sandstone thin sections. *Computers & Geosciences*, 152:104778, 2021. 26, 31

[187] R. Schepers, G. Rafat, C. Gelbke, and B. Lehmann. Application of Borehole Logging, Core Imaging and Tomography to Geotechnical Exploration. *International Journal of Rock Mechanics and Mining Sciences*, 38(6):867–876, 2001. 45

[188] N. Sebe. *Machine Learning in Computer Vision*, volume 29. Springer Science & Business Media, 2005. 17

[189] M. Seifallahi, B. Tokhmechi, A. Soleimani, and A. A. Fard. A novel methodology for fracture extraction from borehole image logs. In *The First International Conference Oil, Gas, Petrochemical And Power Plant, Tehran: SID*, volume 7, 2013. 45

[190] R. Shan, Q. Xing, J. Zhang, J. Wang, Y. Wang, and B. Liu. Lithology identification using well logging images based on improved inception network. In *IEEE Symposium Series on Computational Intelligence*, pages 1–6. IEEE, 2021. 28

[191] S. Shen, H. Li, W. Chen, X. Wang, and B. Huang. Seismic Fault Interpretation Using 3-D Scattering Wavelet Transform CNN. *IEEE Geoscience and Remote Sensing Letters*, 19:1–5, 2022. 22, 37

[192] H. Sheng, X. Wu, X. Sun, and L. Wu. Deep learning for characterizing CO_2 migration in time-lapse seismic images. *Fuel*, 336:126806, 2023. 23

[193] R. Shi, K. N. Ngan, and S. Li. Jaccard index compensation for object segmentation evaluation. In *IEEE International Conference on Image Processing*, pages 4457–4461. IEEE, 2014. 43

[194] C. Shorten and T. M. Khoshgoftaar. A survey on image data augmentation for deep learning. *Journal of Big Data*, 6(1):1–48, 2019. 33

[195] M. V. T. Soares, L. da Silva Bomfim, A. C. Vidal, M. C. K. Avansi, O. R. Cunha, R. G. V. García, and R. S. de Paiva Medeiros. Pre-salt carbonate cyclicity and depositional environment: NMR petrophysics and Markov cyclicity of lacustrine acoustic facies (Santos Basin, Brazil). *Marine and Petroleum Geology*, 157:106494, 2023. 16

[196] S. Song, D. Zhang, T. Mukerji, and N. Wang. GANSim-surrogate: An integrated framework for stochastic conditional geomodelling. *Journal of Hydrology*, 620: 129493, 2023. 38

[197] J. F. L. Souza, M. D. Santos, R. M. Magalhães, E. Neto, G. P. Oliveira, and W. L. Roque. Automatic classification of hydrocarbon "leads"' in seismic images through artificial and convolutional neural networks. *Computers & Geosciences*, 132:23–32, 2019. 37

[198] P. J. Strzelecki, A. Świerczewska, K. Kopczewska, A. Fheed, J. Tarasiuk, and S. Wroński. Decoding Rocks: An Assessment of Geomaterial Microstructure using X-ray Microtomography, Image Analysis and Multivariate Statistics. *Materials*, 14(12):3266, 2021. 27, 40

[199] H. Su-Mei, S. Zhao-Hui, Z. Meng-Ke, Y. San-Yi, and W. Shang-Xu. Incremental semi-supervised learning for intelligent seismic facies identification. *Applied Geophysics*, 19(1):41–52, 2022. 54

[200] H. Sun, S. Vega, and G. Tao. Analysis of heterogeneity and permeability anisotropy in carbonate rock samples using digital rock physics. *Journal of Petroleum Science and Engineering*, 156:419–429, 2017. 27

[201] Y. Sun, Y. Zhao, and L. Yuan. Quantifying nano-pore heterogeneity and anisotropy in gas shale by synchrotron radiation nano-CT. *Microporous and Mesoporous Materials*, 258:8–16, 2018. 27

[202] S. B. Suslick and D. J. Schiozer. Risk analysis applied to petroleum exploration and production: an overview. *Journal of Petroleum Science and Engineering*, 44(1-2): 1–9, 2004. 17

[203] P. Szatmari and E. J. Milani. Tectonic control of the oil-rich large igneous-carbonate-salt province of the South Atlantic rift. *Marine and Petroleum Geology*, 77:567–596, 2016. 55

[204] R. Szeliski. *Computer Vision: Algorithms and Applications*. Springer Nature, 2022. 32

[205] M. Tadayoni, M. Khalilbeyg, and R. Bin Junin. A new approach to heterogeneity analysis in a highly complex carbonate reservoir by using borehole image and conventional log data. *Journal of Petroleum Exploration and Production Technology*, 10:2613–2629, 2020. 45

[206] P. Tahmasebi, S. Kamrava, T. Bai, and M. Sahimi. Machine learning in geo-and environmental sciences: From small to large scale. *Advances in Water Resources*, 142:103619, 2020. 35, 36

[207] D. G. Tang, K. L. Milliken, and K. T. Spikes. Machine learning for point counting and segmentation of arenite in thin section. *Marine and Petroleum Geology*, 120: 104518, 2020. 26, 31, 37

[208] P. Tang, D. Zhang, and H. Li. Predicting permeability from 3D rock images based on CNN with physical information. *Journal of Hydrology*, 606:127473, 2022. 22, 37

[209] M. Tembely, A. M. AlSumaiti, and W. S. Alameri. Machine and deep learning for estimating the permeability of complex carbonate rock from X-ray micro-computed tomography. *Energy Reports*, 7:1460–1472, 2021. 22, 27, 37

[210] J. E. Thomas. Fundamentos de Engenharia de Petróleo. 2ª edição. *Editora Interciência*, 2004. 15

[211] A. Ul-Hamid. *A Beginners' Guide to Scanning Electron Microscopy*, volume 1. Springer, 2018. 25

[212] M. B. Valentín, C. R. Bom, J. M. Coelho, M. D. Correia, M. P. De Albuquerque, M. P. de Albuquerque, and E. L. Faria. A deep residual convolutional neural network for automatic lithological facies identification in brazilian pre-salt oilfield wellbore image logs. *Journal of Petroleum Science and Engineering*, 179:474–503, 2019. 27

[213] S. Van der Walt, J. L. Schönberger, J. Nunez-Iglesias, F. Boulogne, J. D. Warner, N. Yager, E. Gouillart, and T. Yu. scikit-image: image processing in Python. *PeerJ*, 2:e453, 2014. 44

[214] G. Van Rossum and F. L. Drake Jr. *Python Reference Manual*. Centrum voor Wiskunde en Informatica Amsterdam, 1995. 39

[215] A. Vaswani, N. Shazeer, N. Parmar, J. Uszkoreit, L. Jones, A. N. Gomez, Ł. Kaiser, and I. Polosukhin. Attention is all you need. *Advances in Neural Information Processing Systems*, 30, 2017. 69

[216] S. Verma, S. Bhattacharya, T. Fett, P. Avseth, and I. Lehocki. Imaging and interpretation: Seismic, Rock Physics and Image Log Analysis Workflows for Deepwater Systems. In J. R. Rotzien, C. A. Yeilding, R. A. Sears, F. J. Hernández-Molina, and O. Catuneanu, editors, *Deepwater Sedimentary Systems*, pages 555–591. Elsevier, 2022. 28

[217] B. Vissapragada, W. Al-Hanai, and S. Russel. Carbonate Rocks. *The Society of Core Analysts*, Jan. 2000. 17

[218] M. Voorn, U. Exner, A. Barnhoorn, P. Baud, and T. Reuschlé. Porosity, permeability and 3D fracture network characterisation of dolomite reservoir rock samples. *Journal of Petroleum Science and Engineering*, 127:270–285, 2015. 22, 27

[219] A. Voulodimos, N. Doulamis, A. Doulamis, and E. Protopapadakis. Deep learning for computer vision: A brief review. *Computational Intelligence and Neuroscience*, 2018, 2018. 36

[220] H. Wang, L. Dalton, R. Guo, J. McClure, D. Crandall, and C. Chen. Application of unsupervised deep learning to image segmentation and in-situ contact angle measurements in a CO_2-water-rock system. *Advances in Water Resources*, 173:104385, 2023. 23, 27, 31

[221] N. Wang, H. Chang, D. Zhang, L. Xue, and Y. Chen. Efficient well placement optimization based on theory-guided convolutional neural network. *Journal of Petroleum Science and Engineering*, 208:109545, 2022. 37

[222] Y. Wang, H. Liu, M. Guo, X. Shen, B. Han, and Y. Zhou. Image recognition model based on deep learning for remaining oil recognition from visualization experiment. *Fuel*, 291:120216, 2021. 37

[223] Z. Wang, Q. Wang, Y. Yang, N. Liu, Y. Chen, and J. Gao. Seismic facies segmentation via a segformer-based specific encoder–decoder–hypercolumns scheme. *IEEE Transactions on Geoscience and Remote Sensing*, 61:1–11, 2023. 54

[224] X.-L. Wei, C.-X. Zhang, S.-W. Kim, K.-L. Jing, Y.-J. Wang, S. Xu, and Z.-Z. Xie. Seismic fault detection using convolutional neural networks with focal loss. *Computers & Geosciences*, 158:104968, 2022. 66

[225] P. M. Wong, M. Jang, S. Cho, and T. D. Gedeon. Multiple permeability predictions using an observational learning algorithm. *Computers & Geosciences*, 26(8):907–913, 2000. 45

[226] Q. Wu, Y. Liu, Q. Li, S. Jin, and F. Li. The application of deep learning in computer vision. In *Chinese Automation Congress*, pages 6522–6527. IEEE, 2017. 36

[227] S. Wu, Q. Wang, Q. Zeng, Y. Zhang, Y. Shao, F. Deng, Y. Liu, and W. Wei. Automatic extraction of outcrop cavity based on a multiscale regional convolution neural network. *Computers & Geosciences*, 160:105038, 2022. 37

[228] X. Wu, Y. Shi, S. Fomel, L. Liang, Q. Zhang, and A. Z. Yusifov. FaultNet3D: Predicting fault probabilities, strikes, and dips with a single convolutional neural network. *IEEE Transactions on Geoscience and Remote Sensing*, 57(11):9138–9155, 2019. 65

[229] X. Wu, S. Yan, J. Qi, and H. Zeng. Deep learning for characterizing paleokarst collapse features in 3-D seismic images. *Journal of Geophysical Research: Solid Earth*, 125(9):e2020JB019685, 2020. 37

[230] Y. Wu, S. Misra, C. Sondergeld, M. Curtis, and J. Jernigen. Machine learning for locating organic matter and pores in scanning electron microscopy images of organic-rich shales. *Fuel*, 253:662–676, 2019. 26, 31

[231] Y. Wu, P. Tahmasebi, C. Lin, M. J. Munawar, and V. Cnudde. Effects of micropores on geometric, topological and transport properties of pore systems for low-permeability porous media. *Journal of Hydrology*, 575:327–342, 2019. 34

[232] P. Xie, J. Hou, Y. Yin, Z. Chen, M. Chen, and L. Wang. Seismic inverse modeling method based on generative adversarial networks. *Journal of Petroleum Science and Engineering*, 215:110652, 2022. 38

[233] G. Xu and B. U. Haq. Seismic facies analysis: Past, present and future. *Earth-Science Reviews*, 224:103876, 2022. 16, 53, 54

[234] Z. Yan, S. Liu, and H. Gu. Fault image enhancement using a forward and backward diffusion method. *Computers & Geosciences*, 131:1–14, 2019. 22

[235] X. Yang, X. Chen, and M. M. Smith. Deep learning inversion of gravity data for detection of CO_2 plumes in overlying aquifers. *Journal of Applied Geophysics*, 196: 104507, 2022. 23, 37

[236] S. Yarmohammadi, D. A. Wood, and A. Kadkhodaie. Reservoir microfacies analysis exploiting microscopic image processing and classification algorithms applied to carbonate and sandstone reservoirs. *Marine and Petroleum Geology*, 121:104609, 2020. 22, 26

[237] Ö. Yilmaz. *Seismic data analysis: Processing, inversion, and interpretation of seismic data.* Society of Exploration Geophysicists, 2001. 28, 29

[238] J. You, J. Zhao, X. Huang, G. Zhang, A. Chen, M. Hou, and J. Cao. Explainable Convolutional Neural Networks driven knowledge mining for seismic facies classification. *IEEE Transactions on Geoscience and Remote Sensing*, pages 1–18, 2023. 54

[239] N. You, Y. Elita Li, and A. Cheng. ML-based facies classification on acoustic image logs from Brazilian presalt region. In *Second International Meeting for Applied Geoscience & Energy*, volume 1, pages 1870–1874. Society of Exploration Geophysicists and American Association of Petroleum, 2022. 28

[240] N. You, E. Li, and A. Cheng. Automatic facies classification from acoustic image logs using deep neural networks. *Interpretation*, 11(2):1–53, 2023. 45

[241] I. Yousef and V. Morozov. Fractures characterization of carbonate reservoir using core analyses and borehole image logs. *Petroleum Science and Technology*, pages 1–26, 2022. 45

[242] J. Yu, F. Wellmann, S. Virgo, M. von Domarus, M. Jiang, J. Schmatz, and B. Leibe. Superpixel segmentations for thin sections: Evaluation of methods to enable the generation of machine learning training data sets. *Computers & Geosciences*, 170: 105232, 2023. 26

[243] Z. Yuan, H. Huang, Y. Jiang, J. Tang, and J. Li. An enhanced fault-detection method based on adaptive spectral decomposition and super-resolution deep learning. *Interpretation*, 7(3):T713–T725, 2019. 22, 37

[244] W. Yun, Y. Liu, and A. R. Kovscek. Deep learning for automated characterization of pore-scale wettability. *Advances in Water Resources*, 144:103708, 2020. 21, 26, 37

[245] Y. Zang, Q. Wang, H. Wang, B. Wang, K. Tian, T. Wang, J. Li, Z. Zhang, S. Tian, and S. Stanchits. Laboratory visualization of supercritical CO_2 fracturing in tight sandstone using digital image correlation method. *Geoenergy Science and Engineering*, 225:211556, 2023. 23

[246] L. Zeng, W. Ren, and L. Shan. Attention-based bidirectional gated recurrent unit neural networks for well logs prediction and lithology identification. *Neurocomputing*, 414:153–171, 2020. 22

[247] C. Zhang, X. Song, and L. Azevedo. U-Net generative adversarial network for subsurface facies modeling. *Computational Geosciences*, 25:553–573, 2021. 22, 38

[248] G. Zhang, Z. Wang, and Y. Chen. Deep learning for seismic lithology prediction. *Geophysical Journal International*, 215(2):1368–1387, 2018. 22, 37

[249] H. Zhang, H. Yu, S. Meng, M. Huang, M. Micheal, J. Su, H. Liu, and H. Wu. Fast and accurate reconstruction of large-scale 3D porous media using deep learning. *Journal of Petroleum Science and Engineering*, 217:110937, 2022. 27, 37

[250] J. Zhang, J. Li, X. Chen, Y. Li, and W. Tang. A spatially coupled data-driven approach for lithology/fluid prediction. *IEEE Transactions on Geoscience and Remote Sensing*, 59(7):5526–5534, 2020. 22, 37

[251] S. Zhang, M. Zhu, and K. Meng. An automated multi-scale retinex for dim image enhancement. In *IEEE 2nd International Conference on Power, Electronics and Computer Applications*, pages 647–651. IEEE, 2022. 48

[252] W. Zhang, T. Wu, Z. Li, S. Liu, A. Qiu, Y. Li, and Y. Shi. Fracture recognition in ultrasonic logging images via unsupervised segmentation network. *Earth Science Informatics*, 14:955–964, 2021. 45

[253] Y. Zhang, Y. Liu, H. Zhang, and H. Xue. Seismic facies analysis based on deep learning. *IEEE Geoscience and Remote Sensing Letters*, 17(7):1119–1123, 2019. 54

[254] Y. J. Zhang. A survey on evaluation methods for image segmentation. *Pattern Recognition*, 29(8):1335–1346, 1996. 32

[255] D. Zhao, Y. Guo, G. Wang, and X. Mao. Characterizing Nanoscale Pores and its Structure in Coal: Experimental Investigation. *Energy Exploration & Exploitation*, 37(4):1320–1347, 2019. 21, 26, 39

[256] D. Zhao, Y. Guo, G. Wang, W. Jiao, J. Liu, and Y. Hui. Quantitative characterization of nano-scale pores in shale reservoirs of Wufeng-Longmaxi formation based on image processing. *Fresenius Environ. Bull*, 29(5):3992–3999, 2020. 21, 26, 39

[257] M. Zhao, Y. Wang, M. Gerritsma, and H. Hajibeygi. Efficient simulation of CO_2 migration dynamics in deep saline aquifers using a multi-task deep learning technique with consistency. *Advances in Water Resources*, page 104494, 2023. 23

[258] T. Zhao and P. Mukhopadhyay. A fault detection workflow using deep learning and image processing. In *SEG International Exposition and Annual Meeting*. OnePetro, 2018. 64

[259] T. Zhao, F. Li, and K. J. Marfurt. Constraining self-organizing map facies analysis with stratigraphy: An approach to increase the credibility in automatic seismic facies classification. *Interpretation*, 5(2):T163–T171, 2017. 54

[260] Y. Zheng, Q. Zhang, A. Yusifov, and Y. Shi. Applications of supervised deep learning for seismic interpretation and inversion. *The Leading Edge*, 38(7):526–533, 2019. 17

[261] Z. Zhong, A. Y. Sun, Y. Wang, and B. Ren. Predicting field production rates for waterflooding using a machine learning-based proxy model. *Journal of Petroleum Science and Engineering*, 194:107574, 2020. 38

[262] Z. Zhou, M. M. R. Siddiquee, N. Tajbakhsh, and J. Liang. U-Net++: A nested U-Net architecture for medical image segmentation. In *Deep Learning in Medical Image Analysis and Multimodal Learning for Clinical Decision Support*, pages 3–11. Springer, 2018. 68

[263] Z. Zhou, M. M. R. Siddiquee, N. Tajbakhsh, and J. Liang. U-Net++: Redesigning skip connections to exploit multiscale features in image segmentation. *IEEE Transactions on Medical Imaging*, 39(6):1856–1867, 2019. 69

[264] C. Zhu, J. Wang, S. Sang, and W. Liang. A multiscale neural network model for the prediction on the equivalent permeability of discrete fracture network. *Journal of Petroleum Science and Engineering*, 220:111186, 2023. 22, 37

[265] M. Zohreh, R. Junin, and P. Jeffreys. Evaluate the Borehole Condition to Reduce Drilling Risk and Avoid Potential Well Bore Damages by using Image Logs. *Journal of Petroleum Science and Engineering*, 122:318–330, 2014. 45

[266] K. Zuiderveld. Contrast Limited Adaptive Histogram Equalization. *Graphics Gems*, pages 474–485, 1994. 46